NEUTRON DEPTH DOSE DISTRIBUTIONS IN HETEROGENEOUS PHANTOMS

A THESIS

Presented to

The Faculty of the Division of Graduate

Studies and Research

By

John Ware Poston

In Partial Fulfillment

of the Requirements for the Degree

Doctor of Philosophy

in the

School of Nuclear Engineering

Georgia Institute of Technology

June, 1971

In presenting the dissertation as a partial fulfillment of the requirements for an advanced degree from the Georgia Institute of Technology, I agree that the Library of the Institute shall make it available for inspection and circulation in accordance with its regulations governing materials of this type. I agree that permission to copy from, or to publish from, this dissertation may be granted by the professor under whose direction it was written, or, in his absence, by the Dean of the Graduate Division when such copying or publication is solely for scholarly purposes and does not involve potential financial gain. It is understood that any copying from, or publication of, this dissertation which involves potential financial gain will not be allowed without written permission.

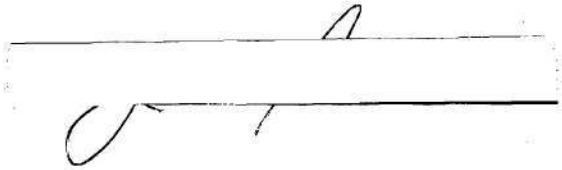

7/25/68

NEUTRON DEPTH DOSE DISTRIBUTIONS IN HETEROGENEOUS PHANTOMS

Approved:

Date approved by Chairman: 3/11/71

ACKNOWLEDGMENTS

I wish to express my sincere appreciation to my thesis advisor, Professor F. W. Chambers, Jr., for his guidance, interest, and understanding during the entire research program.

I am also grateful to the members of my reading committee, Dr. G. Eichholz, Dr. D. S. Harmer, and J. A. Auxier (Oak Ridge National Laboratory), for their interest and useful suggestions in all phases of this work.

I am indebted to many individuals at the Oak Ridge National Laboratory for their willing advice and help. Special thanks go to P. T. Perdue and F. E. Gillespie for their assitance and advice with the electronic circuits. W. H. Shinpaugh deserves special credit for his graphic arts work. The assistance of D. R. Ward and E. M. Robinson during the operation of the Health Physics Research Reactor and the DOSAR Low Energy Accelerator was of particular value.

As always, lively discussions with my fellow graduate students, especially P. H. McGinley, W. H. Wilkie, C. L. Wakamo, and R. F. Boggs, were of lasting value. Thanks also go to Harold Hoey and his fine staff of research machinists at Georgia Tech for their work in fabricating these chambers.

The diligent and loyal assistance of Miss L. Jo Brown during the typing and editing of this dissertation is truly appreciated.

This research was begun at the Georgia Institute of Technology while I was supported by a traineeship supplied by the U.S. Public

Health Service. The project was completed at the Oak Ridge National Laboratory which is operated for the U.S. Atomic Energy Commission by the Union Carbide Corporation. Financial support during all phases of this research is appreciated.

I would like to thank the Division of Graduate Studies and Research, Georgia Institute of Technology for permission to use special pagination and margins in order to comply with the reproduction criteria of the Oak Ridge National Laboratory.

Finally, I wish to thank my wife for all her encouragement, patience, and understanding; our parents for their unquestioning support and understanding; and my children who, I hope, some day will understand what it means for daddy to be a "master" and then a "doctor".

TABLE OF CONTENTS

TABLE OF CONTENTS (Continued)

LIST OF TABLES

LIST OF ILLUSTRATIONS

LIST OF ILLUSTRATIONS (Continued)

SUMMARY

In the past few years, there has been an increasing interest in neutron radiography for both industrial and medical applications. Such use in radiography as well as potential application of neutrons in cancer therapy drew attention to the need for further research to establish reliable data on neutron dosimetry in such cases. These investigations have been directed toward the measurement of dose distributions in various media, including the human body, beam collimation studies, and development of means of imaging both fast and thermal neutrons.

The study reported here was begun with the purpose of establishing neutron dose distributions at bone-tissue interfaces in the human body. Similar measurements performed for photons of up to 200 keV have shown a reduction in the dose delivered to tissue areas shielded by bone of up to a factor of two. The design and operational characteristics of detectors intended to measure analogous distributions due to fast neutrons are described. Measured distributions due to fission spectrum and 14-MeV neutrons are presented and discussed. Results from measurements with fission spectrum neutrons indicate that the high voltage electrodes attached to the front of the detectors were too thick to allow the measurement of the changes in dose distributions very near the interface. However, distributions due to 14-MeV neutrons indicate a reduction in the predicted homogeneous depth dose distribution due to the presence of bone. The reduction is about 20% at a distance in bone of about 2 cm. In tissue at the rear of bone, a buildup or increase in the dose deposited

has been demonstrated which is about 50% more than the interface value at a depth in tissue of 0.8 to 1.0 cm. These results are discussed and compared with available theoretical descriptions.

Also included is a discussion of the problems associated with the use of these detectors, a discussion of the sources of error in the experiment, and a set of recommendations for improvement and further study in this area.

CHAPTER I

INTRODUCTION

Soon after the discovery of x rays by Wilhelm Röntgen in 1895, the possibility of using x-ray pictures in medical and surgical diagnosis was recognized. An editorial in *The Journal of the American Medical Association* in 1896 expressed the cautious opinion that these new rays might have therapeutic applications.[1] In December, 1898, Pierre and Marie Curie announced the discovery of radium, a highly active substance extracted from pitchblende. Rays similar to those reported by Röntgen but more penetrating were found to be one of the three kinds of rays which emanated from the substance. These rays were called gamma-rays.

The effect of gamma-rays on living tissue was observed when Becquerel noted a skin burn from a small vial of radium which he carried in his vest pocket. Pierre Curie intentionally produced a similar burn on his arm. Observations on the effects of gamma rays on body tissues led to the conclusion that radiations from radium might possess curative powers. Further research on the effects of radium rays on microorganisms, seeds, protozoa, ova, and embryos followed. The extensive study of irradiated epithelial cells led Bergonié and Tribondeau to propose the well-known law that in essence states that radiosensitivity of a tissue will be dependent upon the number of undifferentiated cells it contains, the degree of mitotic activity in the

tissue, and the length of time that cells remain in active proliferation.[2] Thus tumors, containing large proportions of undifferentiated and rapidly dividing cells, should be quite susceptible to treatment by x rays or gamma rays. This result formed the base from which experimental and therapeutic uses of radiation began to grow.[3]

The distribution of dose from x rays as a function of depth in the human body was of immediate interest to the radiologist. These distributions were required for diagnostic and therapeutic treatment planning in the use of x- and gamma-ray sources for such applications as cancer therapy. A great deal of the early work was performed to determine distributions in substances, other than tissue, which simulate the radiation absorption of the human body (these simulated bodies are usually called phantoms). In general, the human body was represented by a homogeneous mixture of the major elements which constitute tissue (i.e., mainly hydrogen, oxygen, carbon, and nitrogen). Several excellent textbooks containing detailed depth dose tables have been published[1,4] for use by individuals engaged in x-ray or gamma-ray diagnosis and therapy. These tabulations accurately predict ($\leq$ 5%) the dose as a function of depth in soft tissue, but will be less accurate predictions when bone is introduced at some depth in tissue. In x-ray therapy, the bones tend to cast "shadows" which reduce the depth dose in tissue layers at depths below the bone. As one visualizes the distribution of absorbed dose in tissue, there is the expected decrease due to attenuation of the beam. As radiation passes from one medium into another denser one (for example, bone), the absorbed dose increases due to the strong Z-dependence of the photoelectric interactions. If the interace is

crossed again, at the rear of the bone, returning to the tissue region, one finds the absorbed dose greatly reduced from that which would be expected based on measurements in a homogeneous phantom. The heterogeneous case (i.e., tissue with bone at some depth in the tissue) of x-ray absorption has been an area of considerable research by radiologists for many years. Spiers[5] has recently made an extensive survey of the latest techniques and advances in the area of transition zone dosimetry for monoenergetic photons.

A detailed account of the growth in the field of radiology in the early twentieth century is presented in Reference 1. With Chadwick's discovery of the neutron in 1932 and the intensive research which followed, another tool was added to the list of radiations available for radiation therapy. By 1939, J. H. Lawrence and R. S. Stone had begun the treatment of cancer patients with a neutron beam from a cyclotron.

With the increased availability and use of neutrons in many research areas, the need for similar depth dose information for neutrons became evident. Since 1954, dose and spectrum measurements have been reported in various materials simulating tissue and employing a wide variety of neutron sources. These results are valuable in the assessment of neutron dose for radiation protection purposes as well as in nuclear accident evaluation, neutron therapy, and neutron radiography. Fowler[6] has summarized the current potential of the use of neutrons in radiotherapy. The use of neutrons for radiography is summarized by Barton et al.[7,8] A recent publication by Auxier et al.[9] summarizes the present state of experimental and theoretical neutron depth dose

considerations. Recent improvements in the calculations of neutron depth dose may form a new basis for future estimates of the hazard from neutron exposure.

The major portion of the neutron depth dose investigations has been carried out with homogeneous phantoms in various geometries. The introduction of bone into a phantom, a situation which is obviously more representative of the human body, has been considered little until recently. To date, only a few calculations and no experimental results have been published.[10-12] It appears that the extension of fast neutron depth dose measurements to the heterogeneous case is the next logical step. Further, it appears as in x-ray and gamma-ray diagnosis and therapy, that the region of primary concern may be the tissue-bone interface.[13] Experimental investigations in heterogeneous phantoms, especially at bone-tissue interfaces, should have direct applicability to the areas of radiation protection, neutron therapy, and neutron radiography.

This thesis reports work done with heterogeneous phantoms designed to investigate the dose distributions due to fast neutrons and gamma rays at a bone-tissue interface. These results provide a means of checking the validity of various theoretical models of such systems.

CHAPTER II

GENERAL CONSIDERATIONS

Neutron Interactions in Tissue

Before any discussion of neutron interactions in tissue can begin, a set of definitions must be given. In this discussion, neutrons will be segregated into the categories which follow:[14]

1. Thermal Neutrons. These neutrons are in thermal equilibrium with matter and, in special cases, have a Maxwellian distribution of velocities. In this distribution, the most probable velocity at 295°K is 2,200 meters/sec., corresponding to an energy of 0.025 eV.

2. Intermediate Neutrons. These neutrons are in the energy range 0.5 eV to 10 keV. In this range, there usually exist large resonance peaks in the neutron cross sections; thus the often-used term "resonance neutrons".

3. Fast Neutrons. These neutrons are in the energy range 10 keV to 10 MeV where, in general, the most frequent interaction with matter is elastic scattering.

4. Relativistic Neutrons. This category encompasses all neutrons with energies greater than 10 MeV.

A more detailed discussion of the interaction of neutrons according to energy groups is presented in the following section.

The type of neutron interaction depends strongly upon the kinetic energy of the neutron. For thermal neutrons, the most important

interaction with matter is capture. In tissue, the important reactions at low energy are $^{1}H(n,\gamma)^{2}D$, which produces a 2.2 MeV gamma ray, and $^{14}N(n,p)^{14}C$ which yields a 0.6 MeV proton. In most dose considerations, the energy from the (n,p) reaction is considered to be deposited locally, since the range of the proton is less than ten microns in tissue. Because of the greater range of the 2.2 MeV gamma rays, the size of the tissue sample under irradiation greatly influences the contribution of this reaction to the absorbed dose.

For intermediate energy neutrons, the neutron slowing-down process is the important interaction with matter. Capture and nuclear reactions may also occur in this region.

The most important dose depositing interaction of fast neutrons with tissue is elastic scattering with hydrogen. Collision of a neutron with a nucleus results in deflection of the incident particle, along with the transfer of a portion of the energy of the neutron to the struck nucleus. Energy losses by elastic scattering are dependent on the size of the colliding nucleus and the collision angle (e.g., glancing or head-on). The maximum fractional energy loss by an incident neutron on elastic collision with a nucleus is given by the relation,[15]

$$\frac{E_1 - E_{min}}{E_1} = 1 - \alpha \qquad (1)$$

where E_1 is the kinetic energy of the neutron before collision and E_{min} is the minimum value of the energy to which a neutron can be reduced by an elastic scattering collision. In this relation, α is given by

$$\alpha \equiv \left(\frac{A - 1}{A + 1}\right) \tag{2}$$

where A is the mass number of the target nucleus. For hydrogen, A = 1 and $\alpha = 0$, and thus it is possible for a neutron to lose all its kinetic energy in one collision with a hydrogen nucleus. However, as a consequence of isotropic scattering in the center-of-mass system, each fraction of the neutron energy is given to the proton with equal probability. For hydrogen, elastic scattering may be considered isotropic in the center-of-mass system up to about 14 MeV.[14]

Inelastic scattering becomes important as the neutron energy increases, first occurring for most nuclei at an energy of the order of 1 MeV. At energies above 10 MeV, inelastic scattering may be as probable as elastic scattering. The important inelastic reactions of neutrons in soft tissue are those with carbon, nitrogen, and oxygen.

Cross sections for inelastic processes of interest in tissue become significant at neutron energies greater than 5 MeV and increase generally, but not always monotonically, as neutron energy increases to about 15 MeV. Most of these reactions are accompanied by de-excitation gamma rays, but the proton and alpha particle-producing reactions are of special importance due to the high linear energy transfer (LET) of these particles and the total absorption of their energies near the reaction site. Auxier et al.[9] have tabulated 33 reactions occurring in tissue and have calculated the relative contributions of each reaction to the average dose in a 30-cm diameter cylindrical phantom, 60 cm high. For every neutron energy (fission spectrum, 5, 7, 10, and 14 MeV), elastic

scattering with hydrogen is the major contributor to the average dose in the phantom. In general, elastic scattering with oxygen and the $^{1}H(n,\gamma)^{2}D$ reaction are next in the order of importance, respectively, in terms of relative contributions to the average dose in the cylindrical phantom.

Results of calculations by Wilkie[16] for 14-MeV neutrons incident on an elliptical phantom (30 cm wide, 20 cm thick) indicate that about 95% of the total neutron interactions in tissue are elastic collisions with the four major constituents of tissue (72% with hydrogen nuclei). However, only about 72% of the energy loss (dose) of the neutrons is due to elastic collisions. The remainder of the energy loss comes through inelastic collisions with carbon, hydrogen, and oxygen nuclei. In contrast, the author also reports results for ^{252}Cf fission neutrons which indicate that 99.9% of the interactions are elastic (81% with hydrogen nuclei) and that 98% of the energy loss comes through these elastic collisions.

In the relativistic neutron energy region, especially above about 20 MeV, inelastic scattering is more important than elastic scattering. For high atomic number materials, the elastic cross section may be neglected entirely. However, for hydrogenous materials, such as tissue, elastic processes are still important. The total elastic (n,p) cross section is approximately a factor of two higher than the (n,n') cross section at 14 MeV, and this relation appears to hold up to energies of the order of 200 MeV.

Sources of Neutrons

In a discussion of neutron dosimetry, one should logically consider the neutron spectra, average energy, and output of the available

sources of neutrons. Nachtigall[17] has recently summarized the data for many of the available (α,n) neutron sources. The results of a portion of this survey are presented in Table 1. Tables 2 and 3 list the characteristics of some (γ,n) and spontaneous fission sources, respectively.

Nuclear reactors provide copious quantities of neutrons for many research applications. The leakage spectra from these reactors vary quite widely due to the interposition of moderator, coolant, and shielding material. For example, the leakage spectrum from the Health Physics Research Reactor at ORNL (an unshielded reactor) provides a neutron spectrum that closely approximates that of the fission spectrum. The leakage spectrum from the Zephyr reactor, in contrast, shows many neutrons in the lower end of the fast neutron range with an average energy of much less than 1 MeV.[18] The neutron leakage spectrum of a research reactor is one of the first measurements performed when initial use begins. The results are too numerous to mention or discuss.

Accelerator-produced neutrons are also used quite extensively in many research areas. The most commonly employed reactions are the $^{2}D(d,n)^{3}He$ and the $^{3}T(d,n)^{4}He$ reactions producing neutrons of 3 and 14.5 MeV, respectively. Reference 39 gives neutron spectra resulting from deuterons in the energy range 15-24 MeV impinging on a thick beryllium target.

The use of a Van de Graaff accelerator allows one to produce monoenergetic neutrons over a wide range. Such monoenergetic sources are commonly used for the calibration and intercomparison of neutron dosimetry systems.[19]

Table 1. Comparison of Some (α,n) Neutron Sources[17]

Source	Half Life	Average E_n (MeV)	Max E_n (MeV)	Output for 1 Ci (neutrons/sec)
^{210}Po-B	138.4 d	2.8	5.0	2.0×10^5
^{210}Po-Be	138.4 d	4.0	10.8	2.5×10^6
^{241}Am-Be	458 y	4.3	11.0	2.0×10^6
^{226}Ra-Be	1622 y	4.5	13.2	1.5×10^7
^{239}Pu-Be	2.44×10^4 y	4.1	10.6	1.5×10^6

Table 2. Comparison of Some (γ,n) Neutron Sources[18]

Source	Half-Life	E_γ (MeV)	En calc. (MeV)	En meas. (MeV)	Yield
^{24}Na + Be	15.0 h	2.757	0.966	0.83	1.3×10^5
^{24}Na + D_2O	15.0 h	2.757	0.261	0.22	2.7×10^5
^{88}Y + Be	104 d	1.853	0.166	0.158	1.0×10^5
^{124}Sb + Be	60 d	1.70	0.031	0.0248	1.9×10^5
^{226}Ra + Be	1622 y	many	--	0.7 max	1.2×10^4
^{226}Ra + Be	1622 y	many	--	0.12	0.1×10^4

Table 3. Comparison of Some Spontaneous Fission Sources[18]

Nuclide	Half-Life (spontaneous fission)	Half-Life (α-decay)	Neutrons/g sec
^{236}Pu	3.5×10^{9} y	2.7 y	3.1×10^{4}
^{238}Pu	4.9×10^{10} y	89.6 y	2.3×10^{3}
^{240}Pu	1.3×10^{11} y	6600 y	7.0×10^{2}
^{242}Cm	7.2×10^{6} y	162.5 d	1.8×10^{9}
^{244}Cm	1.4×10^{7} y	18.4 y	1.0×10^{7}
^{252}Cf	85.5 y	2.7 y	2.3×10^{12}

Concepts Important to Radiation Dosimetry

In its simplest form, dosimetry is the measurement of dose by means of dosimeters. Historically, physicists employed the basic concept of energy in studying the interaction of radiation with matter. Generally, the resulting measurements were successful in affording some correlation between the quantity measured and the effects observed.

In the literature, however, dose has been used in several senses; primarily due to the fact that there are several different types of measurements that have been shown to be possible and useful in the study and control of the effects of ionizing radiation on matter. The significant types of measurements can be categorized as follows:[40]

1. Measurement of the absorbed dose in the target matter at the point of interest.
2. Measurement of the energy released by indirectly ionizing particles per unit mass of the target material at the position of interest.
3. Measurement of the number of particles or quanta, or their energy, incident at a given position.
4. Measurement of some function of the number and energy of the particles and quanta incident at a given point. As an example, the function may represent the product of the absorbed dose and the quality factor for radiations of different linear energy transfer.

The International Commission on Radiological Units and Measurements (ICRU) is the principal organization responsible for selecting and defining radiation quantities and units. A summary of the historical

development of the important radiation quantities and units used in radiation dosimetry is given by Attix et al.[40] The ICRU has defined the absorbed dose in the following manner:[41] "The absorbed dose (D) is the quotient of ΔE_D by Δm, where ΔE_D is the energy imparted by ionizing radiation to matter in a volume element, Δm is the mass of matter in that volume element." By the term "energy imparted to matter" one means that energy which appears as ionization or excitation, or as increases in chemical or crystal-lattice energy, etc., in the matter. Energy which is involved in changes in rest mass of the material or the radiation is excluded by definition. In other words, by "energy imparted" to an irradiated material one really means simply that energy which is removed from the radiation field. Thus, one concludes that absorbed dose, like temperature or pressure, is a macroscopic concept. However, its usefulness consists in the fact that it specifies in a single number the energy concentration at the point of interest.

Historically, the concept of linear energy transfer (LET) was introduced by Zirkle[42] who proposed the term to describe the rate of energy loss of a particle along its projected path. This is essentially the same concept as the stopping power, but the concept of LET puts emphasis on the process rather than on the particle or the medium. LET has been defined in terms of local energy transfers; unfortunately, the word local has various connotations. Recent ICRU definitions have sought to avoid this confusion. The following is the most recent definition given by the ICRU:[110]

> The linear energy transfer or restricted linear collision stopping power (L_Δ) of charged particles in a medium is the

quotient of dE by $d\ell$, where $d\ell$ is the distance traversed by the particle and dE is the mean energy loss due to collisions with energy transfers less than some specified value Δ.

$$L_{\Delta} = \left(\frac{dE}{d\ell}\right)_{\Delta}$$

Since the introduction of this concept, the theory has undergone considerable discussion, investigation, and formalization; the above is the "most recent" definition.

Much of the work in the formalization and the measurement of LET distributions has been due to Boag[43] and to Rossi et al.[29,44,45] The measurement of LET is quite difficult requiring complex mathematical analyses of the experimental data in order to derive the required LET distributions.[29,30]

In practical situations of radiation protection, precise information is seldom available concerning the conditions of exposure and subsequent actions of the exposed subject. In addition, at the low levels of dose typical of an occupational exposure, the physiological effects to be expected are not known with precision. For these reasons, the ICRU has recommended that a quality factor (QF), depending only on the LET, be used in place of Relative Biological Effectiveness (RBE) for computing the dose equivalent* for occupational exposure. The inclusion

---

* Relative Biological Effectiveness (RBE) is defined as the ratio of the amount of energy of any radiation required to produce a given effect to the energy required of 200 kVp x rays to produce the same effect.

Dose Equivalent (DE) is defined as the product of absorbed dose, D, quality factor (QF), dose distribution factor (DF), and other necessary modifying factors. The unit of dose equivalent is the rem.

of other modifying factors in the calculation is further recommended, but for exposure to neutrons, only QF is used in the computation of dose equivalent. The quality factor is defined in purely physical terms, since it is only a function of LET, but the basis of the definition is biological. Table 4 presents the quality factor as a function of LET. The quality factor is given as a discrete value for some specified range of LET, simply for convenience and ease of use in the calculation of dose equivalent.

The most successful method of deriving LET distributions in human phantoms under neutron irradiation has been through the use of computers. Snyder[46] has presented calculated LET distributions for fast neutrons in tissue equivalent cylinders sized to simulate a mouse and a rat. These calculations take a form similar to others reported by Snyder in that the calculations consider only neutrons in the range 0.1 to 10 MeV, no consideration is given to contributions to the LET distribution due to gamma rays. These calculations have recently been extended to energies up to 14 MeV for a man-equivalent cylinder,[47] and the results indicate, at 14 MeV, that the LET distribution as a function of depth in the phantom can be characterized by a single distribution. These authors report that, in general, the absorbed dose and dose equivalent as functions of depth in collimated beams are similar to those for broad beams, except that dose distributions due to collimated beams decrease more rapidly with increasing depth. The LET distributions are also similar, but the fraction of dose in the low LET range (< 5 keV/μ) is lower at the greater depths than for broad-beam cases.

Table 4. Quality Factor as a Function of LET[9]

LET (keV/μ)	QF
0 - 3.5	1.00
3.5 - 7.0	1.50
7.0 - 15.0	2.82
15.0 - 25.0	4.47
25.0 - 35.0	6.18
35.0 - 50.0	8.28
50.0 - 62.5	10.3
62.5 - 75.0	11.8
75.0 - 87.5	13.6
87.5 - 100	14.9
100 - 200	17.5
200 -1000	20.0

Proton recoil dose measurements in tissue equivalent phantoms have been used by Lawson and Watt[48,49] to calculate LET distributions. Results were presented as a function of depth for PuBe, (D,D), (D,T), and cyclotron-produced (15.6 MeV) neutrons. In general, excellent agreement was found with theoretical predictions for neutron beams, but some differences were apparent on the exit side of the phantoms. These authors concluded that the theoretical results are in error, since the calculations did not successfully account for the rapid decrease in the average energy of the neutron beam. Other experimental evidence cited in their paper support this view.

In 1958, Roesch[50] reported that there existed a fundamentally important quantity to dosimetry which had neither been defined nor given a name. This quantity gives the energy per unit mass transferred by gamma rays or neutrons into the form of kinetic energy of secondary charged particles at a point of interest in an irradiated medium. He called the quantity, KERM, which was an acronym for kinetic energy released per unit mass. The ICRU, in 1962, established the quantity called kerma, which was similar to Roesch's KERM. It was recommended that kerma be used in place of one of the common interpretations of "first collision dose". During the years since the adoption of this definition, there has been some controversy[51-53] over the use and applicability of this quantity.

In radiation dosimetry, one is still faced with the task of measuring total energy transfer from incident radiation to the medium of interest. A vast amount of research has gone into the more microscopic effects of radiation; for example, such topics as target theory,

oxygen enhancement, enzyme inactivation, etc. In the past several years, a new research area called "microdosimetry" has sprung from within the general field of radiation dosimetry. Microdosimetry has been the topic of two recent symposia.[54,55] In the research reported here, the term dose (or absorbed dose) will refer to the energy imparted to the medium of interest based on the interpretation of the ionization current produced in a small ionization chamber located in a suitable phantom. This macroscopic experimental method does not allow the measurement of LET distributions as part of the research. Although it is recognized that such information is important in radiation dosimetry, the prime concern in this work will be the measurement of energy deposition in the material of interest.

Fast Neutron Dosimetry

Neutron dosimetry or the measurement of neutron dose is important in many areas. The occupational exposure of persons actively engaged in research or isotope production near sources of neutrons (such as reactor) is always of concern to the health physicist. The exposure of patients and hospital personnel during neutron therapy is the responsibility of the medical physicist. With the increased interest in neutron radiography as a diagnostic tool, another need for neutron dosimetry has arisen. Only by neutron dosimetry can the exposure of human beings (either intentional or by accident) be controlled and evaluated.

In this survey of neutron dosimetry, the prime area of interest is the interface formed by bone and tissue in the human body. This interface area is important in all the areas mentioned above. The

heterogeneity of the human body is certain to cause distortions in the dose distributions in the body when exposed to external sources of neutrons. These distributions could prove important in the assessment of exposure of occupationally exposed persons as well as in treatment planning for neutron diagnosis and therapy.

The selection of a detector that will supply the necessary information outlined above must be governed by a set of specific criteria. Such a detector must satisfy as closely as possible the following requirements:

1. The detector must not disturb the radiation field within the medium; therefore, it must be constructed of material equivalent to tissue or bone as required by the experiment. Other material must be kept to a minimum.
2. The detector must be sensitive to fast neutrons. Sensitivity to gamma-rays will not cause rejection of the technique.
3. The detector must be as small as possible and allow the placement of the detector in a suitable phantom.
4. The techniques for use of this detector system should be well established.

In other words, the experiment requires a detector system which, due to the size and materials of construction, will not significantly perturb the radiation field. In addition, the detector must allow the measurement of dose-distributions quite close to the interface. This latter requirement will be found to be the most stringent requirement.

This section is intended to review the methods of fast neutron dosimetry that have been employed in the measurement of neutron depth-dose. Particular mention will be made of those methods that may be applicable to this research. A review of relatively new methods, some as yet unproven, will also be included. Since this research is concerned with fast neutron dosimetry, no consideration will be given to the measurement of incident thermal neutrons.

Neutron dosimetry techniques can be divided into several quite arbitrary categories. For purposes of discussion, the following general classifications will be used:

1. Ionization Techniques.
2. Pulse Techniques.
3. Other Methods.

Although in principle calorimetry techniques should work equally well for neutrons and gamma radiation, these techniques have not been applied to the measurement of absorbed dose from neutrons. The high dose rates required cause this technique to be impractical in most research applications.

Chemical systems include photographic emulsions and aqueous solutions whose radiation chemical response is known. However, chemical systems were eliminated from consideration for use in this research, because, in general, photographic film is much more sensitive to gamma radiation than to neutrons on the basis of absorbed dose in tissue. Thus, methods of fast neutron dosimetry based on film blackening are seldom used. The use of nuclear emulsions for track measurements

presents a tedious, and often complex, technique whereby one can determine the neutron spectrum;[14] the dose can be calculated.

In aqueous systems, the observed chemical yields are usually dependent upon the nature of the radiation. Any possible use of these systems in the dosimetry of mixed radiations requires a broad knowledge of the radiation chemical yields as a function of linear energy transfer (LET) together with detailed information on the energy spectrum of the radiations actually present in the dosimeter. In general, the use of chemical dosimetry in mixed radiation fields must be done by difference techniques, and, in many cases, large errors are inevitable.

Although activation detectors offer the advantage of considerable simplicity, the use of such a method means the introduction of a nontissue-equivalent material into the phantom. The results of such a measurement yield only neutron flux or fluence values with the requirement of a calculation to determine the absorbed dose distribution.

The various techniques used in the dosimetry of mixed fields of neutron and gamma radiation are shown in Table 5. This table summarizes the common techniques of neutron dosimetry, the energy range of the systems, and the applicability of the particular systems to the research problem. The more common techniques employed in depth dose determinations will be discussed in greater detail in the following section.

Of the various detectors listed, ionization chambers have particular advantages in the present context. The use of ionization chambers is based upon the measurement of the ionization produced in a gas-filled cavity by charged particles traversing the cavity. If the value of W, the energy required to produce an ion pair in the gas, is

Table 5. Summary of Neutron Dosimetry Techniques[14]

Detector Type	Radiation Type	Energy Range	Dose or Flux Density Range*	Applicable to Present Problem
Tissue equivalent ionization chamber	n	all neutrons	10^{-7} to 10^{3} sec^{-1}	yes, extensive
Absolute counter dosimeter	n	fast	up to 10^{-2} sec^{-1}	no, too large
Secondary ethylene dosimeter	n	fast	up to 1 sec^{-1}	yes, extensive
LET spectrometer	n	up to 100 MeV		promising, but large
Count rate dosimeter	n	fast	biological tolerance range	doubtful
$BF_3 + CH_2$ moderator	n	fast	up to 2×10^{3} $n/cm^2/sec$	no, too large
CH_2-lined proportional counter	n	fast	up to 3×10^{5} $n/cm^2/sec$	no, too large
Spherical radiator with ZnS screen	n	fast	up to 10^{-4} sec^{-1}	doubtful
Hornyak button	n	fast	10^{-6} to 10^{-2} sec^{-1}	doubtful
Hurst Threshold unit	n	fast	1	no
$^{12}C(n,2n)^{11}C$	n	20 MeV	up to 10^{4} $n/cm^2/sec$	no
$^{209}Bi(n,f)$	n	50 MeV	up to 10^{6} $n/cm^2/sec$	no
$^{197}Au(n,\gamma)^{198}Au$	n	thermal		no

*Refers to total dose in rads unless followed with sec^{-1} which means rads per second. In the case of pulse counting techniques the upper limit for the dose rate or flux density is such that the counting rate is 10^{4} counts/sec.

known, then a measurement of the total amount of ionization produced in the cavity, i.e., the total charge, should indicate the energy imparted to the gas. Of course, the cavity must conform to the requirements of the well-known Bragg-Gray relation.[20] Neutrons do not produce ionization directly; thus, if an ionization chamber is to be used, some means must be found to cause the production of secondary charged particles. Since the interaction of radiation with tissue is the primary interest in dosimetry, a common technique is to construct the walls of the cavity with a material which simulates tissue. The design and construction of several tissue equivalent ionization chambers was reported by Rossi and Failla in 1956.[21] Since that publication, the use of such chambers has spread throughout the world, and chambers of this general type have been constructed in a wide range of sizes and shapes. Many of the chambers are suitable for depth-dose measurements.

In 1937, Failla[22] devised an ionization chamber with movable electrodes for the purpose of measuring the superficial dose in an irradiated material. Measurement of the ionization per unit volume as a function of electrode spacing and extrapolation of the resulting curve to zero volume provide a good estimate of the superficial dose; this type of chamber is called an "extrapolation chamber". Failla pointed out that it is imperative that the extrapolation chamber be constructed of tissue-equivalent material in order that ionization produced by neutron interactions may be measured. However, tissue equivalence is a much more rigorous requirement in the case of fast neutrons than that governing detectors designed for the measurement of electromagnetic

radiations. With appropriate modifications, this type of chamber has found application in several difficult dosimetric problems; for example, the measurement of dose due to a radioactive isotope uniformly distributed in tissue, the dosimetry of beta-ray sources, and the measurement of dose rate in electron beams.[23] Wingate et al.[24] have recently reported the use of an extrapolation chamber for the measurement of the absorbed dose from x rays near the bone-tissue interfaces. It appears that the use of a small extrapolation chamber of special design affords the only possibility for the measurement of dose distributions at and near interfaces. Although chambers of this general type have been employed for similar measurements in the laboratory, the extrapolation chamber technique has never been applied to the measurement of dose distributions at interfaces at depth in a phantom.

Another possibility for the measurement of neutron depth-dose distributions are condenser ionization chambers similar to those of Sievert.[23] These chambers may be constructed of tissue-equivalent materials and may be sized to occupy a very small volume in the phantom. Construction of such chambers employing bone-equivalent material, as well as tissue-equivalent material, shows interesting possibilities. The use of these chambers for the measurement of depth-dose distributions is still a common practice.[25,26] However, measurements with even the smallest chambers available will yield only a very gross dose distribution when applied to interface dosimetry.

Few pulse counting devices are available which are truly suitable for the measurement of neutron depth-dose distributions at interfaces.

Proportional counters designed by Hurst et al.[27,28] have been used extensively in depth-dose measurements. Although the sensitive volume is small, about 1 cm^3, the chamber itself is rather large, 2 cm diameter by 12 cm long, and thus does not satisfy the general requirement of not perturbing the radiation field.

The LET chamber designed by Rossi and Rosenzweig[29,30] has interesting applications, but due to the size of the chamber (about 10 cm diameter) application to depth-dose measurements is not immediately obvious. The design, construction, and testing of a similar chamber with greatly reduced dimensions is under way.[31] A method of generating LET spectra from proton recoil spectra measured in a cylindrical proportional counter has recently been reported.[32]

The use of a detector constructed of a thin layer of plastic scintillator arranged to conform with the Bragg-Gray principle was reported by Watt et al.[33] The authors report that this detector has been used to determine accurate values of absorbed dose, quality factors, and LET distributions for proton recoils at depth in tissue. The detector consisted of a tiny piece of NE 102 plastic scintillator sandwiched between two polyvinyl toluene disks. These disks, which are non-scintillating, had thicknesses greater than the range of the recoil protons generated by elastic collisions in the detector. The scintillator sandwich was coupled through a light pipe to a photomultiplier tube. The authors outlined the several advantages of this system when compared to other methods. Primary disadvantages include a low energy response cutoff at about 400 keV and the requirement for a further correction at neutron energies greater than 10 MeV.

Other methods used for neutron depth dose measurements include solid state detectors and various methods of luminescence dosimetry. Thurston et al.[34] have reported the use of a silicon diode as a fast neutron dosimeter with a wide range of application. Neutron dose is correlated to the reduction in minority carrier lifetime in silicon. This dosimeter has been shown to give agreement when compared to other neutron dosimeters in a "free field" exposure. However, results from tests with a moderated neutron spectrum or an unknown spectrum that was different from the fission spectrum have required large, purely empirical corrections to obtain agreement with other systems.[35] The size of the detector is quite small, and, if the difficulties with moderated systems can be overcome, such a dosimeter should prove to be quite useful in neutron depth dosimetry. However, the requirement of using tissue-equivalent material, negates the application to interface dosimetry.

Other solid state dosimetry devices, such as thermoluminescence dosimetry systems, offer high sensitivity and small size. Major advances in this area have been the subject of two recent conferences.[36,37] The most recent advance in this area has been the introduction of dosimetry by thermally stimulated exoelectron emission (TSEE).[38,39] This technique involves measurement of thermally stimulated emission of low energy electrons from the surface of an irradiated ionic crystal. The number of released (exo) electrons has been shown to be a linear function of dose. The principles and potentials of this method are similar to those of thermoluminescence dosimetry. The substances which have been studied include LiF, BeO, $CaSO_4$, $SrSO_4$, and $BaSO_4$. The use of TSEE

material, coupled with hydrogenous radiators, offers the potential of measuring fast neutron dose with a detector whose response is essentially due to a surface effect.

In summary, it appears that the use of small, specially designed extrapolation chambers should be the most logical approach to the research problem. Further, in order to be more applicable to the problem, these detectors should be constructed of tissue- or bone-equivalent materials. The gas used in the detecting volume should also be equivalent to tissue or bone. The well-known techniques involved in measuring the ionization current in the chamber volume should provide an adequate method for measuring dose distributions in a phantom.

Tissue and Bone

In the literature of radiation dosimetry, the reader often encounters the results of a study to determine the absorbed dose in tissue. Generally, very little additional information is reported. However, when one ventures into the field of histology, it immediately becomes obvious that there are many types of "tissue", and further, that there are many subdivisions under these types of tissue. Four primary tissues are generated from three primitive germ layers in the early development of organisms. These are the epithelium, connective tissue, muscle tissue, and nerve tissue. These tissues are combined and integrated to form functional structures, the organs of the body. However, in an effort to simplify the human body for dosimetry purposes, the elemental constituents of the body are of prime interest.

In surveying the literature, a number of slightly different elemental compositions are given for human tissue. However, those compositions usually referenced are from a few specific sources. Table 6 presents a comparison of the most commonly used tissue compositions. The first four compositions (I - IV) shown in this table correspond to what is called the "standard man" composition. The "standard man" composition results from a homogenation of the entire human body. The effects of including bone, etc., in the homogeneous tissue are easily observed by noting the change in the percent of calcium and phosphorus present in the tissue. The remaining compositions represent what is commonly called "standard wet tissue", adipose tissue, and the tissue approximation of Rossi and Failla.[21] Table 7 compares the three most recent compilations of the chemical composition of muscle. Compositions I and III are thought to be simply revisions of the work of Tipton.[59] Table 8 lists the chemical compositions of several tissue-equivalent materials and gases employed in radiation dosimetry. One readily observes that, in general, the chemical compositions are quite similar. However, variations in the oxygen content could cause difficulties for 14 MeV neutrons due to the $^{16}O(n,\alpha)$ reaction. The main deviation from true tissue equivalence is in the plastic material (TE-I) where carbon is substituted for oxygen in order to make the plastic an electrical conductor.

The degree to which the atomic composition of tissue needs to be duplicated is dependent on the desired accuracy of the measurement as well as the type of radiation to be measured.[14] For most of the spectrum of electromagnetic radiation, plastics represent a reasonably good

Table 6. Comparison of Elemental Tissue

Element	I[56]* 1960 (%)	II[57]* 1957 (%)	III[58]* 1968 (%)	IV[59]* 1969 (%)	V[14]* 1961 (%)	VI[59]* 1969 (%)	VII[21]* 1957 (%)
Oxygen	65.0	65.0	60.0	61.0	73.0	23.0	71.6
Carbon	18.0	18.0	24.0	23.0	12.0	64.0	14.9
Hydrogen	10.0	10.0	10.0	10.0	10.0	12.0	10.0
Nitrogen	3.0	3.0	2.9	2.6	4.0	0.80	3.5
Calcium	1.5	1.5	1.2	1.4	0.01	0.0022	-
Phosphorus	1.0	1.0	1.1	1.0	0.2	0.016	-
Potassium	0.2	0.20	0.20	1.0	-	0.032	-
Sulfur	0.25	0.25	0.24	0.2	0.2	0.073	-
Sodium	0.15	0.15	0.20	0.14	-	0.050	-
Chlorine	0.15	0.15	0.20	0.12	-	0.12	-
Magnesium	0.05	0.050	0.03	0.027	-	0.002	-
Iron	0.006	0.0057	-	-	-	-	-
Manganese	0.00003	0.000029	-	-	-	-	-
Copper	0.0002	0.00014	-	-	-	-	-
Iodine	0.00004	0.000043	-	-	-	-	-

*Reference source.

Table 7. Comparison of Elemental Composition of Muscle

Element	I[58]* 1968 (%)	II[18]* 1964 (%)	III[59]* 1969 (%)
Oxygen	75.0	72.9	75.0
Carbon	11.0	12.3	11.0
Hydrogen	10.0	10.2	10.0
Nitrogen	2.6	3.5	2.6
Calcium	0.0031	0.007	0.0031
Phosphorus	0.18	0.2	0.18
Potassium	0.30	0.3	0.30
Sulfur	0.24	0.5	0.23
Sodium	0.16	0.08	0.075
Chlorine	0.18	-	0.078
Magnesium	0.019	0.02	0.019
Iron	-	-	-
Manganese	-	-	-
Copper	-	-	-
Iodine	-	-	-

* Reference Source

Table 8. Comparison of Tissue-Equivalent Materials and Gases Employed in Dosimetry

Element	TE[21]* I (%)	TE[21]* II (%)	TE[60]* III (%)	Nylon[63]* (%)	Lucite[63]* (%)	TEG[21]* I (%)	TEG[21]* II (%)	ME[24]* I (%)	MEG[24]* I (%)
Hydrogen	10.1	9.8	10.2	68.3	63.4	10.16	9.8	10.25	10.22
Oxygen	-	71.0	74.2	4.7	12.2	40.78	70.99	5.19	73.04
Carbon	86.4	15.6	12.0	22.8	24.4	45.57	15.73	76.05	12.33
Nitrogen	3.5	3.6	3.6	4.3	-	3.5	3.5	3.49	3.51
Calcium	-	-	-	-	-	-	-	2.044	-
Phosphorus	-	-	-	-	-	-	-	-	-
Sulfur	-	-	-	-	-	-	-	-	-
Potassium	-	-	-	-	-	-	-	-	-
Sodium	-	-	-	-	-	-	-	-	-
Chlorine	-	-	-	-	-	-	-	-	-
Magnesium	-	-	-	-	-	-	-	-	-
Fluorine	-	-	-	-	-	-	-	1.933	-
Silicon	-	-	-	-	-	-	-	1.045	-
Argon	-	-	-	-	-	-	-	-	0.90

* - Reference Source
TE - Tissue Equivalent Material
TEG - Tissue Equivalent Gas
ME - Muscle Equivalent Material
MEG - Muscle Equivalent Gas

substitute, but in the case of neutrons, the hydrogen content of the plastic employed is very critical.[61] Experiments with composition TE-I (Table 8) have indicated that, for fast neutrons in the range from 0.5 to 14 MeV, the replacement of oxygen by an equal weight of carbon results in an error of no more than six percent.[21] If exact tissue equivalence is required, it is possible to construct chambers lined with tissue-equivalent gels (TE-II) which match a tissue composition $(C_5H_{40}O_{18}N)_n$ exactly. However, due to evaporation and gas permeability of the gel, the use of such a material presents several difficulties not encountered in the use of rigid plastic materials.

Calculations of kerma due to fast neutrons in tissue-like materials have been reported by Williamson and Mitacek.[62] Curves of kerma versus neutron energy (up to 10 MeV) were given for a number of materials commonly encountered in dosimetry. In addition, data are presented in this paper which give the ratios of these values of kerma to those in standard man. This ratio, for the tissue-equivalent gas used in this study (TEG-I), varies from about 1.01 to 1.02. The substitution of carbon for oxygen in tissue equivalent plastic (TE-I) causes the ratio to vary between 1.00 and 1.08. This result is in fair agreement with the experimental results of Rossi and Failla[21] quoted above.

Calculations by Randolph[63] lead to the conclusion that, for 14-MeV neutrons, the Rossi-Failla[21] tissue formulation was equivalent to both wet tissue and the standard man. Of the materials considered in his calculation, the results indicated that nylon and lucite are suitable materials for tissue approximation.

Neutron fluence-to-kerma conversion factors for the human body were calculated by Ritts et al.[58] in 1968. In addition to tissue, results were reported for muscle, bone, lung, brain, red marrow, and the "standard man" composition. The calculations incorporated the latest cross-sections for the eleven most common elements in man. Neutrons were considered in the range between 0.045 eV and 15 MeV. Several reactions were included which had not previously been considered. Among these were an anisotropic elastic scattering correction, inelastic scattering, (n,2n) reactions, (n, charged particle) reactions, and beta or positron emissions from these reactions. These authors essentially duplicated the calculations of Auxier and Snyder,[64] and the results agreed quite well below 10 MeV. The results in the upper MeV energy range showed marked differences due to cross-section fluctuations. However, the major area of discrepancy was in the energy interval 2 to 100 eV when considering all eleven elements. The calculated results were appreciably higher than those of Auxier and Snyder, primarily due to the 1.71 MeV beta particle released by the (n,p) reaction in phosphorus which dominates in this energy region. At higher energies, the nitrogen capture cross section increases to a point where the contribution to the kerma from this reaction dominates.

The conclusion one draws from this discussion of experimental and theoretical investigations of tissue equivalence is that tissue-equivalent plastics and gases can serve as a reasonable approximation to tissue over the range of neutron energies encountered in this research.

Bone is a hard, specialized connective tissue, with a calcified collagenous intercellular substance. It performs a mechanical function

in forming the skeletal support of the body; it protects the vital organs of the cranial and thoracic cavities and lodges the bone marrow. Bone serves as a store for calcium and thus plays an important part in meeting the immediate needs of the body for this element.[65]

Mammalian bone is either spongy (cancellous) or compact in structure. Spongy bone consists of intercrossing connecting osseous bars of varying thickness and shapes. These branch, unite with one another, and partially surround intercommunicating spaces filled with bone marrow. Compact bone, in contrast, appears as a continuous hard mass in which spaces can be observed only with the aid of a microscope. No sharp boundary can be drawn between the two types of bone tissue. These tissues merely represent two different arrangements of the same histological elements. In fact, essentially every bone contains both types of osseous tissue.

The greatest part of the mass of the bone is made up of layers (called lamellae) of calcified bone matrix. The lamellae have been found to be fibrillar in structure. Embedded within the interstitial substance are cavities (lacunae) which are completely filled with bone cells (called osteocytes). On the surface of the bone are osteoblasts and osteoclasts which are associated with the apposition and the reconstruction of the bone, respectively. These cells are much more numerous during the active development and growth of the skeleton.

Spiers[5] has characterized the two component materials to be considered in bone dosimetry as (1) soft tissue and (2) a mineralized matrix or mineral bone. For absorbed dose calculations, the make-up of bone must be somewhat idealized. In one idealized model, the osteocytes

are found in small (5 micron) cavities throughout the bone. Where the layers of bone are relatively thick, the osteocytes surround a Haversian canal (50 to 100 microns in diameter). The marrow spaces in trabecular bone, which contain the red marrow, are larger than the spaces of the Haversian canals (on the average about 400 microns in diameter). In the Haversian canals, osteogenic cells form a lining on the bone approximately ten microns thick. Thus, the tissues of interest in the dosimetry of bone are (a) tissue within small cavities of the bone; (b) tissue within larger bone cavities; and (c) tissue shielded by bone.[2]

The exact elemental composition of bone is probably unknown. However, as in the case of tissue, several compilations are available for radiation dosimetry purposes. Several of these are listed in Table 9 along with chemical compositions of a bone-equivalent plastic and a bone-equivalent counting gas. Again, the variation in elemental composition is evident. In this case, these variations are probably due to the method of preparation of the samples as well as statistical fluctuations between human beings due to variations in diet, age, etc. To further complicate matters, at least two compilations of the distribution of bone marrow in the human body are available.[67,68] Variations greater than a factor of two are apparent between these summaries. In both cases, however, the data were accumulated for a very limited number (about 20-30) of patients, over a wide range of age, weight, and physical well-being. Of these compositions, the most up-to-date is composition V due to Tipton.[59] In compiling this composition, the results of four separate investigations were used.

Table 9. Comparison of Bone Composition and Equivalent Materials and Gases

Element	B-I[58]* (%)	B-II[18]* (%)	B-III[14]* (%)	B-IV[66]* (%)	B-V[59]* (%)	B-VI[16]* (%)	BE-I[24]* (%)	BEG-I[24]* (%)
Hydrogen	7.1	6.4	4.0	3.39	4.1	7.6	6.39	4.69
Oxygen	39.5	41.0	48.0	44.1	43.0	52.2	3.06	40.25
Carbon	22.4	27.8	17.0	15.5	16.0	16.7	53.41	53.41
Nitrogen	4.7	2.7	5.0	3.97	4.3	3.7	2.67	2.67
Calcium	12.37	14.7	20.0	22.2	21.0	14.8	17.69	-
Phosphorus	13.16	7.0	5.0	10.2	10.0	6.8	-	-
Sulfur	0.41	0.2	0.2	0.31	0.31	-	-	-
Potassium	-	-	-	-	-	-	-	-
Sodium	0.08	-	-	0.06	0.62	-	-	-
Chlorine	-	-	-	-	-	-	-	-
Magnesium	0.28	0.2	-	0.21	0.22	-	-	-
Fluorine	-	-	-	-	-	-	16.77	-
Argon	-	-	-	-	-	-	-	25.73

* - Reference Source
B - Bone
BE - Bone Equivalent Material
BEG - Bone Equivalent Gas

In the bone-equivalent plastic, the carbon content has been increased to produce a conducting plastic. In addition, fluorine has been introduced into the mix in place of phosphorus. In the bone-equivalent gas mixture, argon is substituted for calcium and phosphorus. These equivalent compositions are based on matching the x-ray absorption coefficients of the substitute materials and the actual materials. In addition, the relative electron stopping power of the substitute materials compared to the real materials must be energy independent. As previously stated, similar substitutions in tissue-equivalent plastics and gases have been shown to cause a small error in the measurement of neutron dose. No data for these bone-equivalent materials is available which predicts the significance of using these bone-equivalent materials for the measurement of neutron dose.

CHAPTER III

NEUTRON DOSE DISTRIBUTIONS WITH DEPTH

Dose Distributions at the Bone-Tissue Interface

The renewed interest in neutron radiotherapy coupled with the rising interest in neutron radiography as a diagnostic tool have indicated the extension of fast neutron depth dose measurements to the heterogeneous case. Further it appears that, as in x-ray and gamma-ray diagnosis and therapy, the region of primary concern may be the bone-tissue interface region. To date, only a few calculations and no experimental results have been published.

Lawson[10] has reported calculations of the recoil proton dose at a bone-tissue interface irradiated by fast neutrons. The calculation, performed for 14-MeV neutrons, was essentially a modification of the calculation of Charlton and Cormack[69] on the dissipation of energy by electrons in finite cavities. The only conclusion drawn by the author is that the upper limit of the dose given to tissues in and around the bone is simply the dose which would be delivered to soft tissue if the bone were replaced with soft tissue.

Calculations of the radiation dose from high energy nucleons in targets containing soft tissue and bone are reported by Turner et al.[11] However, only neutrons and protons with energies of 100, 250, and 400 MeV, and two simple geometries were considered in this study. The first phantom was a cylinder 8.0 cm in length and 2.5 cm in diameter consisting of a

soft-tissue center enclosed in concentric bone and soft-tissue rings. This phantom was designed to simulate the arm or leg of a small primate. The second phantom was a large parallelepiped with outside dimensions 20 x 31 x 60 cm. The large slab was assumed to be constructed of soft tissue and surrounded a smaller slab 10 x 15 x 30 cm assumed to have the composition of bone. It was assumed that this simulated the human torso.

In a discussion of the concept of kerma, the ICRU has presented absorbed dose and kerma distributions in and near bone irradiated by 2 MeV neutrons.[70] The kerma in bone is less than that in tissue. This is principally due to the lower concentration of hydrogen in the bone. At the bone tissue interface, the ratio of the dose in tissue to that in bone is given as 1.8 times the ratio of the mass stopping powers. The report concludes that the important tissue doses in bone inclusions are not as much different from those in the tissue away from the bone as in the case of x rays.

A recent neutron radiographic study has been reported by Budinger et al.[12] These authors describe a Monte Carlo calculation of the dose distribution through a simulated human arm. Fission-spectrum neutrons, as well as monoenergetic neutrons of 0.001, 0.120, and 14 MeV, were considered. The authors concluded that the limited resolution possible through tissues thicker than 3 cm make neutron radiography essentially impractical. The dose calculations reveal as much as a twofold increase in dose deposited in the bone cortex, compared to surrounding contiguous tissues. However, it appears obvious that this is a highly inaccurate estimate of the dose, since the calculations require that all photons be absorbed locally. The authors attempt to escape this trap by pointing

out that this is the upper limit of the energy absorbed, and thus, "is a more desirable value considering the conservative approach which should be adopted toward irradiating living human tissue with neutrons."[12]

Neutron isodose distributions through the chest region of a heterogeneous phantom have been reported by Wilkie.[16] A Monte Carlo technique was employed in calculating dose distribtions in a phantom from ^{252}Cf fission neutrons and from a 14-MeV neutron source. These data, although not directly relevant to this research problem, clearly show the distortion of such dose distributions due to changes in the chemical compositions of the organs and bones present in the phantom as well as the air voids due to the introduction of lungs into the phantom. The immediate and most obvious conclusion drawn from these data is that dose distributions based upon a homogeneous approximation can be in serious error.

Theoretical Depth Dose

Most early work in neutron depth dose was directed toward calculation of the maximum permissible exposure to neutrons. Capron et al.,[71] Mitchell,[72] and Snyder[73] presented data for thermal neutrons while Mitchell[74] and Tait[75] reported calculations of energy deposition in tissue by fast neutrons.

Probably the most significant early work in this area was that of Snyder and Neufeld[76] in 1955. These calculations employed Monte Carlo techniques to determine the depth dose in tissue from a broad beam of fast neutrons. This work was incorporated (in a revised form) in NBS Handbook 63[57] in 1957, and has formed the base for much of the

subsequent work, both theoretical and experimental, in the field of neutron depth dose.

Kogan et al.[77] have published the results of calculated depth distributions of neutron dose for energies ranging from thermal to 1 MeV. The calculation considered neutrons impinging normal to the face of a paraffin block. Results of this author's calculations were compared to experimental results[90] as well as the theoretical results of Snyder and Neufeld. Similar depth dose measurements in a paraffin block have been described by Stipcic.[78]

To assess the hazard to astronauts in outer space, Kinney and Zerby[79] reported a calculation of the dose in tissue due to nucleons in the range 100 to 400 MeV. These calculations were extended by Irving et al.[80] for neutrons with energies from 0.5 to 60 MeV. It is interesting and worthwhile to point out that calculations at 1.0 and 10.0 MeV were performed to compare with the results of Snyder and Neufeld in Handbook 63. Duplication of these early calculations yielded identical results. In fact, the replacement of the Snyder-Neufeld approximations in a systematic fashion by more exact treatments showed no noticeable change in depth dose profiles in the improved calculations.

In 1966, Snyder et al.[81] presented modifications to their early work. A Monte Carlo program was written which provided an estimate of dose in a tissue phantom from neutrons in the energy range from thermal to 14 MeV. In this calculation, the 30 cm semi-infinte slab was replaced by a right cylinder 60 cm high and 30 cm in diameter. In the energy range up to 10 MeV, the maximum doses calculated did not differ greatly from the results in NBS Handbook 63. A greater difference was

found, however, when results for cylinders and slabs were compared at depths well below the irradiated surface.

The evolution of neutron dose calculations can be seen by referring to a number of reports by Auxier et al.[9,82-84] In 1965, dose distributions in a 30-cm diameter by 60-cm high cylindrical phantom were reported for fission spectrum neutrons.[82] In 1966, geometrical symmetry was invoked to increase the statistical reliability of calculations for ten monoenergetic neutron energies.[83] The effect of slant incidence on the dose distribution was reported in 1967.[84] A rather extensive group of calculations was published in 1968.[9] These calculations considered thirty-three possible interactions of fast neutrons with the four major elements of tissue.

Experimental Depth Dose Measurements

The measurement of neutron dose as a function of depth in homogeneous phantoms has been reported for nearly twenty years. Experiments have been performed employing a wide variety of substances approximating tissue as well as a wide range of neutron energies. In a recent survey, Hubbell and Auxier[85] have pointed out the many parameters which influence the absorbed dose from neutrons as a function of depth.

The purpose of some of the early publications of neutron depth dose measurements was twofold. The primary intent was to check the calculations of Snyder and Neufeld.[86] A secondary purpose was simply to relate the dose measured by a neutron dosimeter to the dose received by a human in the same radiation field. The calculation of the dose distribution in a slab of tissue irradiated by a broad beam of neutrons

was experimentally verified for a neutron energy of 2.5 MeV by Barr and Hurst[87] in 1954. A related study using a small phantom and neutron energies of 2.5 and 4.6 MeV was reported by Mills and Hurst.[88] In both studies, isotopic neutron sources were employed. Neutron dose was measured with a tiny Hurst proportional counter (commonly called a "phantom counter").

Kogan et al. reported the results of experiments to measure the reflection of neutrons from paraffin and water[89] as well as neutron density as a function of depth in a paraffin slab.[90] Depth dose measurements in a small phantom were presented by Frigerio[91] during a study of neutron penetration directed toward neutron capture therapy.

The first practical application of depth dose measurements was described in 1961 by Hurst et al.[92] Measurements of the dose in man phantoms positioned around the natural uranium heavy water reactor at the Boris Kidric Institute, Vincâ, Yugoslavia were performed in order to assess the dose received by workers exposed during a criticality accident.

Smith and Boot[93] presented the results of an extensive study directed towards the experimental verification of the early calculations of Snyder and Neufeld[86] and Kogan et al.[77] An experimental investigation of the flux density distribution of thermal neutrons in and around a phantom irradiated by a broad beam of thermal neutrons was reported by Boot and Dennis.[94]

A number of depth dose studies have been performed with accelerator-produced monoenergetic neutrons. Blosser and Freestone[95]

have measured dose distributions of 14.1-MeV neutrons in a 42-cm diameter, spherical, water-filled, Lucite phantom. Smith and Boot[93] included 2.5- and 14.1-MeV neutrons in their comprehensive study. Tiny semiconductor detectors were employed by Stone and Thorngate[96] to measure the energy spectrum of recoil particles in a tissue-equivalent liquid from incident 3- and 15-MeV neutrons. Depth dose distributions for components of dose due to $^{1}H(n,\gamma)^{2}D$, $^{14}N(n,p)^{14}C$, and proton recoils for 3-MeV and 14-MeV incident neutrons have been reported by Lawson et al.[97] Design considerations for a 14-MeV neutron radiotherapy unit were described by Greene and Thomas.[98] Recently, Clifford[99] measured little effect on fast neutron depth distributions by phantoms of different geometries irradiated with a broad beam of 2.95-MeV neutrons.

Several other investigations of neutron dose distributions have been reported. In 1964, Watt et al.[100] presented data giving the energy deposited at depth in tissue by neutrons from a PuBe source. Neutron and gamma-ray dose distributions in several phantoms irradiated by the leakage spectrum of a fast reactor were described by Johnson and Poston[101] and Jones et al.[102]

A somewhat novel technique of neutron depth dose determination was introduced by Hightower and Swartz.[103] In this study, cadavers were frozen to liquid nitrogen temperatures, exposed to a beam of neutrons, sectioned, and the ^{24}Na activity induced in the sections counted using standard techniques. After radioactive decay, the sections were reactivated together with suitable sodium standards to correct for variations in sodium content within the sections.

Some important conclusions from this survey of theoretical and experimental depth dose investigations should be enumerated. First, the early calculations of Snyder and Neufeld and their extension by Snyder, Auxier, and others rather accurately predict the distribution of neutron and gamma-ray dose in human phantoms. Many variations of geometry, tissue-equivalent material, and neutron source have been considered. One can easily conclude that the neutron dose distribtuion in a homogeneous phantom simulating the human body is well known. However, it is extremely important to emphasize that all these investigations have been performed in homogeneous phantoms. When bone is introduced into the phantom, one author[10] has concluded that the upper limit to the dose in bone is simply the dose in tissue with the bone removed. Although this may be quite satisfactory for radiation protection purposes, a knowledge of these distributions is required for treatment planning in neutron therapy. The need for measurements in a heterogeneous phantom is evident and, furthermore, appears to be a quite logical step in terms of the further development of neutron depth-dose dosimetry.

Purpose of Research

The purpose of this research is as follows:

1. The design and construction of a detector suitable for the measurement of fast neutron dose distributions in a heterogeneous phantom.
2. The measurement of dose distributions near bone-tissue interfaces, resulting from a broad-beam irradiation of neutrons, in a suitable phantom.

3. Comparison of the results of such measurements with theoretically predicted distributions and recommendations for the improvement in the models.

CHAPTER IV

EQUIPMENT AND INSTRUMENTATION

Description of Detector System

The detectors chosen for this study were extrapolation ionization chambers. The wide applicability of the extrapolation technique to similar problems involving surface and interface dosimetry indicated the extension of this technique to neutron dose measurements at the bone-tissue interface.[22,24,104,105] An extrapolation chamber affords the investigator a detector which has an adjustable sensitive volume. The significance of this technique lies in the fact that the ionization per unit volume in the detector has a definite value even when the volume is vanishingly small. Thus, by measuring the ionization per unit volume as the detector volume is decreased, one can plot a relation between ionization per unit volume and electrode gap-spacing. Extrapolation of this plot to zero gap-spacing yields the ionization per unit volume in the material of interest (assuming the material of interest and the detector material are equivalent) in the absence of any detecting cavity. Failla[22] has suggested that such chambers constructed of tissue-equivalent materials would be suitable for measurements of neutron dose in tissue. However, in order to be suitable for use in a homogeneous phantom, such a chamber must be of a special design. During the design and construction of these chambers, every effort was made to restrict the amount of nontissue- (or bone-)

equivalent material. A schematic diagram is shown in Figure 1. Basically, the chamber is a right circular cylinder 4.92 cm O.D., the height of the cylinder is adjustable from 6.35 cm to 11.43 cm. The sensitive volume is defined by two circular parallel plates with gap spacing adjustable from 0.05 to 2.54 cm. The outer ring and the body of the chamber are joined through precision threads (15.75 threads per cm) and allow the accurate adjustment of the gap spacing. Measurements of electrode separation with a depth-micrometer showed a reproducibility in gap spacing of ± 1% over the full range gap spacings. These results were confirmed by comparison of the chamber capacitance with a set of standard capacitors.

The detector also features a guard ring around the collecting electrode. The collecting electrode and the guard ring are an integral part of the body of the detector. However, the collecting electrode is insulated from the guard ring and the body of the detector by 0.0178 cm of Teflon. Electrical and gas-flow connections to the collecting electrode are made through a conducting glue to the underside of the electrode. A cross-sectional view of the sensitive volume of the chamber is shown in Figure 2.

The high voltage electrode is attached to, but insulated from, the movable ring. The electrical connection to the top of the thin electrode is also made with a conducting glue. Figure 3 shows a photograph of a fully assembled detector.

Six of these chambers were constructed during the course of this study. Of these, three were fabricated from A-150* tissue-equivalent

*Dr. F. R. Shonka, St. Procopius College, Lisle, Illinois.

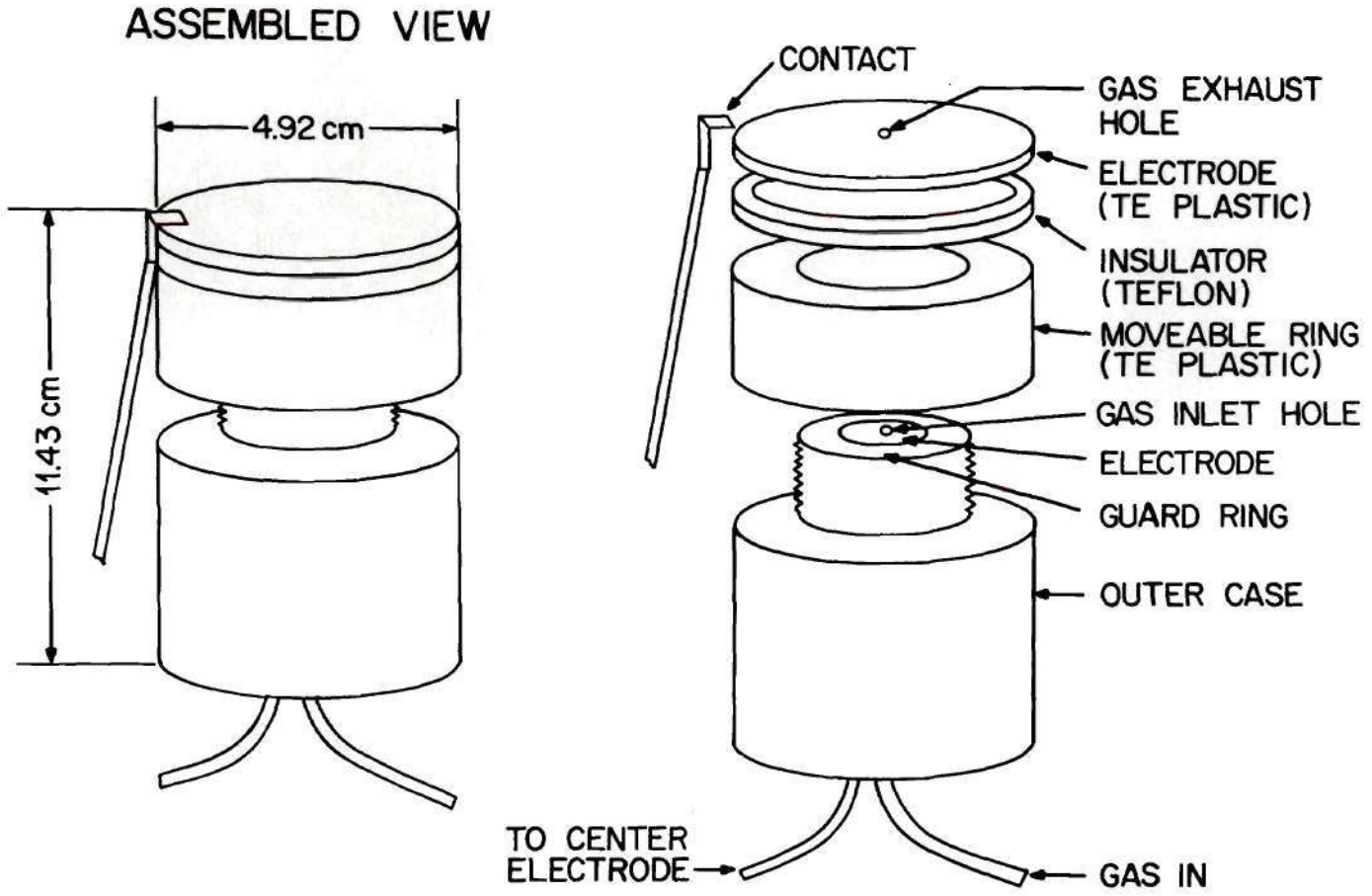

Figure 1. Sketch of Extrapolation Ionization Chamber.

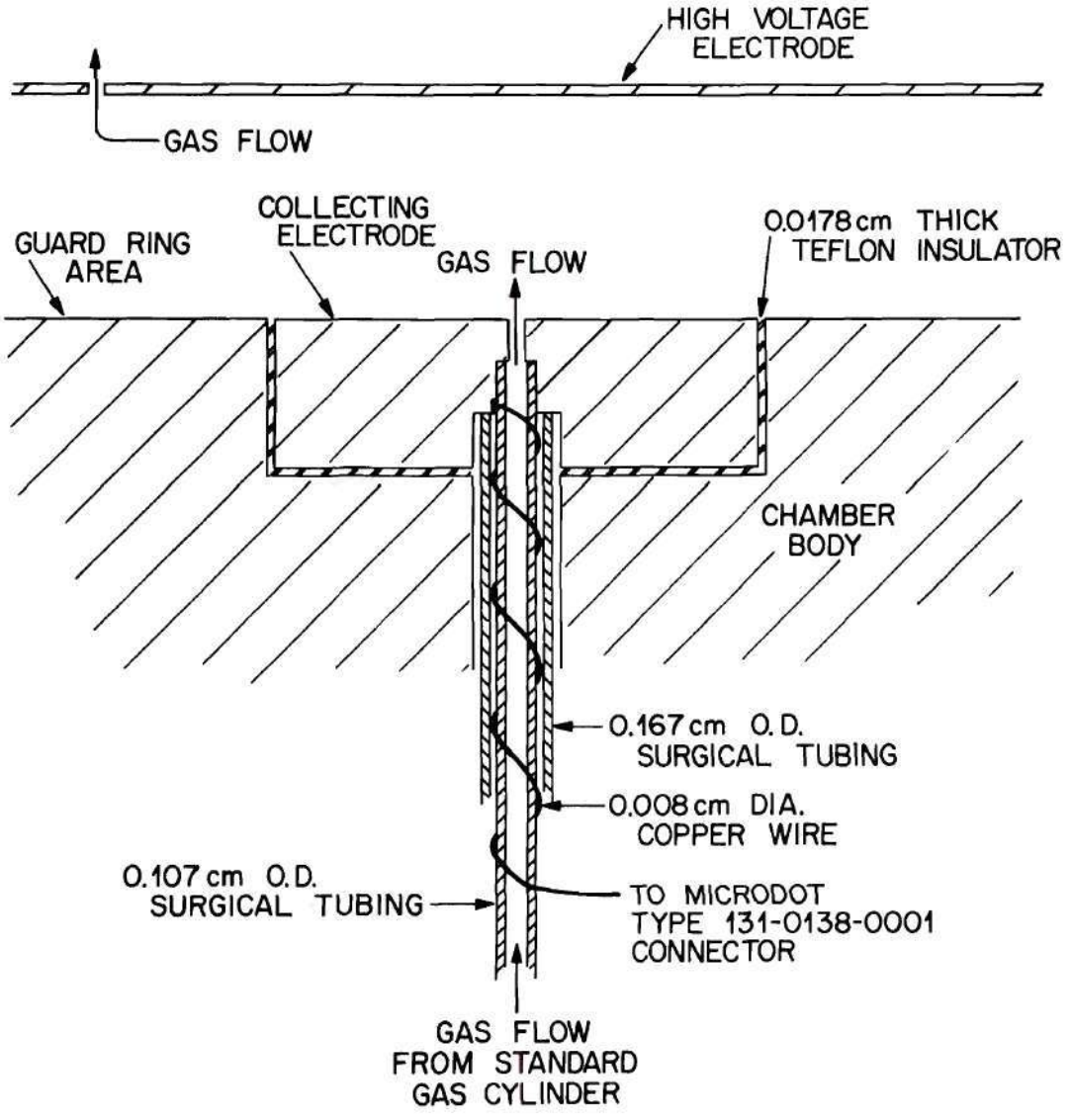

Figure 2. Cross-Section of Sensitive Volume of the Extrapolation Chamber.

Figure 3. Photograph of Typical Ionization Chambers.

(Te-I in Table 8) plastic and three from B-100* bone-equivalent (Be-I in Table 9) plastic. In each group, collecting electrodes of three different areas (1, 2, and 4 cm^2) were constructed. However, due to the low intensity of many of the sources used in this study, only those chambers with 4 cm^2 collecting electrodes were employed for dose measurements.

Although the ionization chambers could be operated at fairly large electrode gap-spacings, for this research, the electrode gap-spacings were restricted to the range 0.05 to 0.025 cm. This restriction was based on an optimization of the number of electrode spacings which could be investigated to allow extrapolation to zero electrode gap-spacing. Thus, the saturation characteristics of the ionization chambers were investigated over a wide range of electrode gap-spacing to ensure that the chambers were always operated on the saturation plateau. Figure 4 shows a typical set of saturation curves in the range 0.465 to 0.147 cm. These curves were "fit" with the aid of a computer to straight lines above an applied voltage of 50 volts. On the basis of these results, an operating voltage of 100 volts was selected for all gap spacings. The data in Figure 4 illustrate that these chambers were in saturation at electrode gap-spacings much larger than the restricted range employed in these measurements.

The directional response of a typical detector is shown in Figure 5. Response readings were normalized for end-on readings as 1.0. The electrode spacing was 0.6 cm (to make the chamber more sensitive for these measurements), and the operating voltage was + 300 volts.

*Dr. F. R. Shonka, St. Procopius College, Lisle, Illinois.

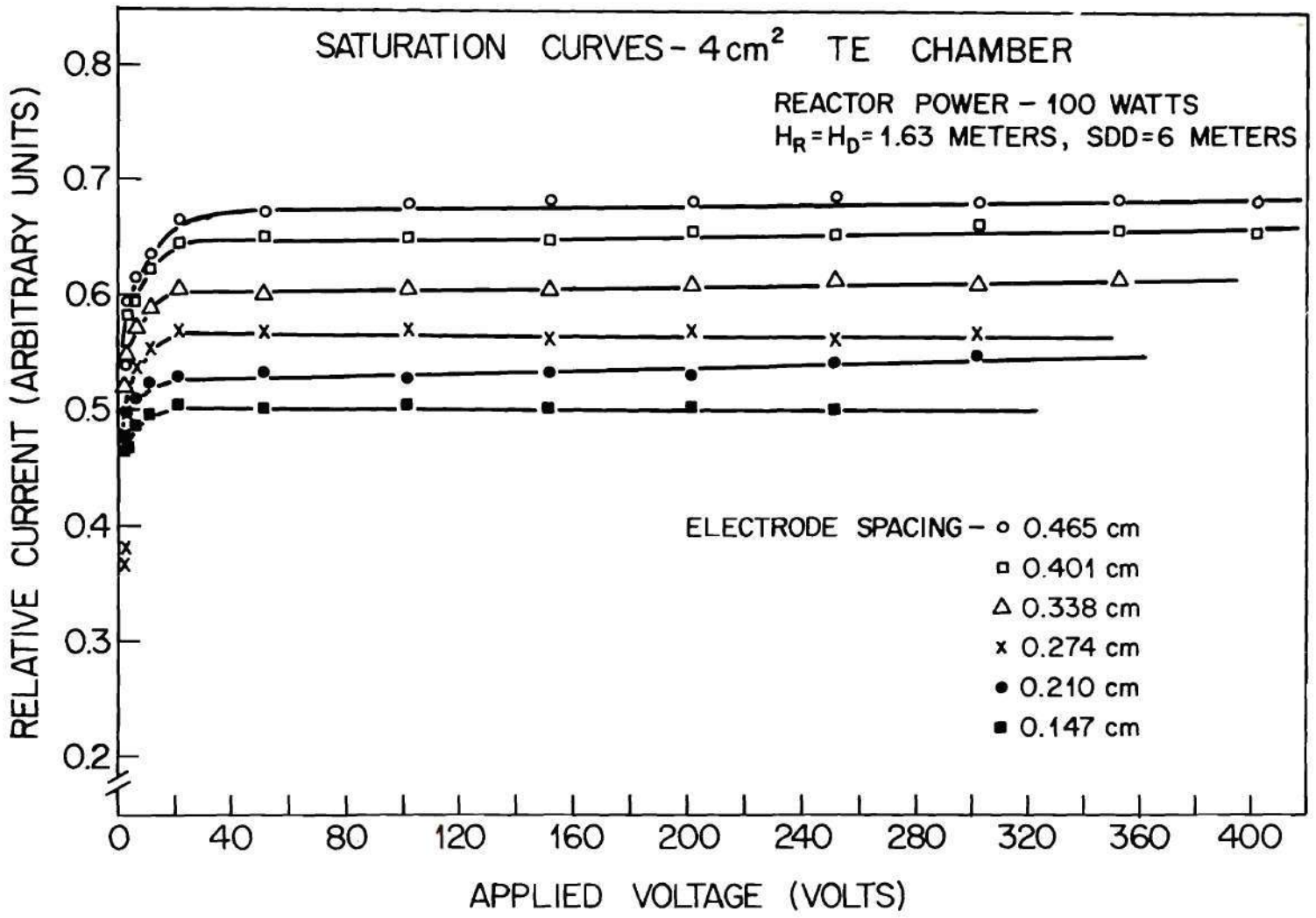

Figure 4. Typical Saturation Curve for 4 cm^2 Tissue-Equivalent Chamber.

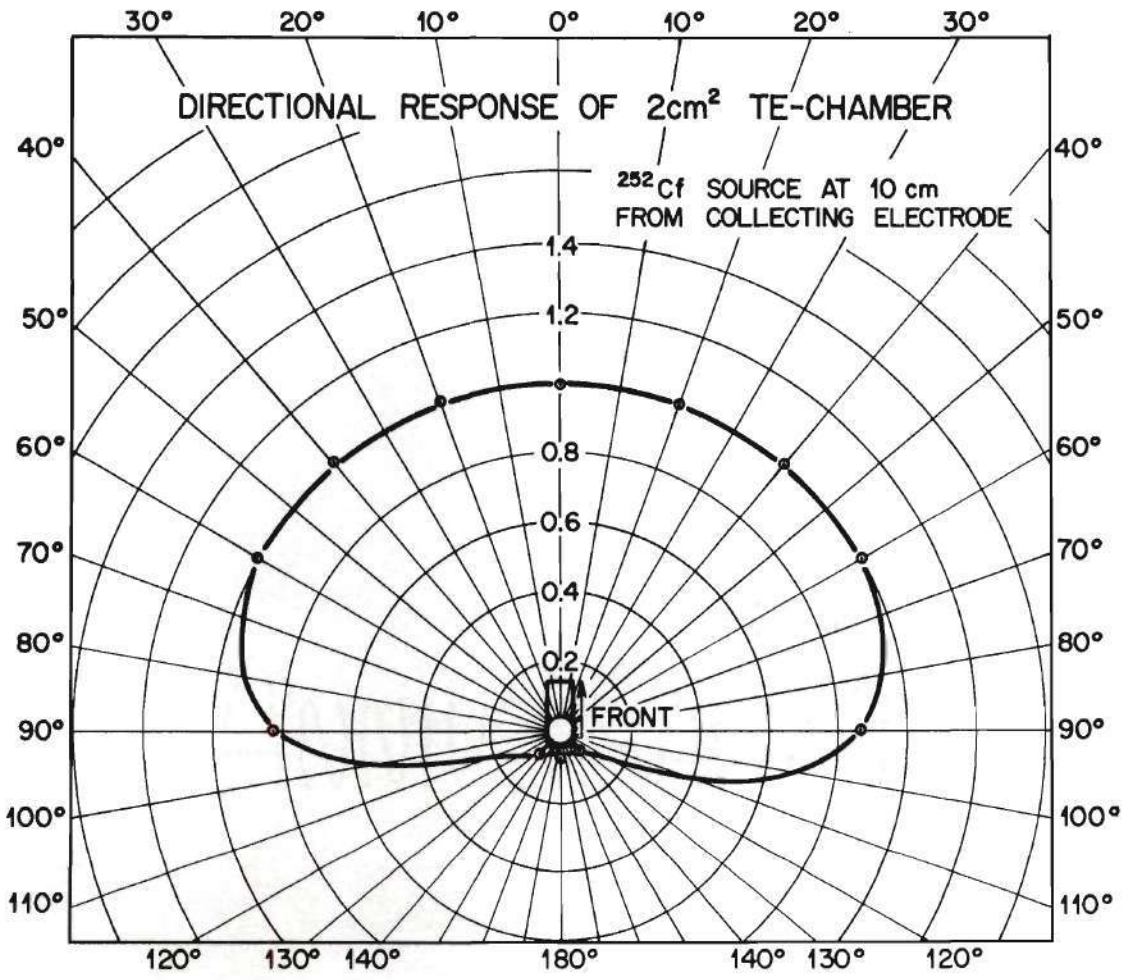

Figure 5. Directional Response of a Typical Chamber.

The source of neutrons was ^{252}Cf located at 10 cm from the collecting electrode. The detector and source were placed in a Styrofoam calibration rig which was mounted on an aluminum table, 1.4 meters above the floor. Such a setup allows relatively reproducible positioning of source and detector during calibration. The ^{252}Cf source capsule was in the form of a right circular cylinder 0.75 cm in diameter and 1.5 cm high. At 10 cm separation, the assumption was made that the source simulated a point source. The geometry effects inherent in this detector are apparent from the directional response curve. The front of the chamber (through the thin [0.02 cm thick] high voltage electrode) is most sensitive. As the source is moved around the chamber, the effect of the thicker side walls (0.56 cm) becomes evident. This effect is even more predominant as the source approaches the very thick ($\sim$ 6 cm) rear of the chamber. It was concluded that this effect was primarily due to the experiment arrangement (i.e., source and detector in air) and the indicated directional response of this detector would not hold when the detector is enclosed in the phantom. Inside the phantom, the detector is completely shielded by tissue-equivalent material, and the effects of the very thick rear portion of the detector on the directional response will be minimized.

In order to investigate the effect on the chamber characteristics of increasing the collecting electrode area while decreasing the guard ring size, a series of measurements were made in a reproducible geometry. In this test, the three tissue-equivalent chambers were exposed, one at a time, to an ^{241}AmB neutron source in a fixed geometry. Data were

taken at two different operating voltages, both of which were shown to be on the flat portion of the chamber saturation curves. In all cases, the same high voltage electrode was used to eliminate variations due to electrode thickness, etc. Electrode gap spacings were 0.19 cm for the 4 cm^2 TE-chamber, 0.18 cm for the 2 cm^2 TE-chamber and 0.21 cm for the 1 cm^2 TE-chamber. Ionization current, corrected for temperature and pressure variations and normalized per unit volume, was plotted as a function of electrode area. The results are shown in Figure 6. The limited data make it difficult to draw concrete conclusions as to the true effect. However, one can reasonably conclude that within the errors of the experiment, there is no effect due to reducing the ratio of field height to diameter in the chamber. This conclusion, of course, is only valid as long as the electrode gap-spacing is significantly less than the electrode diameter.

Since the chambers designed for this research were sensitive both to neutron and gamma radiation, it was soon recognized that some method of separating these two contributions to the measured dose would be required. For this reason, a chamber, otherwise identical to the others, was fabricated from graphite. Based upon the measured sensitivities of the other chambers, the chamber contained a 4-cm^2 collecting electrode. The graphite chamber provides a chamber with low neutron sensitivity. Rossi and Failla[21] have reported the neutron sensitivity of such a chamber to be strongly dependent upon the neutron energy. At a neutron energy of 0.5 MeV, the sensitivity rises to about 25%. At neutron energies below 100 keV, the sensitivity is essentially zero.

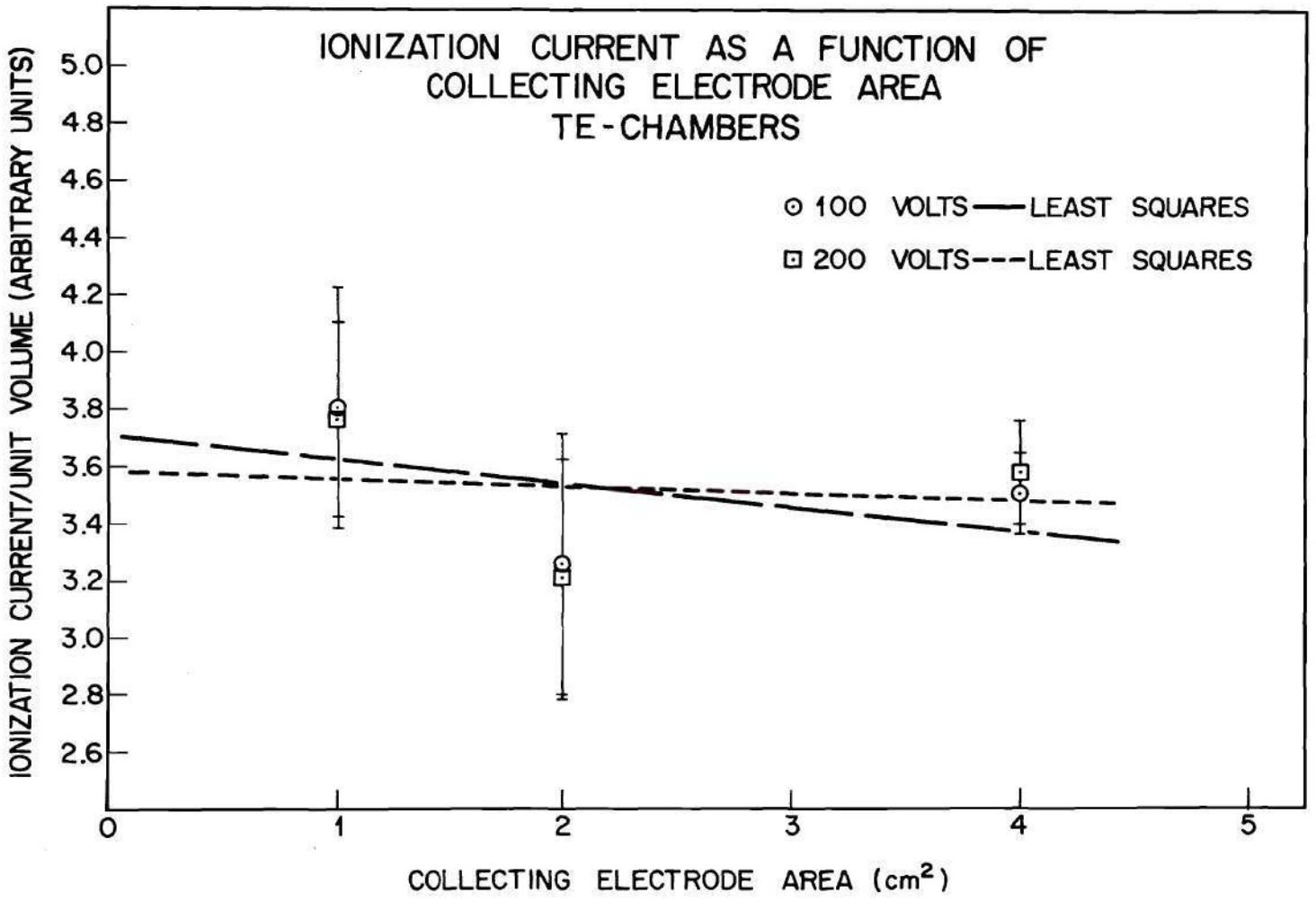

Figure 6. Ionization Current as a Function of Collecting Electrode Area.

The characteristics of this detector were quite similar to those previously described. Saturation curves, shown in Figure 7, illustrate this point. In this case, the gas flowing through the chamber volume was CO_2 rather than one of the special tissue- or bone-equivalent mixtures. Only one high voltage electrode, 0.0381 cm thick, was fabricated for use with this chamber.

Ionization currents from the detectors were measured through a semiautomatic electrometer (model Q-2102*) designed and built at the Oak Ridge National Laboratory. This instrument was intended for use in measuring ionization currents at large distances (up to 500 meters) from the detector unit. The electrometer features a matched pair of electrometer tubes (CK5886), one located in a unit near the ionization chamber and the reference tube located at the instrument readout. The circuit diagram for the remote unit is shown in Figure 8. A block diagram of the electrometer is given in Figure 9. Ionization current in the detector produces a D.C. voltage at the grid of the remote electrometer tube. This results in a change in potential of the grid of one side of the cathode follower tube (6201), which is directly coupled to the anode of both the remote electrometer tube and the reference electrometer tube. The change induces an unbalance in the galvanometer circuit of a Brown recorder amplifier. The balance motor in the Brown recorder serves as a mechanical feedback system acting through a precision voltage source to null the ionization current.

---

* Oak Ridge National Laboratory Drawing Nos. Q-2102-3, Q-2110-2, Q-826D-1, and Q-2110-1.

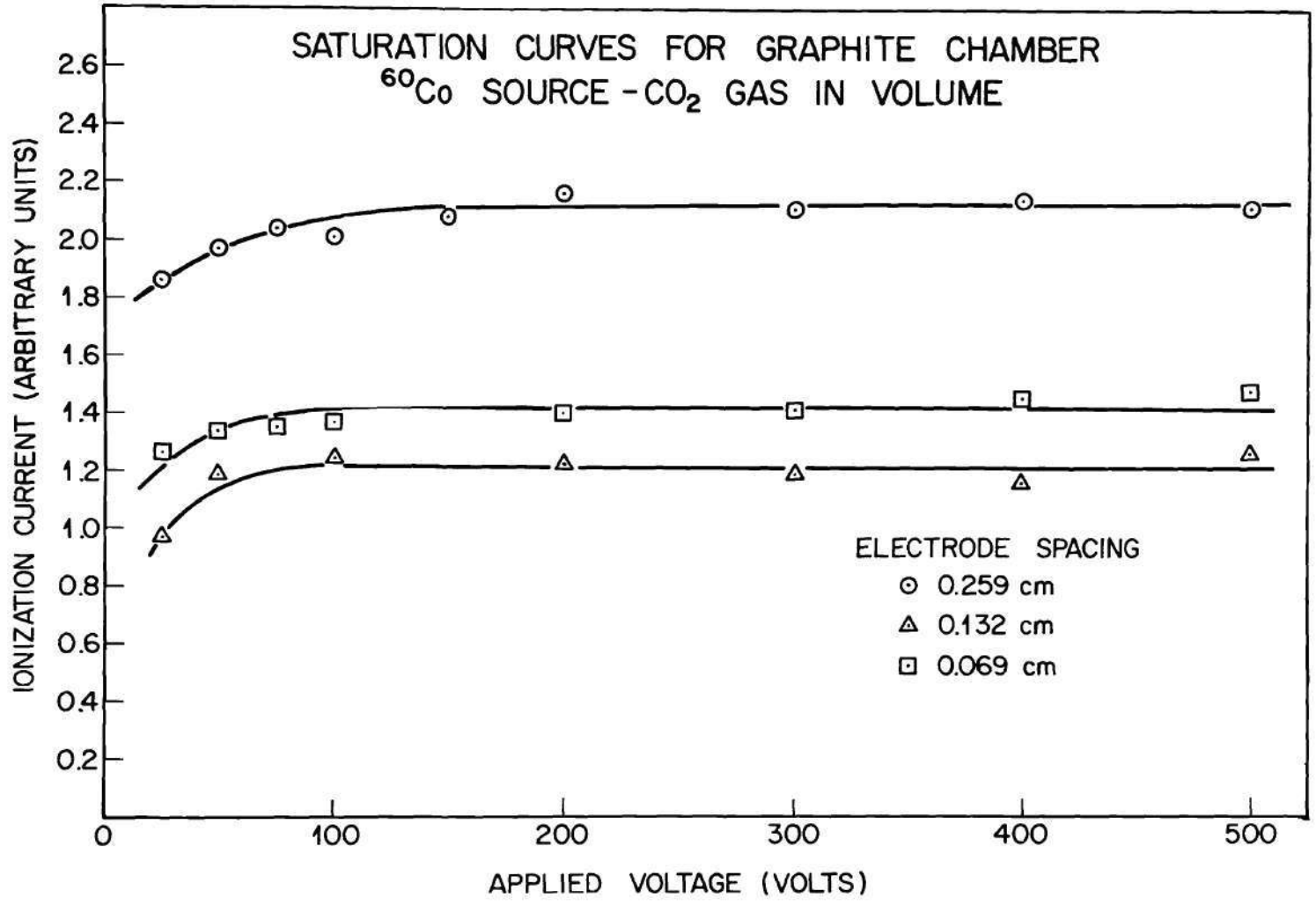

Figure 7. Saturation Curves for the 4 cm^2 Graphite Chamber.

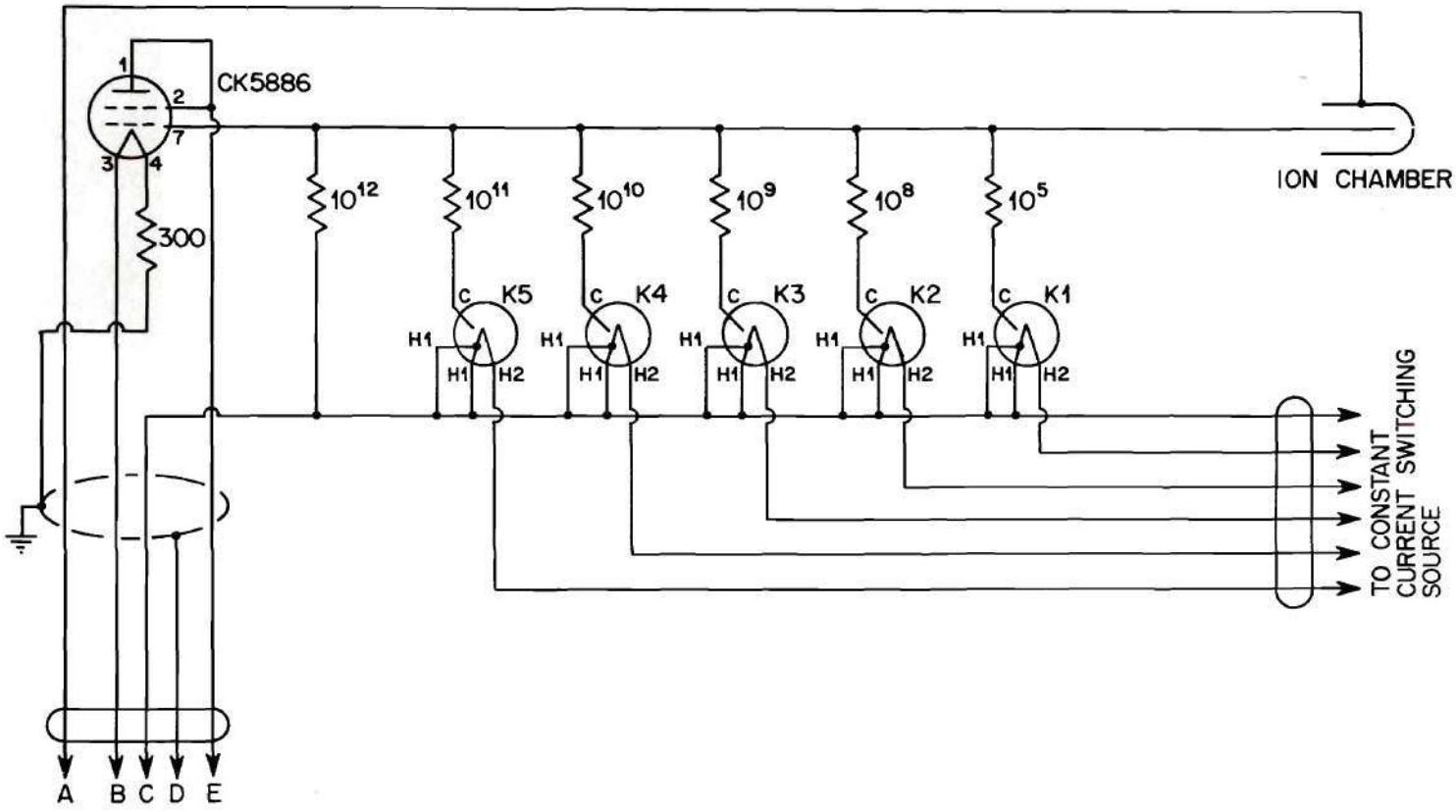

Figure 8. Circuit Diagram of Remote Head.

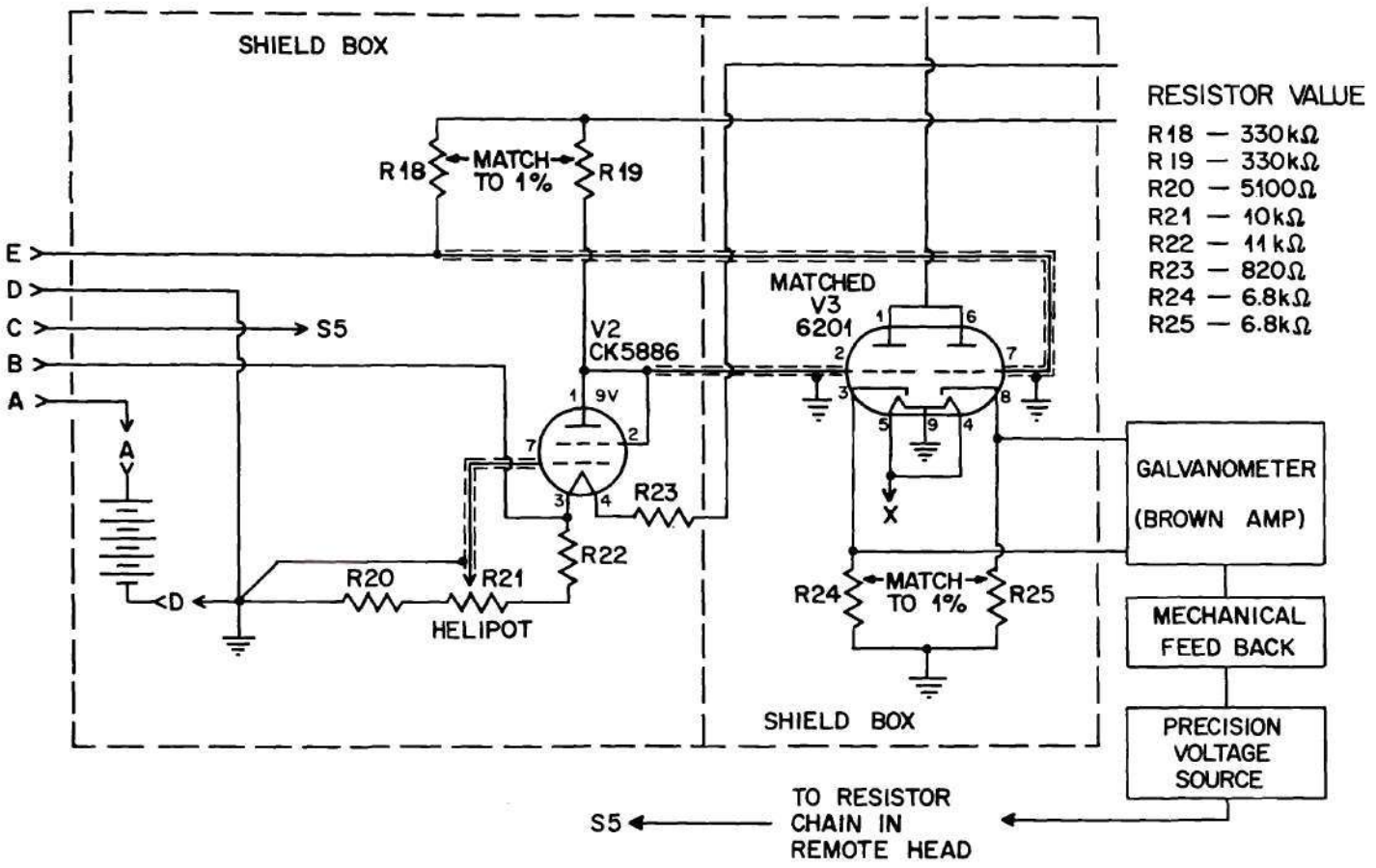

Figure 9. Diagram of Semiautomatic Electrometer.

The instrument featured the ability to remotely select from a series of precision high megohm resistors (R), located in the remote unit, for use in the feedback circuit. In effect, this feedback voltage was coupled to the ground side of the precision resistor in use. This voltage was integrated by a capacitor in the remote unit to reduce as far as possible extraneous input voltages. This arrangement was necessary to prevent the well-known charge transfer phenomena induced in measuring circuits due to the use of long, high capcitance cables on the electrometer input. Thus, the recorder deflection (E, in millivolts) indicated the magnitude of the ionization current (I) produced in the chamber through the simple relation I = E/R. Also included in the design of this instrument was the ability to check and adjust the zero of both the galvanometer and the precision voltage source during use. The ability to select either positive or negative polarity signals was another valuable feature of this instrument.

To reduce A.C. pickup, all cables had a braided shield. In addition, ground loops, etc., were eliminated by ensuring that all ground connections are made at a common point.

A separate neutron-sensitive system was in use to monitor data-taking sessions and to provide normalization between exposures. This channel employed a small Hurst proportional counter (called a "phantom counter") as the neutron detector. The signal is routed through an ORTEC 109PC transistorized preamplifier to a linear amplifier and a discriminator. The output pulses of the discriminator are counted on a Wang Model 2029A scaler.

In general, the data-taking sessions were divided into many two-minute intervals. That is, the remote electrometer was allowed to draw a trace on the strip chart recorder for two minutes. Simultaneously, a two-minute count was taken on the scaler reading the normalization channel. At the end of this period, the electrometer was returned to the zero check position. The normalization count and the electrometer current were recorded and the procedure repeated. A block diagram of the data channel and the monitoring channel are shown in Figure 10.

Calibration of Detectors

The ionization chambers were calibrated at the variable dose rate facility operated by the UT-AEC Agriculture Research Laboratory in Oak Ridge, Tennessee. This facility has available a large number of ^{60}Co source rods which produce a relatively uniform radiation field within the irradiation space. However, during this calibration, only one of the source rods was used.

The detectors to be calibrated were arranged at a distance of 63 cm from the source rod. The detectors were centered 85 cm above a 2.54 cm thick plywood table and 163 cm above the concrete floor of the facility. Two remote-reading Roentgen-meters were placed in the array to monitor the source intensity. The Roentgen-Meters also provided exposure rate information for use in the calculation of the calibration factors. During the calibration period, the temperature and pressure were continuously recorded to allow correction to standard temperature and pressure. Ionization currents from the detectors were measured for

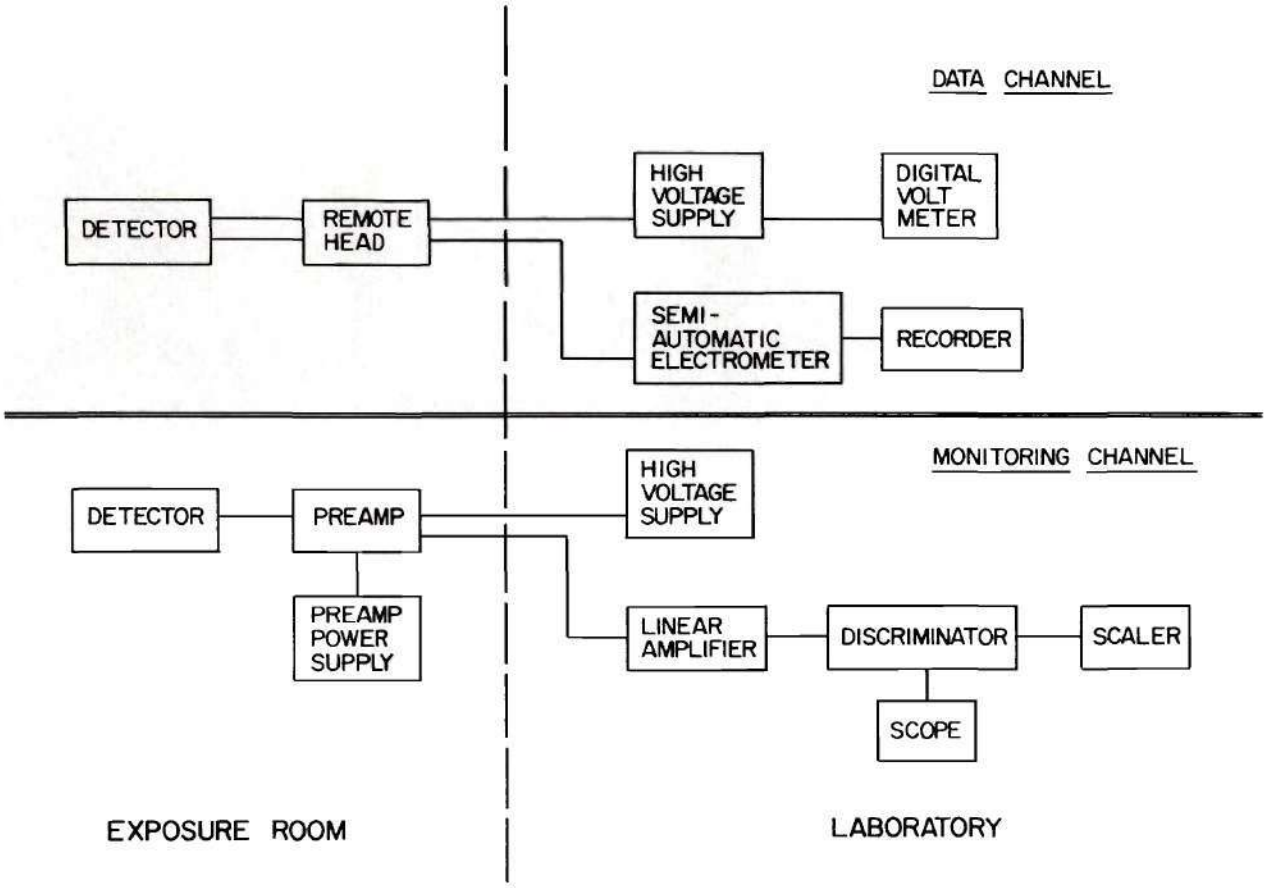

Figure 10. Block Diagram of Detector Systems.

all electrode gap spacings employed in this study. The calibrations were made over a period of two hours; thus no correction for radioactive decay of the source was necessary.

The detectors were also calibrated using a 14-MeV neutron source. The purpose of this work was to determine the relative sensitivity of the detectors compared with the previously measured gamma-ray response. The measurements should furnish necessary constants which must be known in order to separate a coexistent neutron and gamma-ray field into two components.

The ionization chambers were placed 20 cm from the target of the DLEA accelerator (see section on accelerator exposures for details). Ionization currents were measured as a function of electrode spacing, as in the previous calibration. Data were normalized through the use of the accelerator long counter channel; temperature and pressure corrections were applied where necessary. Rather than assume that the radiation field was composed entirely of neutrons, the gamma radiation component was measured by radiophotoluminescent techniques. These measurements indicated that the gamma radiation component was about 7% of the total (in terms of absorbed dose measured in air). Corrections for this contamination of the neutron radiation field were incorporated in the calibration calculations.

In both calibrations, the data were treated in the same manner. The normalized currents were corrected for temperature and pressure variations as well as differences in the sensitive volume of the detectors. Corrected data were then plotted as a function of electrode

gap-spacing, and extrapolated current was then divided by the dose rate to give a calibration factor in units of amperes/rad/min.

The results of the detector calibrations are given in Appendix I.

Phantom

The phantom used in this research was constructed as recommended by the International Commission on Radiological Units and Measurements.[106] The phantom is a 30-cm cube constructed of 0.635-cm thick Lucite sheet. The hollow cube was filled with tissue-equivalent liquid. A Lucite tube, 5-cm I.D. with 0.635-cm thick walls, is located along the center line of the phantom. This tube passes through two parallel faces of the phantom, allowing the movement of the detector through the phantom but isolating the detector from the liquid. Space in the tube not occupied by the detector is filled with tissue-equivalent material (see Chapter II for bone and tissue used in detector, also section on Experiment Arrangement below).

The tissue-equivalent liquid used in the phantom was that suggested by Rossi and Failla.[21] This liquid was intended to have the chemical formula of $C_5H_{40}O_{18}N$. Compounds used to supply these elements were water (27 kg), sucrose (9.3 kg), and urea (3.3 kg). The solution thus contained 10% hydrogen, 74% oxygen, 12% carbon, and 4% nitrogen. A small amount of thymol was added to the liquid to prevent bacterial growth.[87] The phantom was sealed from the atmosphere so that loss of water due to evaporation was minimized.

Experiment Arrangement

Reactor Exposures

For measurements employing fission spectrum neutrons, the Health

Physics Research Reactor (HPRR) was used. A description of this research reactor has been given by Auxier;[107] Johnson and Poston[108] have reported a compendium of dosimetry measurements that describe the reactor neutron spectrum, etc. Briefly, the reactor is a small, bare-metal, fast reactor designed specifically for health physics and radiobiological research. The reactor is unshielded and uncooled, the neutron leakage spectrum is a slightly moderated ^{235}U-fission spectrum. The power level of the reactor is easily varied from a fraction of a watt to 10 kW.

The front face of the phantom was located at a distance of 6.0 meters from the center line of the reactor. This distance was chosen as optimum to simulate the broad beam case while giving statistically significant results on both the data and the monitoring channels. At this distance, the neutron-to-gamma dose ratio was 5:1. The neutron dose as measured in air at the front face of the phantom (with the phantom removed) was $\sim$ 2 mrad/watt - min. Previous dosimetry investigations[108] have shown the radiation leakage from the HPRR to be radially symmetrical ($\pm$ 3% measured at 2.0 meters from the reactor). Thus the assumption of a uniform radiation field across the front face of the phantom (30 cm cube) located at 6.0 meters from the reactor appears valid. Both the reactor and the phantom were located with center lines at 1.63 cm above the reactor room floor. The normal operating power of the HPRR during data-taking sessions was 100 watts. The monitoring channel was located at the same distance (6.0 meters) and height (1.63 meters) in air near the phantom.

For reactor exposures, the ion chamber was positioned remotely through the use of a positioning device. The position of the detector

was noted by observing the experiment through closed-circuit television. Measurements were made in 5-cm steps. As the detector moved through the phantom, a 5-cm block of tissue-equivalent material was pushed out of the front of the phantom. The positioning device was then adjusted so that the detector was in the proper position. The void space left by the forward movement of the detector and the pushing out of a 5-cm plug was filled by the ram of the positioning device which was also constructed of tissue-quivalent material. Photographs of the experimental arrangement are shown in Figures 11 and 12. Figure 11 shows a close-up of the phantom (on the left) and the detector attached to the remote positioner. The cylindrical object in the center of the photograph is the remote electrometer unit. The bare reactor is shown in the right background of Figure 12, the phantom and positioning device are on the left, the monitoring detector is shown at the far right.

Accelerator Exposures

The DOSAR Low Energy Accelerator (DLEA)[109] was the source of 14-MeV neutrons for that portion of the study. The DLEA is a Texas Nuclear Model 9999 accelerator of the Cockcroft-Walton design. Neutrons of approximately 14.5 MeV are produced by the $^{3}H(d,n)^{4}He$ reaction. The DLEA provides ion beams slightly in excess of 1.5 milliamperes with an accelerating potential of 200 kilovolts. The targets used in this study consisted of tritium adsorbed onto a thin layer of titanium which had been evaporated onto a 0.025 cm thick copper disk. The active (tritiated) area of the target disk is 2.54 cm in diameter - the overall diameter was 3.175 cm. The targets have been shown to have an operative half-life for neutron production of approximately 30 minutes.

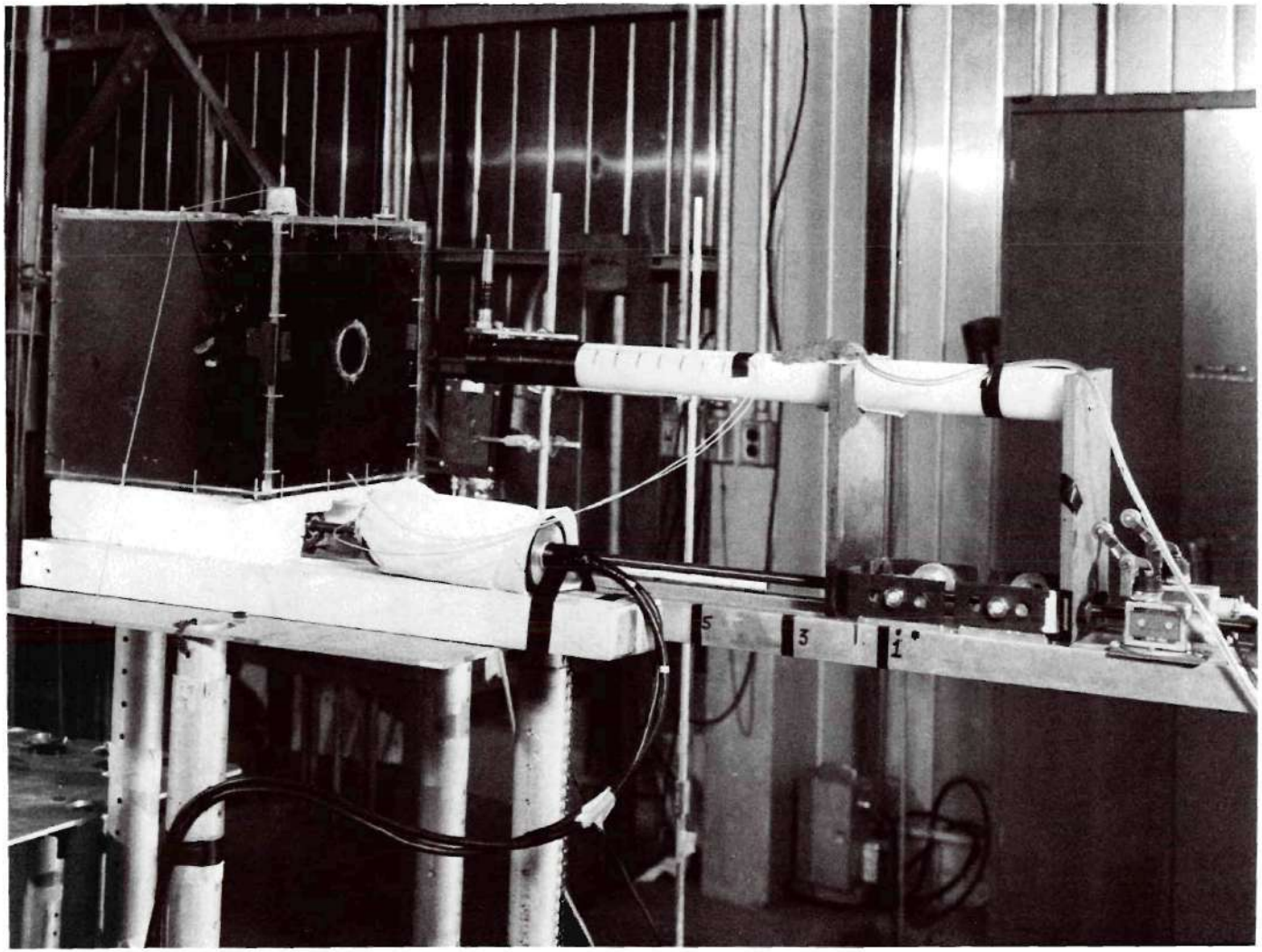

Figure 11. Photograph of Experiment Arrangement for Reactor Exposures. (Side View).

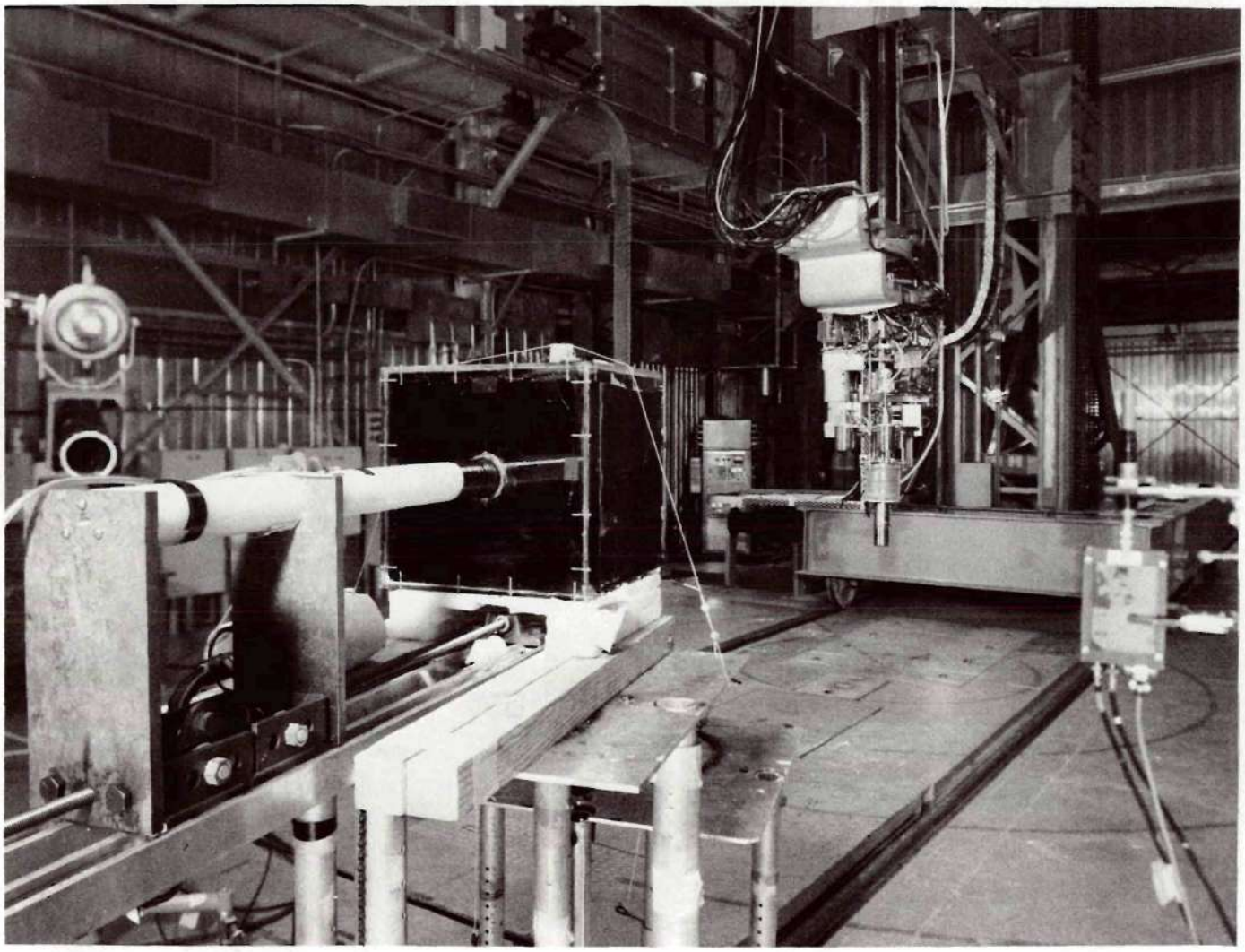

Figure 12. Photograph of Experiment Arrangement for Reactor Exposures. (Rear View).

The front of the phantom was located at a distance of 0.50 meters from the accelerator target. The center line of the phantom and the target were 0.96 meters above the building floor. Monitoring data were provided by a long counter associated with the accelerator normalizing channel. The detector was positioned at 5.0 meters height and at 7.0 meters separation from the accelerator target.

In this phase of the experiment, the detector was positioned in the phantom manually. Each time the detector was moved in the phantom, the void space was refilled with a tissue equivalent material. Measurements were made only with the interface located at a depth of 5 cm below the front face of the phantom. In both phases of the above experiment, the ion chamber had to be removed from the phantom in order to manually adjust the electrode gap-spacing. The experimental arrangement for the accelerator is shown in Figures 13 and 14 . The phantom is shown in the right-hand portion of Figure 13. Also visible at the rear of the phantom are the gas and electrical leads and the tissue-equivalent ram. The accelerator and target assembly occupy the left of this photograph. Figure 14 is another photograph of the experiment arrangement showing the relative of the phantom and the target assembly.

Bench Tests

There are a number of isotopic neutron sources in routine use in many laboratories throughout the world. The source neutron emission rate does not allow the use of these sources in either of the experimental situations just described. However, some depth dose data are available for these sources. In addition, these sources are of general interest in dosimetry research areas for many years. For these reasons,

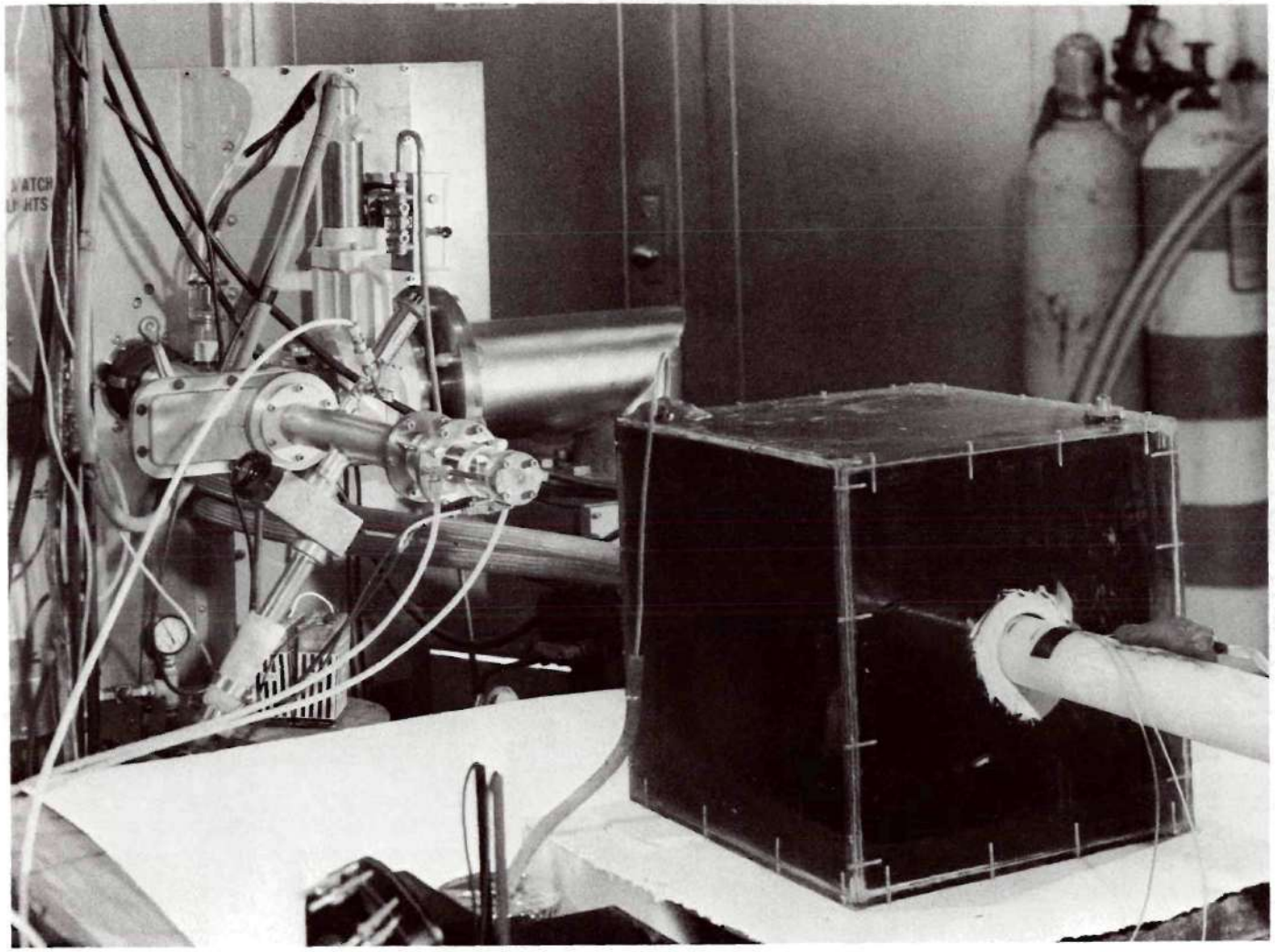

Figure 13. Experiment Arrangement for Accelerator Exposures. (Rear View).

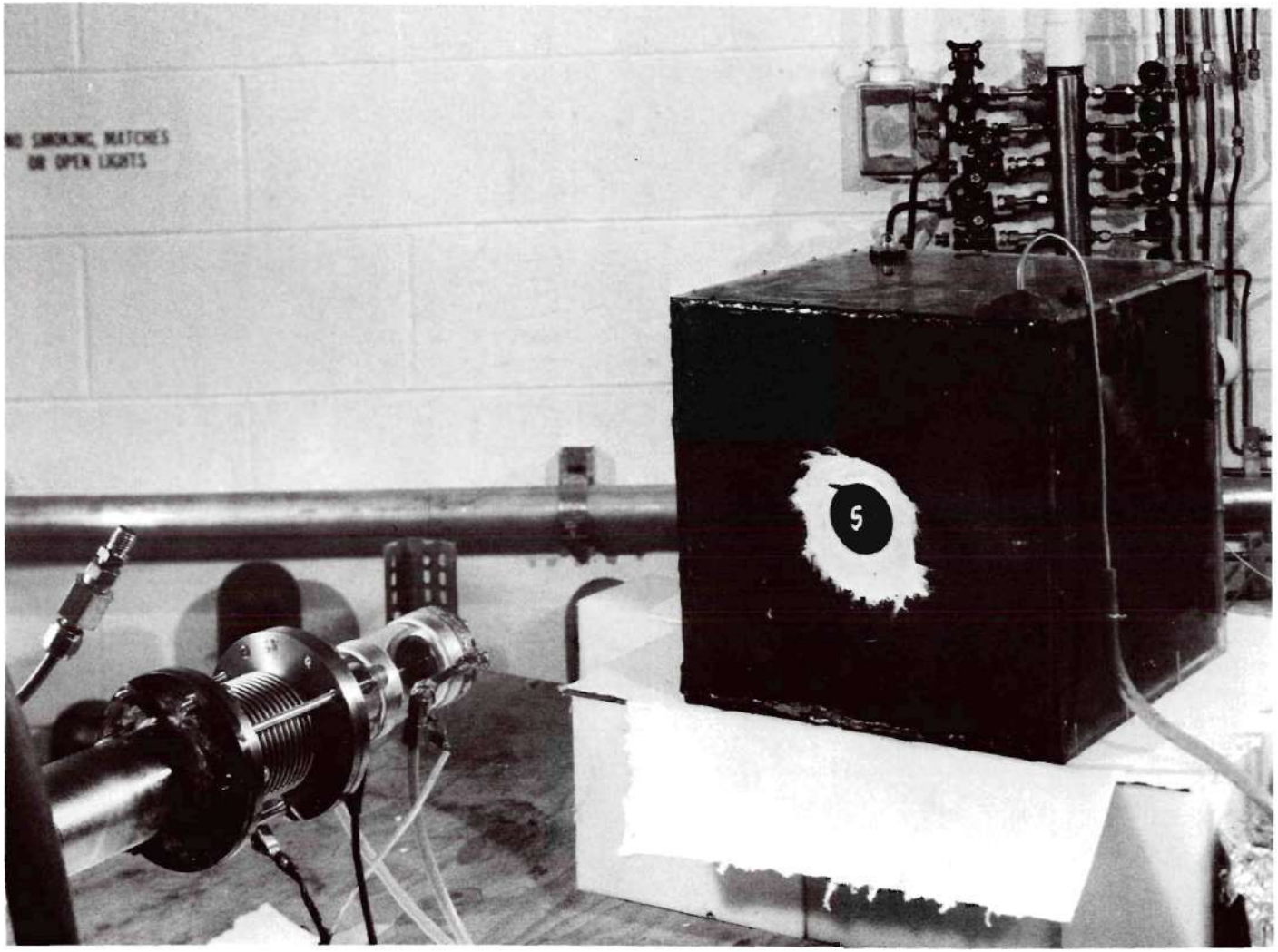

Figure 14. Experiment Arrangement for Accelerator Exposures. (Front View).

a series of experiments were undertaken to investigate dose distributions due to several of these sources, including ^{241}AmB, ^{241}AmBe, and ^{239}PuBe. Table 10 presents physical data on the neutron sources used.

In these studies, the detector, the source, and the interface material were enclosed in a cylindrical, polyethylene shield. A sketch of the experimental arrangement is shown in Figure 15. Basically, the source was located approximately 7.5 cm from the interface; neutrons from the source passed through about 5 cm of tissue- or bone-equivalent material before intercepting the interface region. Calculations based upon the solid angle dispersion relationship for radiation fall-off indicate the variation of fluence across the sensitive volume to be only about 2%. Experimental measurements of fast neutron attenuation[111] in water and paraffin show that the fast fluence with energy greater than 0.5 MeV is about 60% of the total fluence impinging upon the detector volume. All materials used inside the shield were either tissue- or bone-equivalent materials.

Ionization currents produced in the chamber volume were measured using a vibrating reed electrometer and associated equipment. The output of the vibrating reed electrometer was routed to a strip-chart recorder for ease of data accumulation. For each measurement, the recorder was allowed to draw a trace for about 3 minutes. Then a mean reading was selected as indicative of the chamber output. The ionization current from the chamber was determined for each measurement by recording the recorder reading (in mV), and the value of the high megohm resistor (R) selected in the preamp head, and calculation of the current from the simple relation $I = E/R$.

Table 10. Characteristics of Isotopic Neutron Sources

Type	Activity (Ci)	Mean Energy* (MeV)	Neutron Output (neutrons/sec)
^{241}AmB	10	3.0	5.75×10^{6}
^{241}AmBe	5	4.4	1.27×10^{7}
^{239}PuBe	4	4.4	7.65×10^{6}

* Based on measured fluence-to-dose conversion factors.

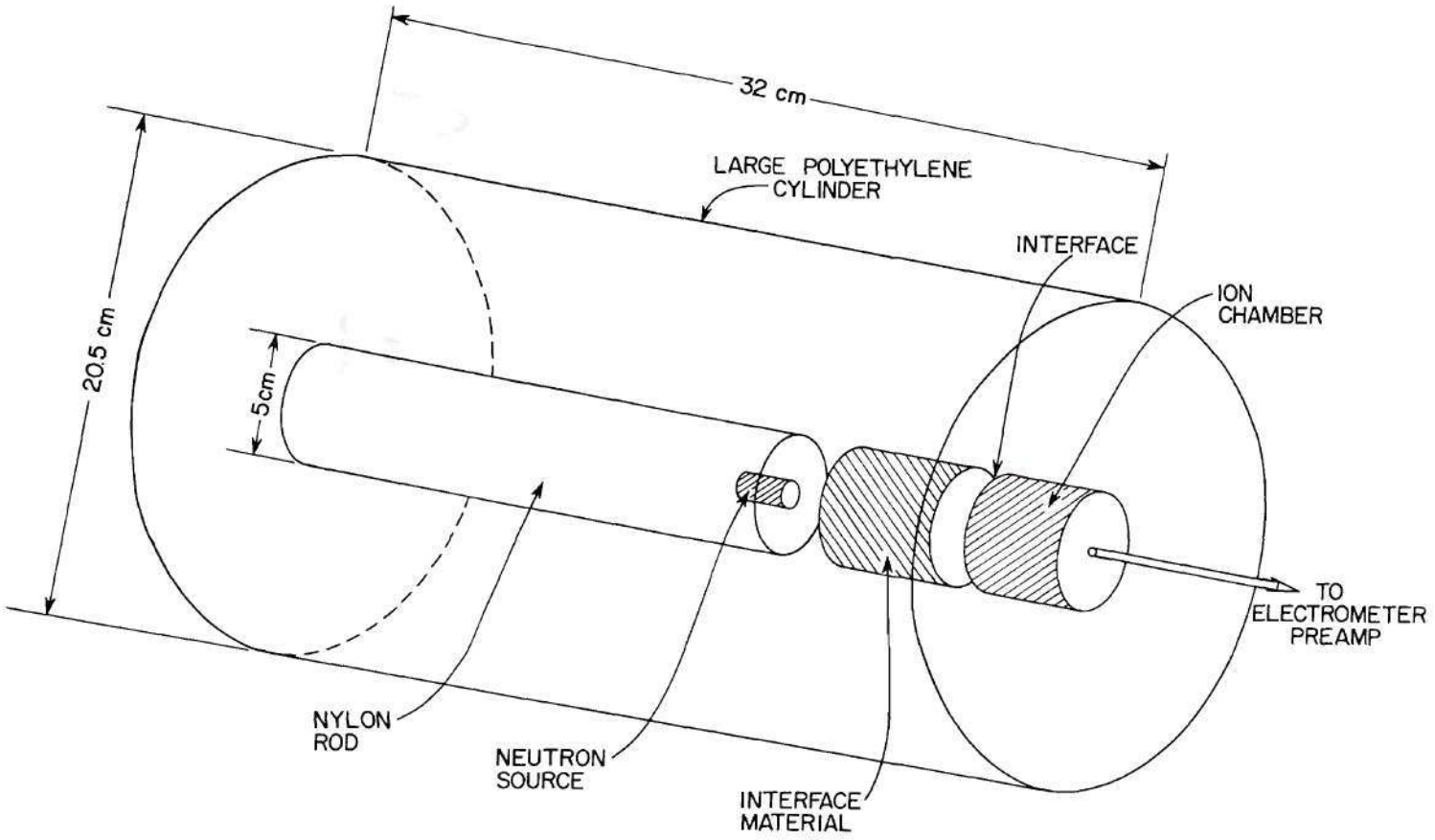

Figure 15. Schematic Arrangement for Isotopic Source Experiments.

In this series of measurements, ionization currents were measured in the tissue-equivalent, bone-equivalent, and graphite chambers. Corrections were applied to the measured ionization currents to account for temperature and pressure variations, as well as source-to-detector separation.

CHAPTER V

RESULTS AND CONCLUSIONS

Data Analysis

During this entire research project, the data have been reduced in essentially the same manner. As previously stated, ionization currents from the extrapolation chambers were measured with an electrometer. The signal from the electrometer is routed to a strip-chart recorder which provides a visual and permanent record of each measurement. The recorder is allowed to operate for a fixed period of time (usually two minutes) while the normalization channel monitors the neutron radiation field. At the end of the observation period, both the strip-chart recorder and the normalization channel are stopped. The mean of the ionization current is recorded along with the result from the normalization. In addition, temperature and barometric pressure readings are recorded in the exposure room. These parameters, with the source-to-detector separation and the chamber gap spacing, provide all the input information necessary for treatment of the data.

The initial data reduction is performed with a short computer program which takes as input the ionization current from each set of measurements. The current is corrected for source intensity change by dividing by the normalization count. Measurements under the same conditions are averaged and corrected for variations in the temperature and pressure in the exposure room. The electrode gap spacing is used

to put the data into terms of ionization current per unit volume by dividing by the chamber volume. In addition, a correction for the reduction of source intensity due to the inverse distance squared effect is applied. Thus, the output from this program provides a normalized ionization current per unit volume at a number of different electrode gap-spacings.

The output of the above program is used as the input for another computer program which uses the normalized ionization current per unit volume and the electrode gap-spacing in a calculation of the ionization current for zero volume. This is accomplished by "fitting" a straight line (using the least-squares method) to the data points and evaluating the fit for the zero gap-spacing intercept. In addition, the probable error in the intercept point and the slope is calculated. The method used in this calculation is described in Reference 112. Briefly, if the linear equation is of the form, $y = a + bx$, the formulas for the probable errors are relatively simple:

$$P_a = r_e\sqrt{\frac{\Sigma x_i^2}{D}} \qquad P_b = r_e\sqrt{\frac{n}{D}} \tag{3}$$

where

$$r_e = 0.6745\sqrt{\frac{\Sigma d_i^2}{(n - 2)}} \tag{4}$$

$$D = n\,\Sigma x_i^2 - (\Sigma x_i)^2 \tag{5}$$

$$d_i = x_i - \bar{x} \tag{6}$$

n = number of data points

These calculations are done easily and rapidly in conjunction with the least squares fit to the data points.

Finally, the calculated zero intercept data are plotted as a function of distance from the interface. All the data points are normalized to the point closest to the interface in each case. The error bars shown in these graphs (e.g., Figures 16-21) are simply the most probable errors calculated as described above. These are the results which will be presented and discussed.

Sources of Error

In the data analysis, some consideration must be given to the sources of error in the experiment. Fairstein[113] has provided a detailed discussion of possible sources of error in the use of ionization chambers and electrometers. Evans[114] has pointed out that the major features of the statistical behavior of ionization chambers can be inferred by comparison with detailed statistical theory for counters. However, the development of a detailed theory is prevented by variations in the number of ion pairs produced in the ionization chamber per ionizing particle. This quantity depends not only on the type of particle but on a statistical distribution about some mean value, even for identical incident particles of identical initial energy. Another fact which can increase the fluctuations in ionization is that several types of ionizing particles may be acting simultaneously on the chamber. Circumstances can easily occur in which heavily ionizing particles, such as recoil protons, may produce only a small portion of the total ionization but may dominate the statistical fluctuations in ionization.

This section is intended to enumerate and quantify sources of error in this research. Table 11 lists in short form the variations of major importance in this work. Perhaps the largest variations are those in the measurement of the ionization current from the extrapolation chamber. In general, the average variation of the trace drawn by the strip-chart recorder (and thus the indicated ionization current) has been found to be ± 10%. The variation in the mean reading chosen as representative of the ionization current was ± 4% for repeated measurements under identical conditions. These are the major variations in the experiment. The other variables are either known or can be easily estimated. One exception to this general statement is the exact distance of the chamber from the interface. The percent error here probably increases as the distance from the interface decreases. The chamber is separated from the interface by interposing various thicknesses of tissue-equivalent (or bone-equivalent) plastic between the high voltage electrode and the interface. A check of the thickness variation of several of these plastic pieces showed that these pieces could be considered as essentially "precision" pieces. In the manufacture, the machinist worked diligently to produce plastic spacers which corresponded exactly with the specified dimensions. Variations in thickness were all less than ± 1% of the desired thickness. However, this is not a true indication of the interface detector separation.

In an effort to provide some insight into the positioning variations, a program of repeated measurements was undertaken on the laboratory bench. *In the first phase of this* experiment, a series of

Table 11. Summary of Errors

Source of Variation	Estimated Error
Variation in Ionization Current	± 10%
Variation in Mean Current	± 4%
Precision Resistors (in Measuring Circuit)	± 1%
Chamber Electrode Spacing	± 1%
Plastic Spacer Thickness	± 1%
High Voltage Electrode Thickness	± 2%
Source Intensity (Reactor)	± 1%
(Accelerator)	± 5%
(Isotopic Source)	± 3%
Chamber Replacement	± 4%
Source and Interface Replacement	± 2%
Uniformity of Source on Phantom (Reactor)	± 1%
(Accelerator)	± 4%
(Isotopic Source)	Not Applicable
Measurement of Temperature	± 1%
Measurement of Barometric Pressure	± 1%

readings were taken with the source, interface material, plastic spacing material, and the extrapolation chamber in a fixed position. Then the source interface material and plastic spacer were removed, separated, and replaced. Another series of ionization current measurements were made. This procedure was repeated many times to accumulate sufficient readings to be considered statistically valid. These measurements yielded a standard deviation of $\sim$ 2% for measurement of the ionization current under the test described above. In a second study, the source, interface material, and plastic spacer were removed from the bench test rig. In addition, the high voltage to the chamber was switched off, and the chamber was disconnected and removed from the test rig. Then the test conditions were reestablished. A standard deviation of less than 4% was calculated for the results of these measurements. Thus, although the positioning error remains unknown, these measurements point out that conditions can be established and reestablished many times to within $\pm$ 4%.

Several corrections, although routinely applied, may not be of great importance. For instance, a change in barometric pressure of 10 torr requires a correction of only 1.3%. Such a change in barometric pressure is easily measured in the laboratory. Similarly, a correction of only 1.7% is required for a change in temperature of 5°C.

As previously stated, the error bars shown in the dose distribution graphs are the calculated probable error of the extrapolated intercept (the zero volume conditions). Based on the preceding summary of sources of variation, it can be concluded that this error

(which ranges up to about 15%) is a good indication of the overall error of the measurements. To the first approximation, variations in the data points used in the computer fit, are reflected by an increase in the calculated probable error for the intercept point.

Results

Before examining the dose distributions closely, it should be instructive to describe the contributing phenomena and attempt to visualize the shape of the distributions. In general, one would expect a decrease in the neutron dose distribution as the detector moved from a "tissue" environment into a "bone" environment. This is based simply on the fact that there is a decrease in the hydrogen content in the bone. (In the plastic used to simulate tissue, the hydrogen content is 10%, while in the bone-equivalent material, the hydrogen content is reduced to about 4-6%.) Calculations by Williamson and Mitacek[62] indicated that there will be more than a factor of two difference between the kerma/unit fluence in tissue and in bone as the neutron energy approaches 14 MeV. For similar reasons, when crossing from bone into tissue, a slight buildup region would be anticipated with the distribution attaining the same slope (the magnitude is uncertain) as the depth dose distribution in a homogeneous tissue medium.

In contrast, the situation is reversed when one considers the distribution of gamma rays (or x rays) across the same interface. That is, the strong dependence of the photoelectric effect on the atomic number of the material should cause an increase in absorption in the bone-equivalent material for low energy photons. In this case,

experiments[24] have confirmed the existence of a buildup region when crossing into a "bone" region from a "tissue" region (this buildup is less pronounced as the photon energy increases). However, the result is a lowering of the dose in tissue directly behind the bone material. Again, the slope of the distribution should become the same as the slope for the distribution in a homogeneous phantom. Thus, the distributions measured with the tissue-equivalent and bone-equivalent ionization chambers should be a composite of the two distributions described above. This conclusion is based on the fact that these two detectors have essentially equal sensitivity to both neutron and gamma-radiation.

The anticipated effects discussed in the preceding paragraphs rely on reasoning based on a knowledge of neutron interactions, neutron cross-sections, the elemental compositions of the materials of interest and previous data from similar measurements with x- and gamma-radiation. A closer examination of the available literature will be presented here to facilitate comparison with the experimental data.

There are few papers in the literature which discuss the effects of bone on neutron depth dose distributions. The majority of these are calculational studies employing Monte Carlo techniques. Of these, the results of Turner et al.[11] can be ignored based on the fact that only neutron (and proton) energies between 100- and 400-MeV were considered. In addition, the dose and dose-equivalent were averaged over the volume elements with no fine structure distribution being given near the interfaces.

The calculations of Wilkie[16] give a very good indication of the dose distributions in a heterogeneous phantom when irradiated with ^{252}Cf

fission neutrons and 14 MeV-monoenergetic neutrons. However, these results are presented as isodose curves in a 20 cm by 30 cm elliptical phantom, and again the necessary fine structure is missing.

The study of Budinger et al.[12] gives distributions which could provide a valuable comparison to these measurements. A close analysis of these calculations leaves little doubt that these results, although very conservative, are suspect. The first major fault in this work is that the authors allow the energy from all gamma-rays produced by neutron interactions to be deposited at the interaction site. Thus, for 14-MeV neutrons, the distribution near the interface crossing from tissue into bone shows a factor of two increase. This result is more what one would expect for incident 30-50 kV x-rays.[24]

A second point of concern is the input data used in the calculations. These authors present a table showing the mean free path for neutrons as a function of energy in tissue and bone. This compilation covers the energy range from 2×10^{-8} to 14.1 MeV. These data indicate that the mean free path in bone is greater than the mean free path in tissue for all neutron energies up to almost 4 MeV. A compilation by Jones,[115] based on available data (total cross-section and relative abundance), indicate that the mean free path in tissue is always higher than the mean free path in bone for neutron energies of 0.025 eV to 14 MeV. In fact, the mean free path in tissue, according to this compilation, is essentially a factor of two higher than the mean free path in bone for all neutron energies considered. These differences are yet to be resolved.

All that remains is a calculation reported by Lawson[10] in 1967. As discussed previously, this calculation is based upon similar work by Charlton and Cormack[69] for electrons generated from photon interactions in bone and tissue. On the surface, the results of Lawson can be compared directly to the distributions measured in this research for 14-MeV neutrons. According to this author, distributions at the bone-tissue interface for any other neutron energy can be derived simply by reducing the distance parameter in his calculation by the ratio of the proton ranges in the medium of interest.

For 14-MeV neutrons, a buildup region is shown in tissue as the distance from the bone slab is increased. The buildup is approximately 60-80% of the interface value with a plateau or equilibrium condition established at about 0.16 cm. In contrast, the calculated distribution in bone shows a decrease to about 30% of the interface value with a plateau at about 0.1 cm. The experimental results will be discussed in relation to the calculations of Lawson.

Reactor Exposures and Bench Tests

Distributions measured in tissue- and bone-equivalent materials, using the HPRR as a neutron source are shown in Figures 16 through 20. These figures show distributions measured at depths of 5, 10, 15, 20, and 25 cm in the tissue-equivalent phantom. As stated previously, data points shown in these figures are the extrapolated intercept (zero electrode separation) determined by plotting ionization per unit volume against the electrode gap-spacing. In all cases, the radiation is impinging on the interface from the left of the drawing. The curves drawn

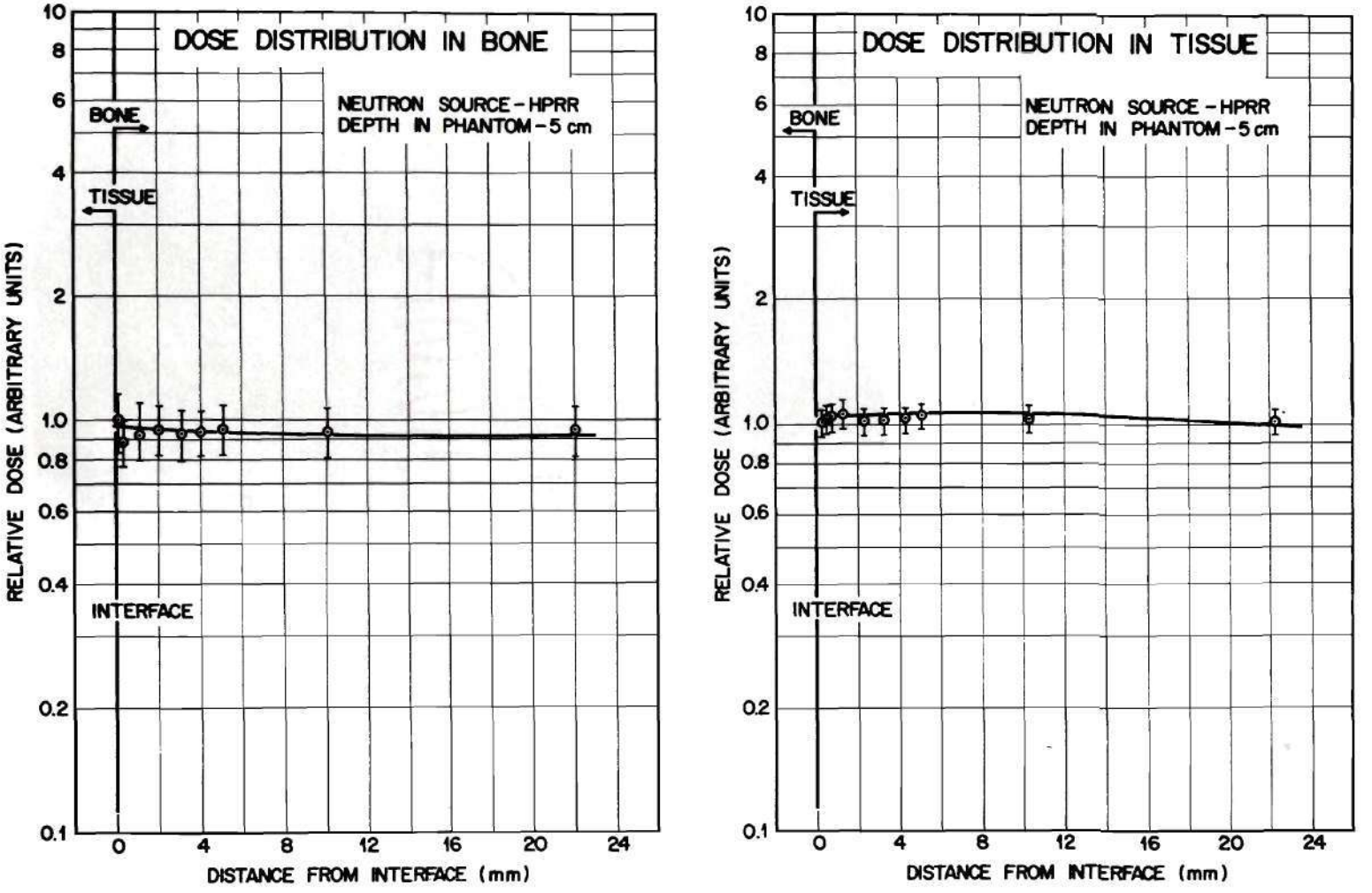

Figure 16. Dose Distributions at a Bone-Tissue Interface Due to Fission Neutrons (Depth 5 cm).

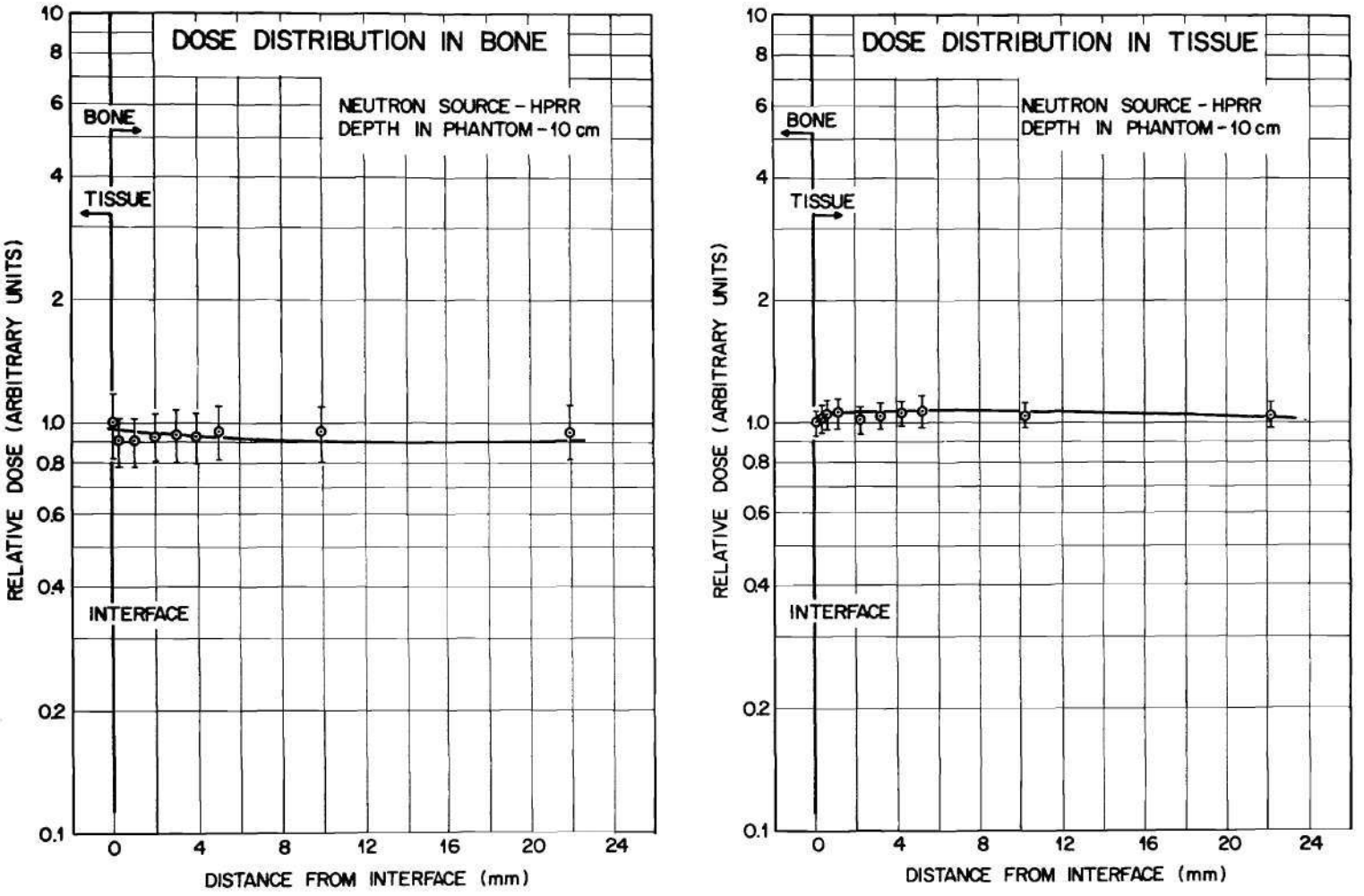

Figure 17. Dose Distributions at a Bone-Tissue Interface Due to Fission Neutrons (Depth 10 cm).

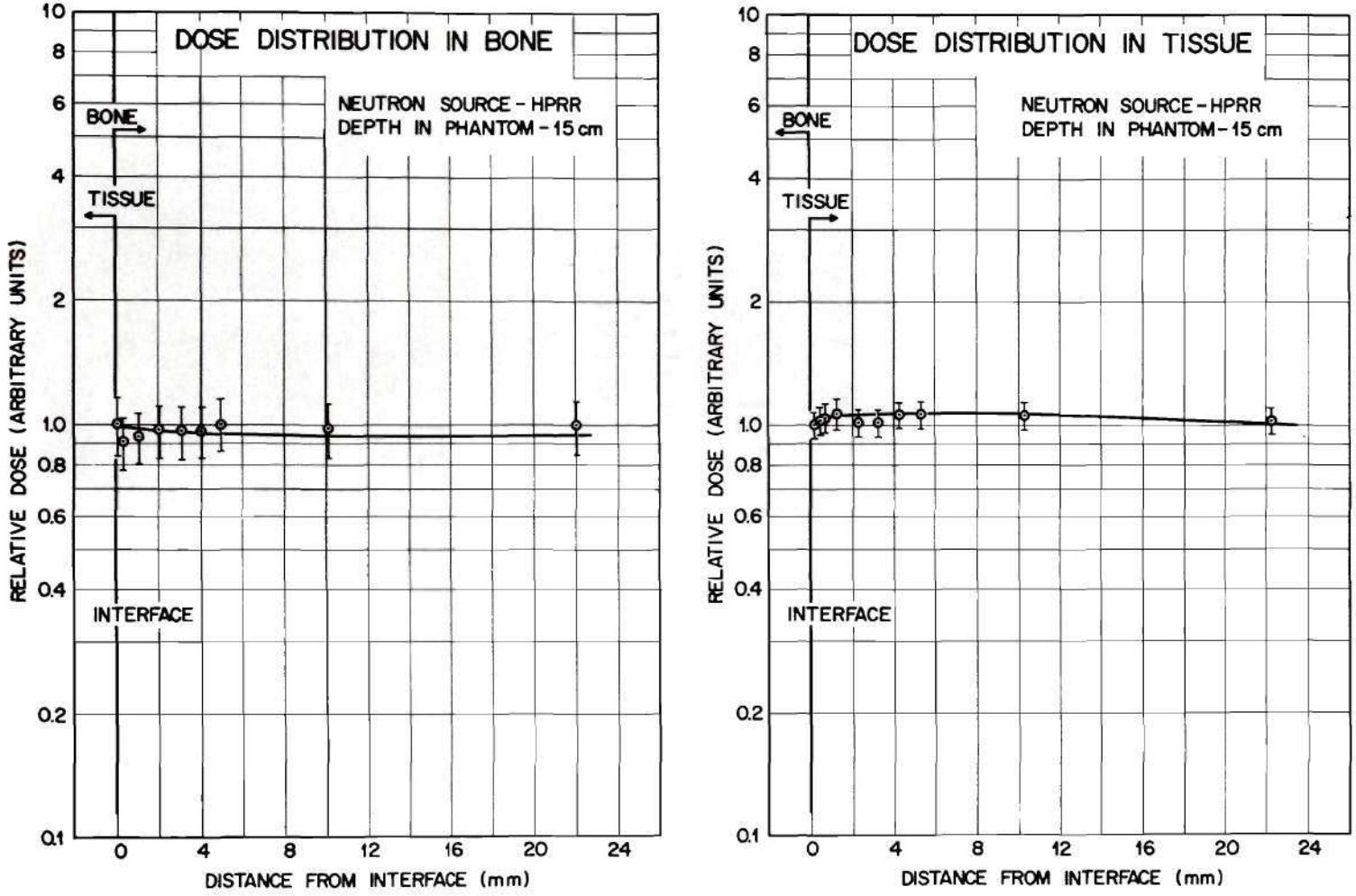

Figure 18. Dose Distributions at a Bone-Tissue Interface Due to Fission Neutrons (Depth 15 cm).

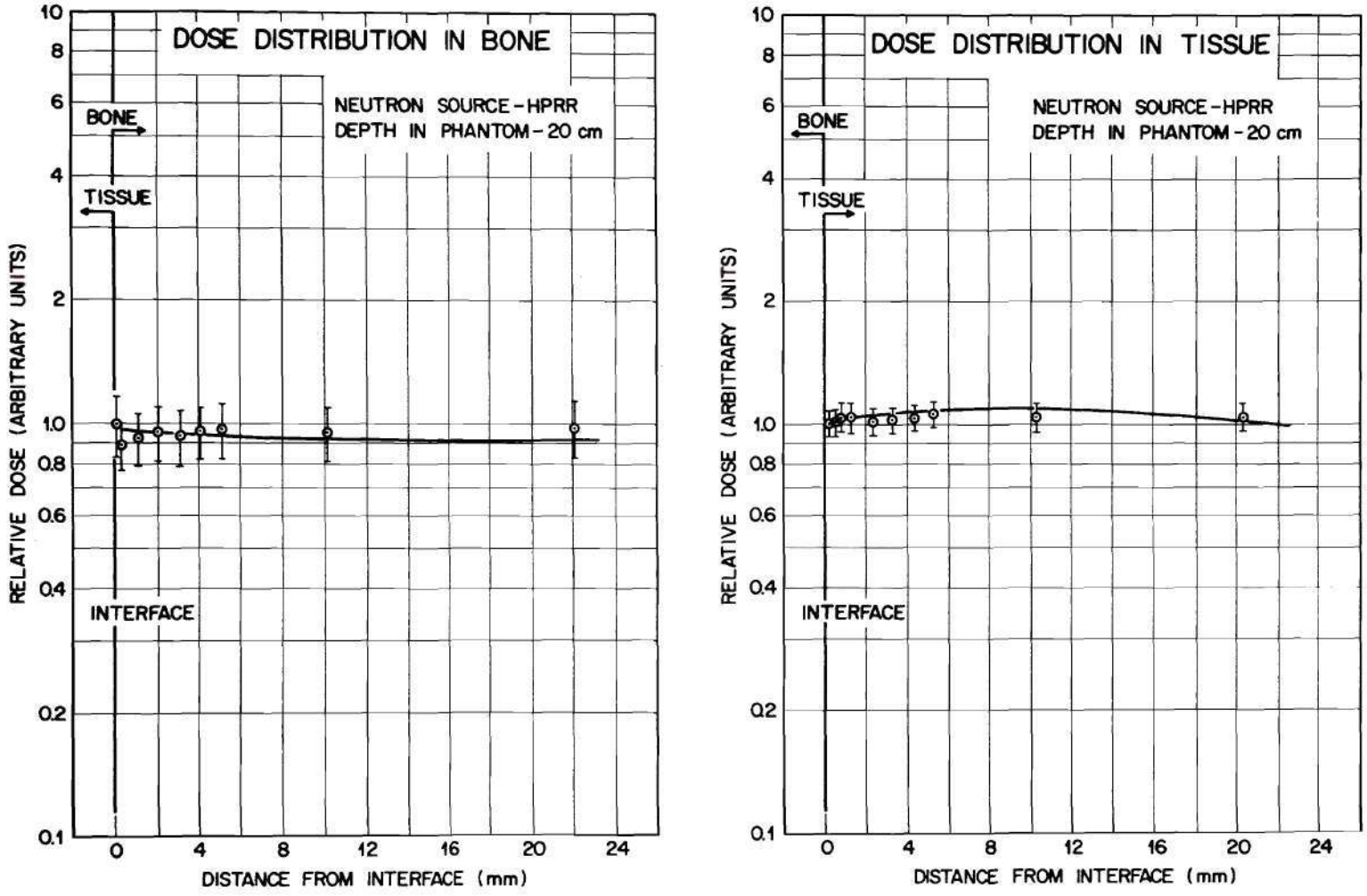

Figure 19. Dose Distributions at a Bone-Tissue Interface Due to Fission Neutrons (Depth 20 cm).

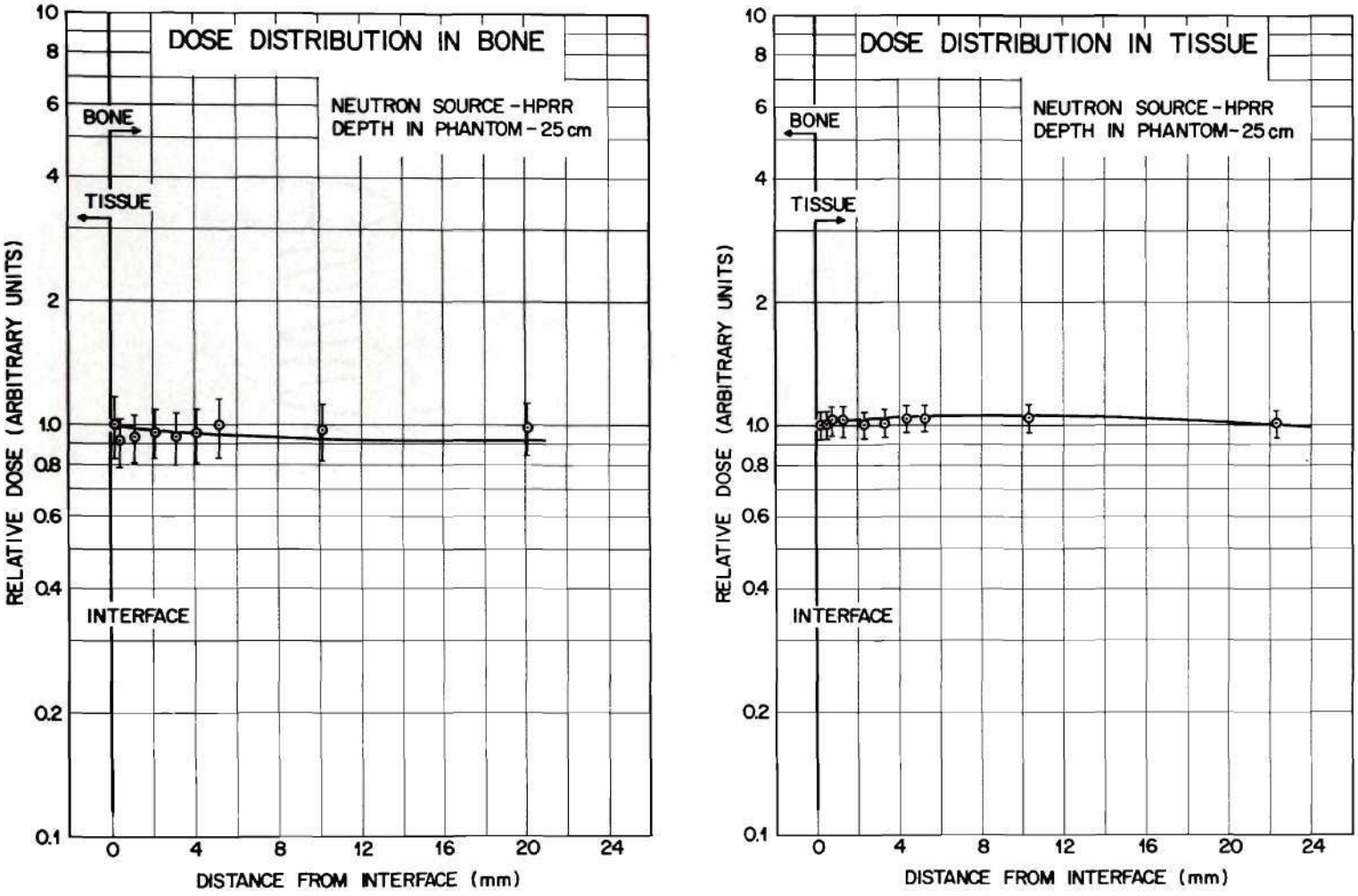

Figure 20. Dose Distributions at a Bone-Tissue Interface Due to Fission Neutrons (Depth 25 cm).

through the experimental points are simply to indicate the trends expected based on the previous discussions.

It is difficult to draw concrete conclusions from distributions such as these. The probable errors are about 7% for distributions in tissue and range up to about 17% in the measured distributions in bone. However, based on the plotted points and the knowledge of neutron and gamma-ray interactions, there are two general trends apparent in the data. First, in the case of the tissue-equivalent material, the data point nearest the interface is always the lowest in magnitude of all the measured data points. There appears to be an increase in dose of about 5 to 6% as one moves away from the interface into tissue. This change is essentially the same as the errors, and thus the significance of this trend is in question. Distributions measured in bone demonstrate a similar trend with the dose nearest the interface always greatest in magnitude than at other positions of measurement. Again, the same trend is seen, the decrease in magnitude is in the range 5 to 10% when moving away from the interface into the bone material. However, the situation is worsened by the fact that the errors are larger than the trend indicated.

By using Lawson's suggestion, a comparison of the results for fission neutrons can be made. The average energy of the HPRR leakage neutron spectrum is about 1.5 MeV.[108] By reducing the distance parameter according to the instructions by Lawson, one finds that the position of the maximum in the distribution occurs at 0.0029 cm in tissue and 0.0195 cm in bone. If the assumption is more correctly made that only one-half

of the neutron energy is transferred to the proton (i.e., assume 0.75 MeV rather than 1.5 MeV) the position of the maximum is further reduced to 0.0026 cm in tissue and 0.0172 cm in bone.

Thus, in considering the results of the measurements at the HPRR, the conclusion is reached that these distributions are of little value, since the techniques employed are not sensitive enough to detect the expected changes. The high voltage electrode on the front of each chamber had a thickness which was essentially the same as the distance over which the maximum change should occur. The tissue equivalent chamber had an electrode which was 0.025 cm thick, essentially one order of magnitude thicker than the region of change. The electrode used on the bone-equivalent chamber was thinner (0.011 cm), but only slightly thinner than the region of maximum change. Thus, even though the possibility of detecting a change near the interface exists, other parameters and sources of error in the experiment have probably negated the opportunity.

Similar arguments can be applied to all the measurements made in the bench test arrangement. In addition, the poor geometry of the arrangement, which was necessitated by the low neutron emission rates of the isotopic sources and the large number of gamma-rays emitted from the source material makes this data of questionable value and interest. Thus, although measurements on the bench provided valuable insight into the many parameters of the experiment, these data will not be presented here. The results from the bench tests are discussed in Appendix II.

The attempt to resolve the neutron- and gamma-radiation components in the radiation field employed a graphite chamber which has been

previously described. During these measurements, the graphite chamber was simply substituted for the tissue-or bone-equivalent chamber. Again, although the trends in the data were apparent, efforts to separate the radiation field into two components by solving a set of simultaneous equations[21] were unsuccessful. There were several possible explanations for this failure. First, in the case of a 14-MeV source, the gamma-component of the radiation field was small, measurements indicated about 4-6% of the total dose. Thus, the ionization current from the chamber was very small and difficult to measure accurately. In many cases, the measured current was only about twice the leakage current in the chamber.

A second effect, which has some bearing on this problem, has just recently been pointed out by Wall and Burke.[116] Results of measurements at interfaces using ^{60}Co gamma-radiation have shown a strong effect of beam direction on dose distributions at interfaces formed by two dissimilar materials. This effect has not been previously noted in the literature. The data of Wingate et al.,[24] although for lower energy photons, showed no effect on the shape or magnitude of the dose distributions due to change in beam direction. However, Wall and Burke report that the dose at a critical point can be changed by a factor of 1.5 simply by changing the beam direction.

In addition, the interposition of a third material (e.g., bone-equivalent plastic, tissue-equivalent plastic and graphite) causes the measured distribution to be some function of the distributions at the two interfaces formed by joining the three different materials. Further, this distribution will be influenced by the particular arrangement of

the materials (which is another method of changing the effective beam direction).

For the above reasons, the attempt to resolve the components of the dose distributions was abandoned. Consequently, the results of measurements with the graphite chamber will be presented and discussed in Appendix II.

Accelerator Exposures

Dose distributions near the interface resulting from a 14-MeV monoenergetic neutron source are shown in Figure 21. These results are essentially as expected; there is an increase in the dose as the interface is crossed from bone into tissue. The buildup is about 50% at a depth of 9-10 mm in the tissue. In the bone environment, there is a reduction of about 20% at a depth of 20 mm. Comparison of the results shown in Figure 21 to those of Lawson[10] shows that the magnitude of the buildup region (about 50%) is in fair agreement with the measured result. However, the position of the maximum increase appears to be at a distance of 0.9 to 1.0 cm in tissue.

In contrast, the calculated distribution in bone shows a decrease to about 30% of the interface value with a plateau at about 0.1 cm. The measured distribution in bone (Figure 21) shows a decrease to about 80% of the interface value at a depth in bone of approximately 2 cm and no true indication of any plateau or equilibrium region.

There are two possible explanations for the differences in the measured and calculated distributions. First, the ionization chambers are sensitive not only to neutron radiation but also to gamma-radiation.

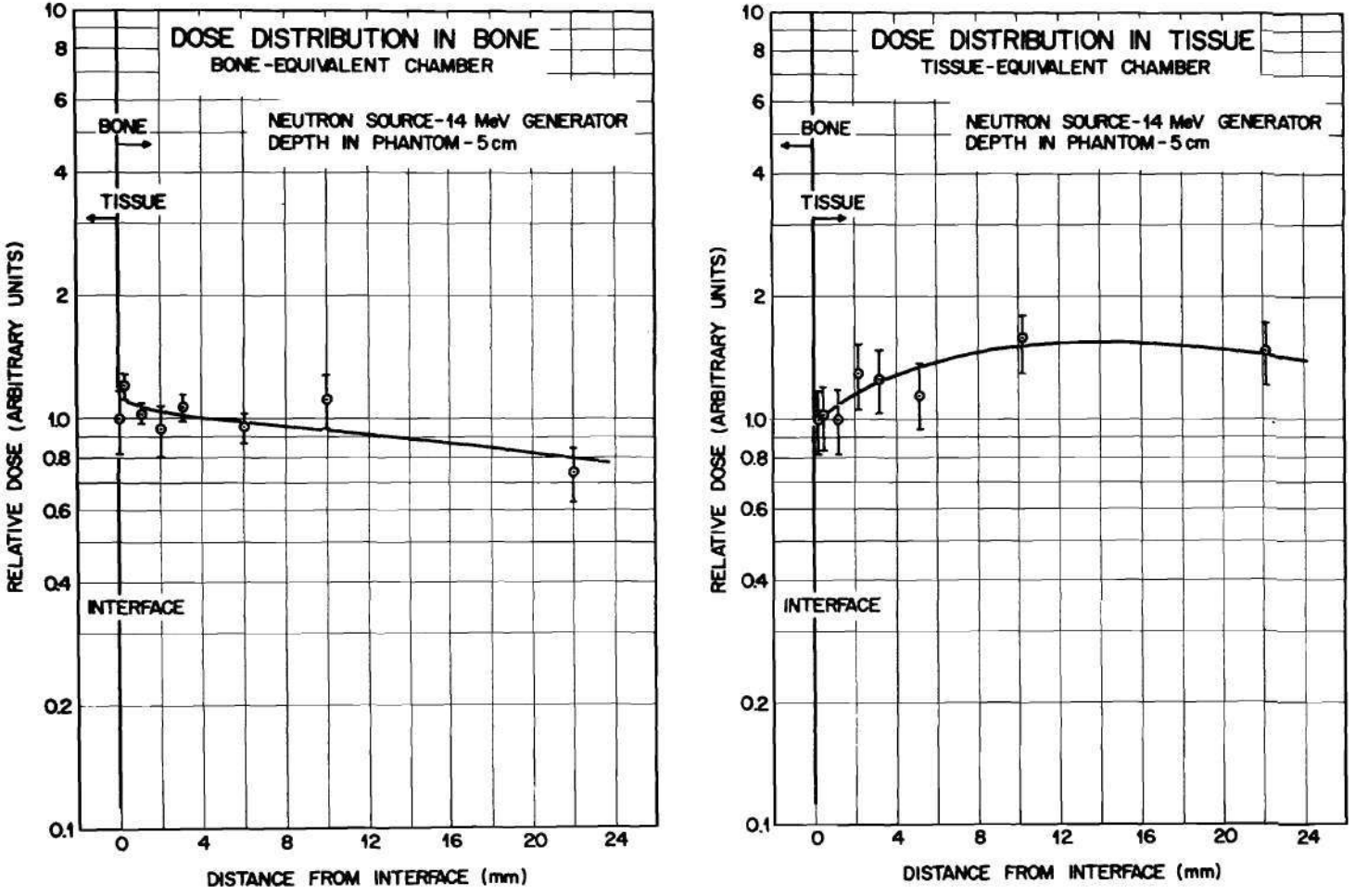

Figure 21. Dose Distributions at a Bone-Tissue Interface Due to 14-MeV Neutrons (Depth 5 cm).

Further, there is essentially equal sensitivity if one ignores the slight difference in the W-values for electrons and protons. Thus, the measured distributions, in contrast to those of Lawson, represent a summation of the distribution imposed on the region by neutron and gamma radiation.

The second point has to do with the method of normalization of the data points. All the distributions were normalized to the point closest to the interface. In retrospect, this appears to have been a poor choice. As previously stated, this point has the largest error in exact position, and, in general, the calculated probable error of this point is always larger than any of the other calculated errors. In addition, the calculation of Lawson indicates that the dose changes very rapidly as the distance from the interface is increased. Again, the thickness of the high voltage electrode does not allow measurements very near the interface. The change in the experimental results are computed in relation to the data point closest to the interface and not the value at the interface. Thus, normalization to the nearest point to the interface coupled with the inability to perform measurements very near the interface could cause large discrepancies when comparing magnitudes of measured and calculated values.

With the increased interest in the use of 14-MeV neutrons in neutron radiography and therapy, further discussion of this ionization chamber data will be presented here. Lawson[10] concluded from his calculation that the upper limit of the dose given to tissues in a heterogeneous environment is simply the dose in tissue in the absence of bone. Based on Lawson's calculations and the results of the research reported

here, depth-dose curves have been constructed to illustrate probable distributions at a bone-tissue interface located in a tissue equivalent phantom. Similar distributions have been constructed as illustrations of photon interactions and are published in textbooks on radiology.[4]

The left-hand part of Figure 22 shows measured and calculated depth-dose distributions from a 14-MeV source. The calculated points, from Auxier et al.[9] are for a broad beam of monoenergetic 14-MeV neutrons impinging on the front of a 30 x 60 cm cylindrical tissue phantom. These results include not only the proton recoil dose, but the contribution from the $^{1}H(n,\gamma)^{2}H$ reaction. The measured data points, by McGinley,[117] are the results of condenser-type, tissue-equivalent ion-chamber measurements in a 30-cm cubical phantom filled with tissue-equivalent liquid. These measurements were made under essentially the same exposure conditions as the reported research with the exception that no bone material was present in the phantom. The intent here is simply to establish the shape of the 14-MeV neutron depth-dose distribution in a homogeneous phantom.

Based on the shape of this curve, a heterogeneous depth dose curve has been constructed (see the right-hand portion of Figure 22). It is apparent that these curves are somewhat idealized; however, corrections have been applied to the data to account for some of the known phenomena. For example, the curves in bone have not only been reduced by the magnitude indicated by the data, but have been further reduced by the assumption that the attenuation of the radiation will be the same as the attenuation in tissue. In addition, the buildup factor (in tissue)

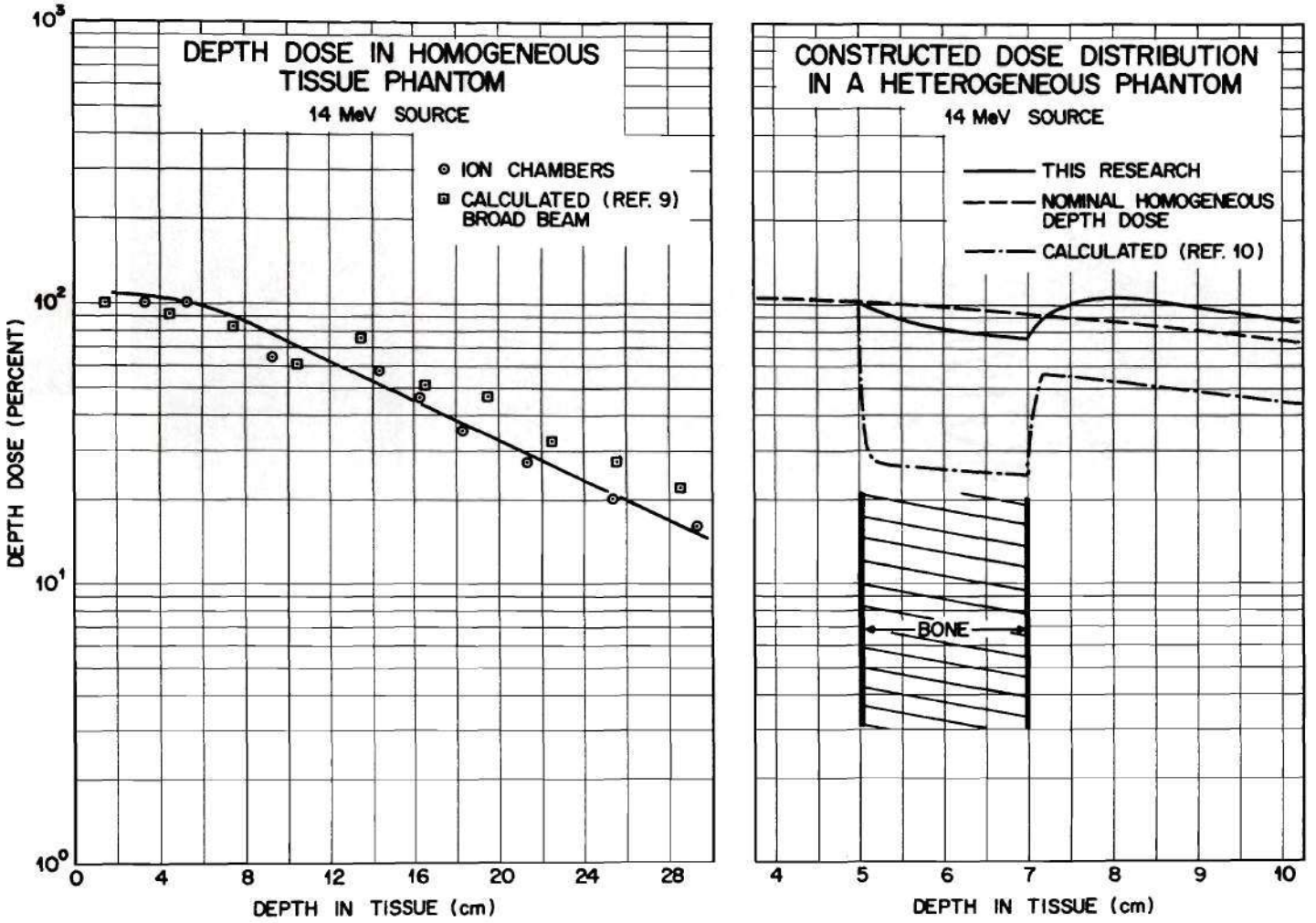

Figure 22. Comparison of Homogeneous Depth Dose Distribution from 14-MeV Neutrons and Idealized Distributions in a Heterogeneous Medium.

indicated by the results is applied to the attenuated value at the interface. No gain in the interface value is claimed for protons generated in tissue very near the interface which contribute to the dose on the bone side of the interface.

The conclusions from these constructed curves are important. Based on Lawson's calculations, the assumption that the upper limit of dose is simply the dose in the absence of bone is certainly valid. At almost every distance behind the bone-tissue interface, the dose can be seen to be about 60% of that indicated for the homogeneous case. However, based on the measured distributions at 14 MeV, the dose appears to be about 20% higher than that indicated by the homogeneous depth-dose curve. As has been discussed previously, the difficulty in the application of the measured results may lie in the normalization procedure. The point nearest the interface was chosen as the point of normalization. Lawson's data indicate a very large rapid change in the dose distribution near the interface. Thus the discrepancy in the magnitude of the measured and calculated changes could be attributed to the lack of the ability of measuring the distribution very near the interface. Therefore, it is difficult to conclude whether the indicated "gain" in dose in tissue behind the bone is real. It is not completely impossible, due to the reduction in the dose deposited in bone material, that the dose in tissue near the interface could be higher than indicated by the homogeneous depth dose curve, resulting in an increased dose deposition in the tissue at the rear of the bone over and above that indicated by the homogeneous depth dose curve. Further study of this phenomenon appears to be warranted.

Conclusions

At the conclusion of many research projects, the researcher must ask himself, "Did I accomplish what I set out to do?" Without exception, the answer to this question must be, "Yes, but...", or "No, but...". This research is a perfect example of the above.

The first task, the designing, fabrication, and checkout of a detector to measure dose distributions at a bone-tissue interface, was accomplished early in this research. After further investigations on radiation detectors and the utilization of the extrapolation ionization chamber in this project, there is no doubt that this technique is the preferred method. In fact, it appears that the extrapolation technique is the only method which is truly suitable for experimental investigation of these distributions.

The second task, the use of the detectors to measure dose distributions at bone-tissue interfaces, was also accomplished. However, this task was hampered by a number of experimental and physical problems. One of the major problems was that the detectors, because of the necessity of maintaining tissue and/or bone equivalence, were sensitive to both neutrons and gamma-rays. No satisfactory solution which would allow separation of these components of the radiation field was found.

The physical size of the high voltage electrode precluded, in some cases, the measurement of distributions near enough to the interface to provide meaningful data. This was especially apparent in the results of measurements at the HPRR. It is doubtful that this problem can be easily solved due to limitations on the minimum thickness of electrodes

which can be produced. In addition, the extreme fragility of the thicker electrodes indicate that thinner electrodes will not have the strength and durability to be of use. Many bone-equivalent electrodes developed tiny cracks, for no apparent reason, after attachment to the movable ring and storage in a desiccator for future use.

Comparison of these data to other existing experiments or calculations has been accomplished within the limitations of the experiment and the calculations. It is fair to say that there is no adequate treatment in the literature with which the data can be compared. The use of computers for Monte Carlo calculations directed toward solving this problem can still be important, but significant results will not be forthcoming until more detailed cross-section information (for elements such as calcium and phosphorus) become available. However, based on the 14-MeV neutron distributions, it can be concluded that there could be an advantage to neutron therapy due to the reduced deposition in bone and the buildup region in tissue shielded from the radiation beam by bone. This increase, coupled with the other advantages of neutron therapy (improved RBE and OER), point out the value and the need for further research in the use of 14-MeV neutrons in therapy.

Recommendations

In reviewing this research, a number of recommendations for improvements and extension of this work are apparent.

In the case of the detectors, several comments seem necessary. First, due to the limited intensity of most available neutron sources, only the chambers with the largest collecting electrodes were employed

in the measurements. It is recommended that chambers with larger collecting electrodes be fabricated for more accurate assessment of the interface dose distributions.

Due to the inherent problems involved in measuring small ionization currents, often at points far removed from the laboratory, improvements in the measuring systems are necessary. It is recommended that two methods be investigated. First, a voltage-to-frequency converter coupled to an electrometer located very near the detector could facilitate data accumulation and analysis. Such a device would provide a pulse of a fixed magnitude which could be routed large distances to a readout device. One readily available and easily used readout device is a timer-scaler unit. By use of this unit, the signal is effectively integrated as a function of time. This should provide increased reliability in the measurements and also allow the application of typical pulse counting statistical analysis to the data.

Secondly, the conversion of the ionization chambers to pulse - ionization chambers is recommended. Again, the advantages in routing, accumulation, storage and manipulation of the signals afforded by pulse techniques are strong reasons for any effort expended toward this goal. As previously stated, the use of pulse techniques allows the application of well-known statistical techniques to the accumulated data.

A change in the phantom to a more realistic geometry, such as a cylindrical or elliptical phantom, is recommended. However, it should be pointed out that at present the cubical phantom is still the only geometry recommended in any of the ICRP publications. In addition, the

use of more realistic geometry for the bone is recommended. The solid piece of bone-equivalent material was intended to be only a first approximation primarily dictated by the design of the detectors and the available materials.

An increase in source intensity, especially in the 14-MeV work, is highly desirable. This requirement has been known for several years, and many research projects are under way attempting to solve this problem. An increase in source intensity and target life-time would have allowed not only more accurate measurements but also increased the number of positions in the phantom at which measurements could be made. In addition, the entire experiment could have been moved to a more important source-to-detector separation, for instance, 1.25 meters.

Finally, it is recommended that these investigations be continued in order to determine more precisely the magnitude of the effect of bone-tissue interfaces upon dose distributions. Experimentally, it is apparent that only distributions due to a 14-MeV neutron source can be measured effectively. Fortunately, this source is the most important and interesting because of its importance for neutron therapy.

Calculations, such as Monte Carlo investigations, have been hampered by the lack of adequate cross-section values for elements such as calcium, phosphorus and magnesium which are present at high percentages in bone. In addition, the fine structure necessary to correlate with experimental results has not been achieved due to inherent limitations in Monte Carlo techniques. It is recommended that calculations be undertaken which are designed to overcome the obvious deficiencies in previous calculations. These deficiencies have been discussed previously.

APPENDIXES

APPENDIX I

CALIBRATION FACTORS FOR EXTRAPOLATION IONIZATION CHAMBERS

The detailed calibration procedure has been discussed previously in the main text. The primary objectives of this calibration were two-fold: First, calibration of these detectors in terms of absorbed dose per unit ionization current and secondly, to facilitate the separation of the two components of the radiation field. To accomplish the second goal required the exposure of the detectors to a high intensity gamma-radiation field and a neutron source with relatively little gamma-ray contamination.

Dose conversion factors were determined at each electrode gap spacing; the resulting curve was extrapolated to zero gap-spacing to determine the factor to be applied to the extrapolated ionization current from a series of measurements. The extrapolated conversion factors from the gamma-ray calibration were:

Tissue-Equivalent Chamber - 1.431×10^{-11}

Bone-Equivalent Chamber - 0.545×10^{-11}

Graphite Chamber - 1.695×10^{-11}

Units on these factors are amperes/rad/minute.

Based on these constants and exposure of the chambers to a 14-MeV neutron source, parameters for solving simultaneous dose equations were derived. After correcting the measured ionization current for the appropriate gamma contamination, it was assumed that the response of

graphite chamber to the gamma source would be taken as unity, and the ratio of the response of each chamber to this chamber would be taken. The results are as follows:

	Γ-Factor	N-Factor
Tissue-Equivalent Chamber -	0.845	0.361
Bone-Equivalent Chamber -	0.322	0.110
Graphite Chamber -	1.00	0.187

Thus, based on these results, the equations for calculating dose become:

$$T = 0.361\ N + 0.845\ \Gamma$$

$$B = 0.110\ N + 0.322\ \Gamma$$

$$C = 0.187\ N + 1.00\ \Gamma$$

where T, B, and C represent the dose measured by the tissue-equivalent, bone-equivalent, and graphite ionization chambers, respectively. The parameters N and Γ are the neutron and gamma doses.

APPENDIX II

DOSE DISTRIBUTIONS RESULTING FROM ISOTOPIC NEUTRON SOURCES

This appendix is intended to present results of measurements of dose distributions resulting from several isotopic neutron sources. These results are separated from the main text for reasons given in the section entitled "Reactor Exposures and Bench Tests". The experiment arrangement, source intensity, and general procedure also have been discussed in the main text.

Measurements were made inside the moderator (see Figure 15) employing the tissue-equivalent, the bone-equivalent, and the graphite extrapolation ionization chambers and several isotopic neutron sources. Dose distributions resulting from an ^{241}AmBe neutron source are shown in Figures 23 and 24. The distributions measured with the bone-equivalent and tissue-equivalent chambers are given in Figure 23. These distributions appear to be as expected based on general trends, but the reduction in relative dose as a function of depth in the bone material is difficult to explain. The situation is further confused by the results from measurements with the graphite chamber, see Figure 24. The results from the graphite chamber show a buildup in tissue similar to the results measured with the tissue-equivalent chamber. In the bone material, there is a reduction of dose with respect to distance into bone, but this reduction is not as pronounced as the reduction measured with the bone-equivalent chamber.

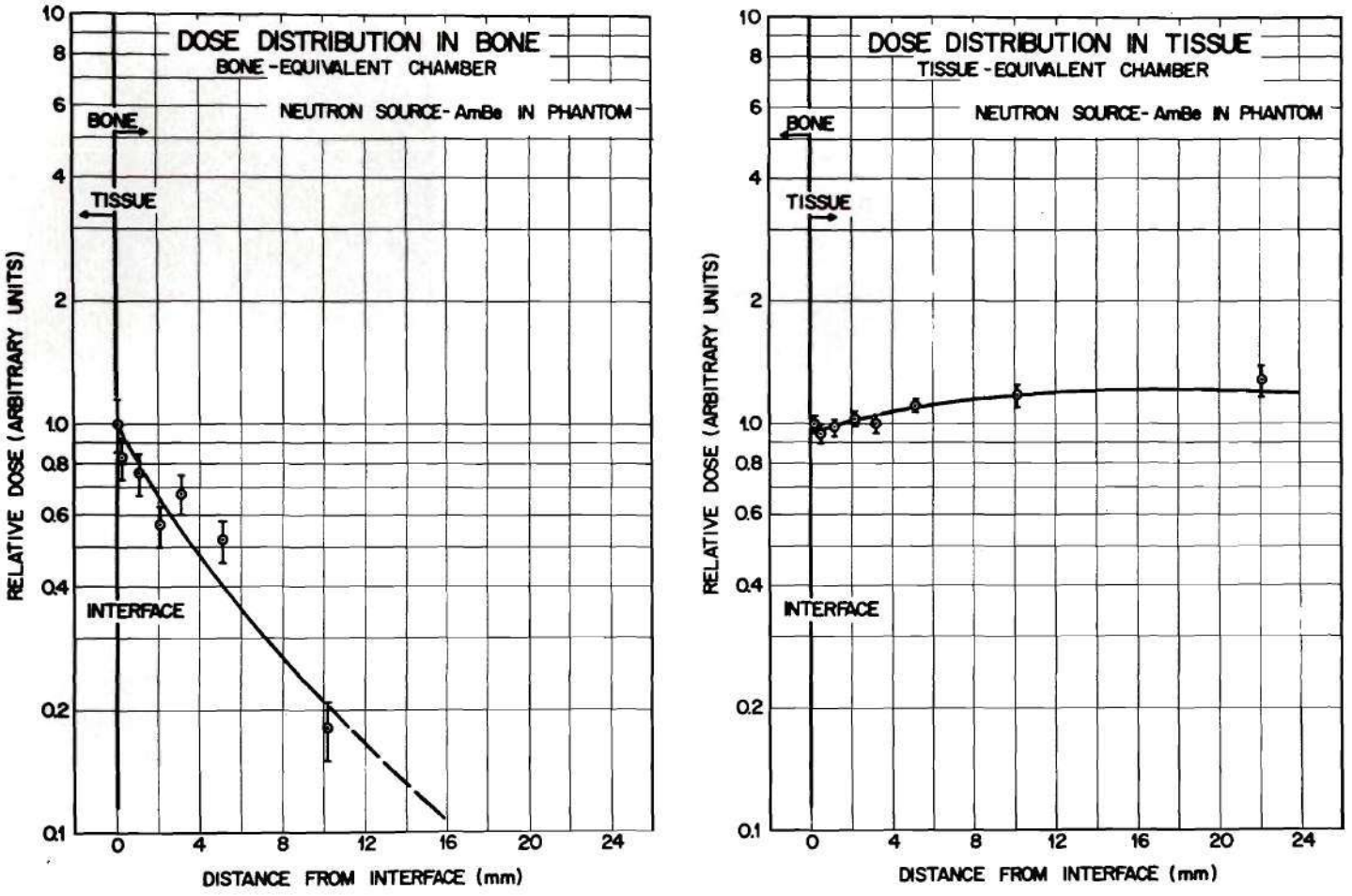

Figure 23. Dose Distributions at a Bone-Tissue Interface Due to Neutrons from an AmBe Source.

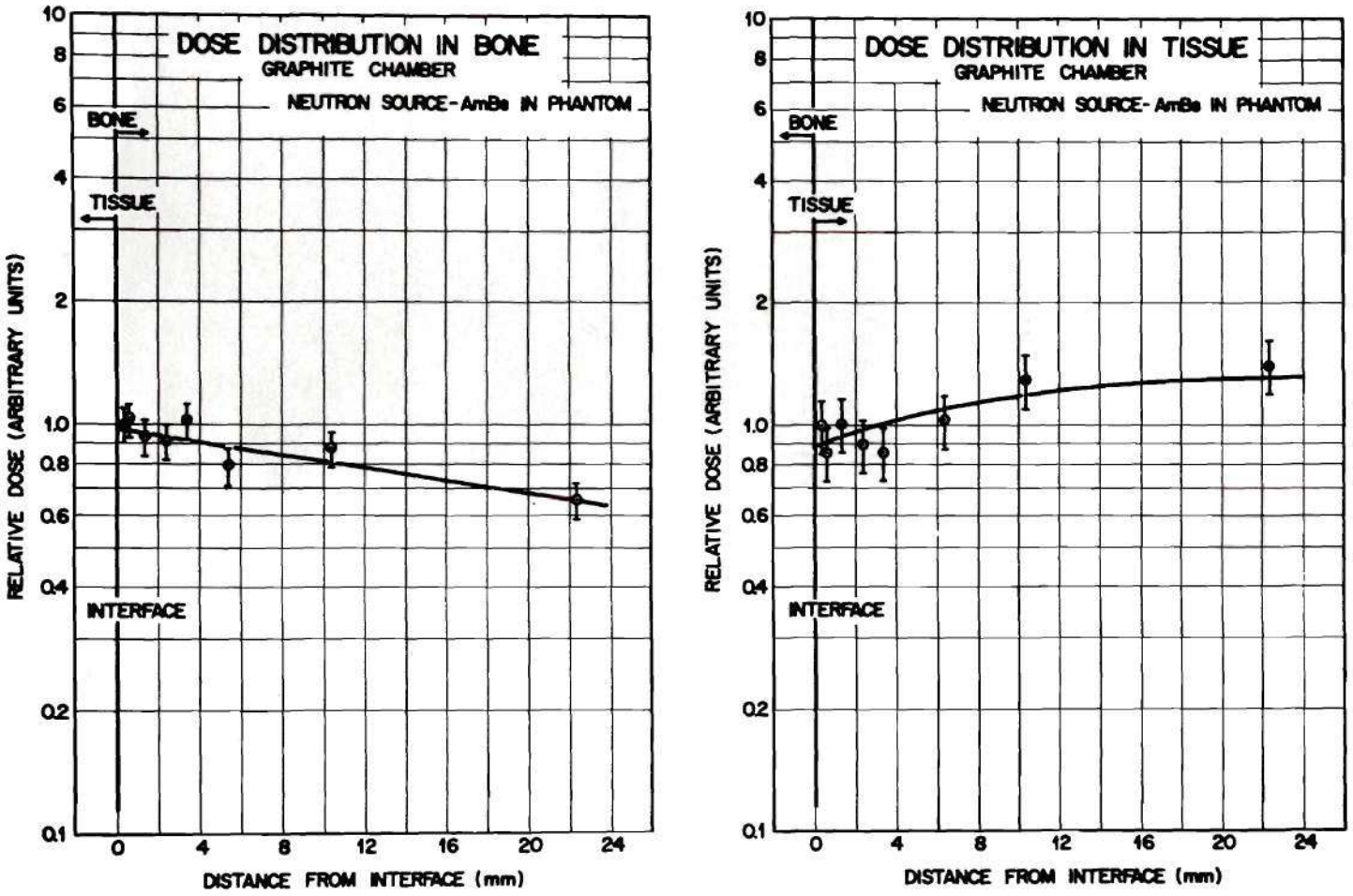

Figure 24. Dose Distributions at a Bone-Tissue Interface Due to an AmBe Source (Graphite Chamber).

One of the most likely explanations for these anomalies is the sensitivity of the chambers to neutron and gamma radiation. The tissue-equivalent and bone-equivalent chambers have essentially equal sensitivity to neutron and gamma radiation. In addition, the neutron sensitivity of the graphite chamber is above 25% for an average neutron energy in the range of 4 MeV.

A second factor which contributes to this confusion is the unknown gamma component of dose for these measurements. An inspection of available data on isotopic neutron sources indicates that there are more than 13 different gamma-rays emanating from this source with photon energies up to 4.43 MeV. Drake et al.[118] have presented results which show that the emission rate of 4.43 MeV gamma-rays from an α-Be source is about 0.5 gamma-rays per neutron. However, most of the gamma-rays emitted from the source material (and daughter products) are in the region of 1 to 300 keV. It is extremely difficult to predict the distribution due to these mixed neutron-gamma radiation fields. Similar statements can be made about the other sources, ^{241}AmB and ^{239}PuBe.

The recent results of Burke and Wall[116] have been discussed in the text. These results indicate that the shape of the dose distribution at an interface is dependent upon the beam direction and the effective atomic number of the materials forming the interface. Further, the use of three materials (e.g., tissue, bone, graphite) can easily impose a distribution near the interface which is a composite of at least two distributions. This composite is dependent upon the arrangement of the materials (another way of changing beam direction), the atomic number of the materials, and the energies of the gamma-ray source used in the experiment.

Dose distributions in tissue and bone material due to neutrons and gamma-rays from an ^{241}AmB are shown in Figure 25. Results of measurements with the graphite chamber employing the same source are presented in Figure 26. Again similar trends in the distributions are apparent. The gamma rays emitted by the source are identical to the emissions from the ^{241}AmBe with the exception for the 4.43 MeV gamma-ray which is not present when boron is substituted for beryllium in the source matrix. The average neutron energy for this source is about 3 MeV.

Dose distributions at a bone-tissue interface due to a ^{239}PuBe neutron source are presented in Figure 27. In the tissue region, there is an apparent buildup region and a corresponding decrease in dose in the bone material. Based on the previous discussions, measurements with the graphite chamber for this source were not attempted. The gamma-ray emissions are quite similar to those discussed for the ^{241}AmBe source. The average neutron energy is about 4.4 MeV; however, the dose distributions are not very similar to those reported for ^{241}AmBe neutrons.

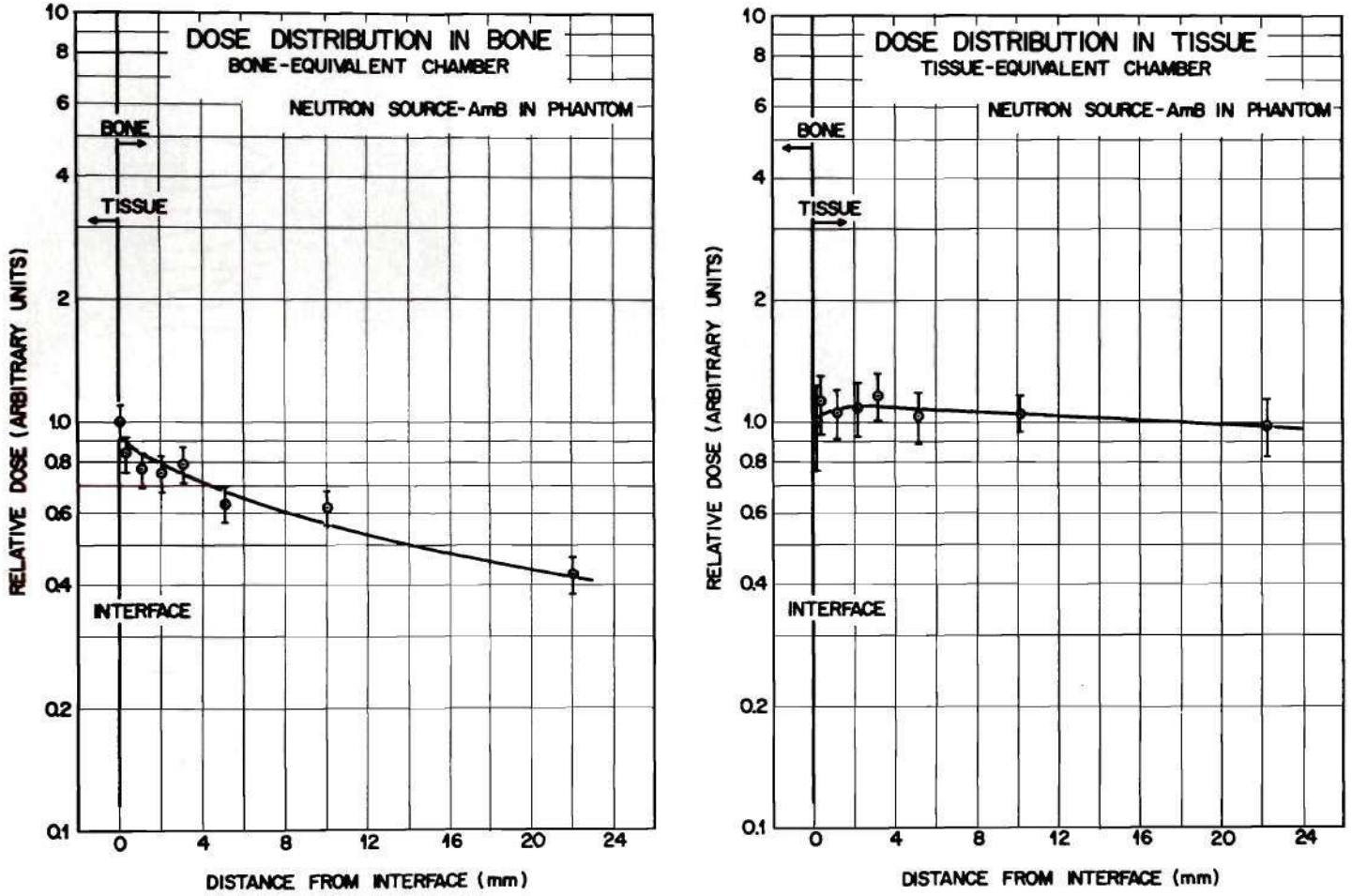

Figure 25. Dose Distributions at a Bone-Tissue Interface Due to Neutrons from an AmB Source.

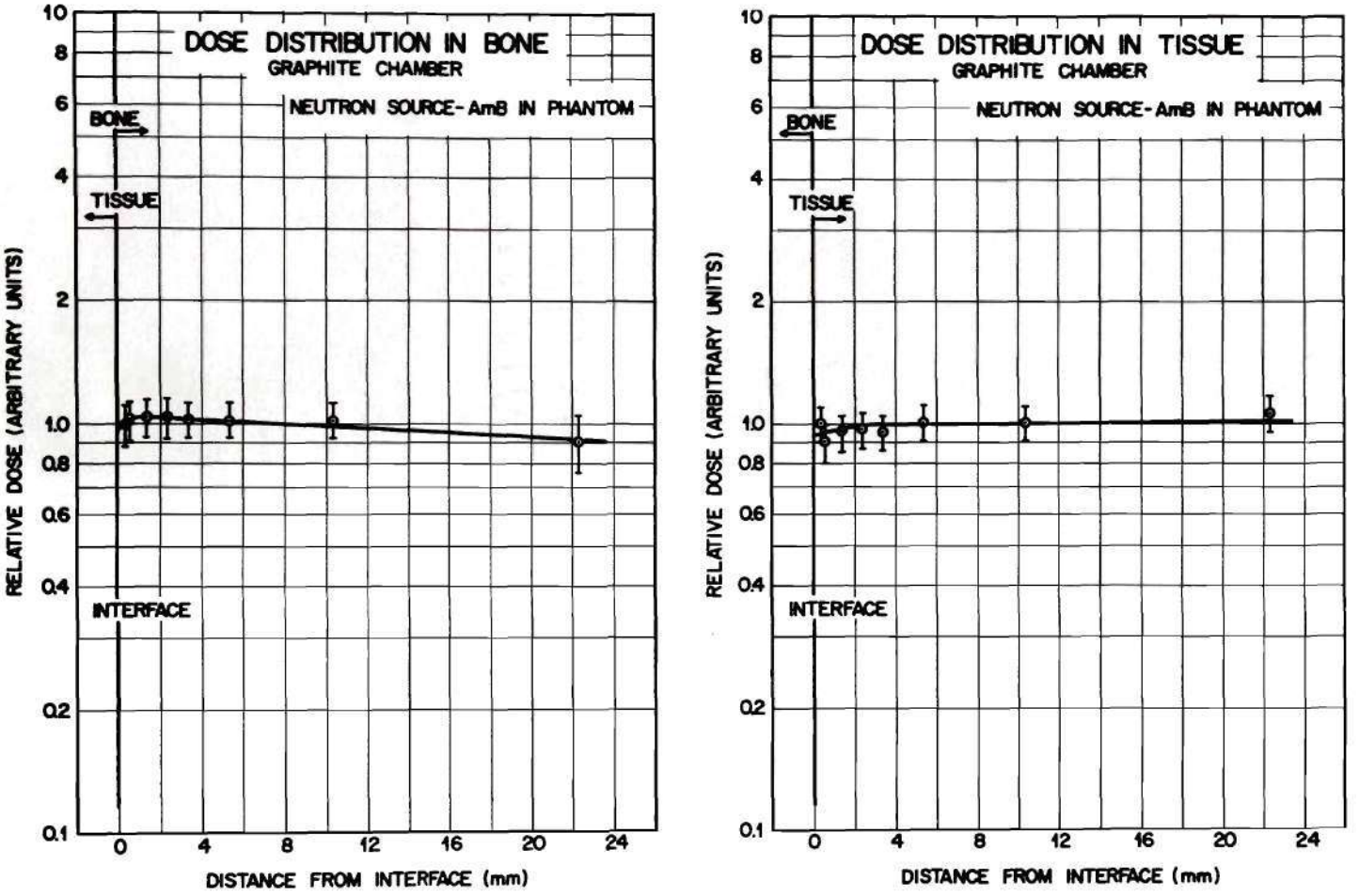

Figure 26. Dose Distributions at a Bone-Tissue Interface Due to an AmB Source (Graphite Chamber).

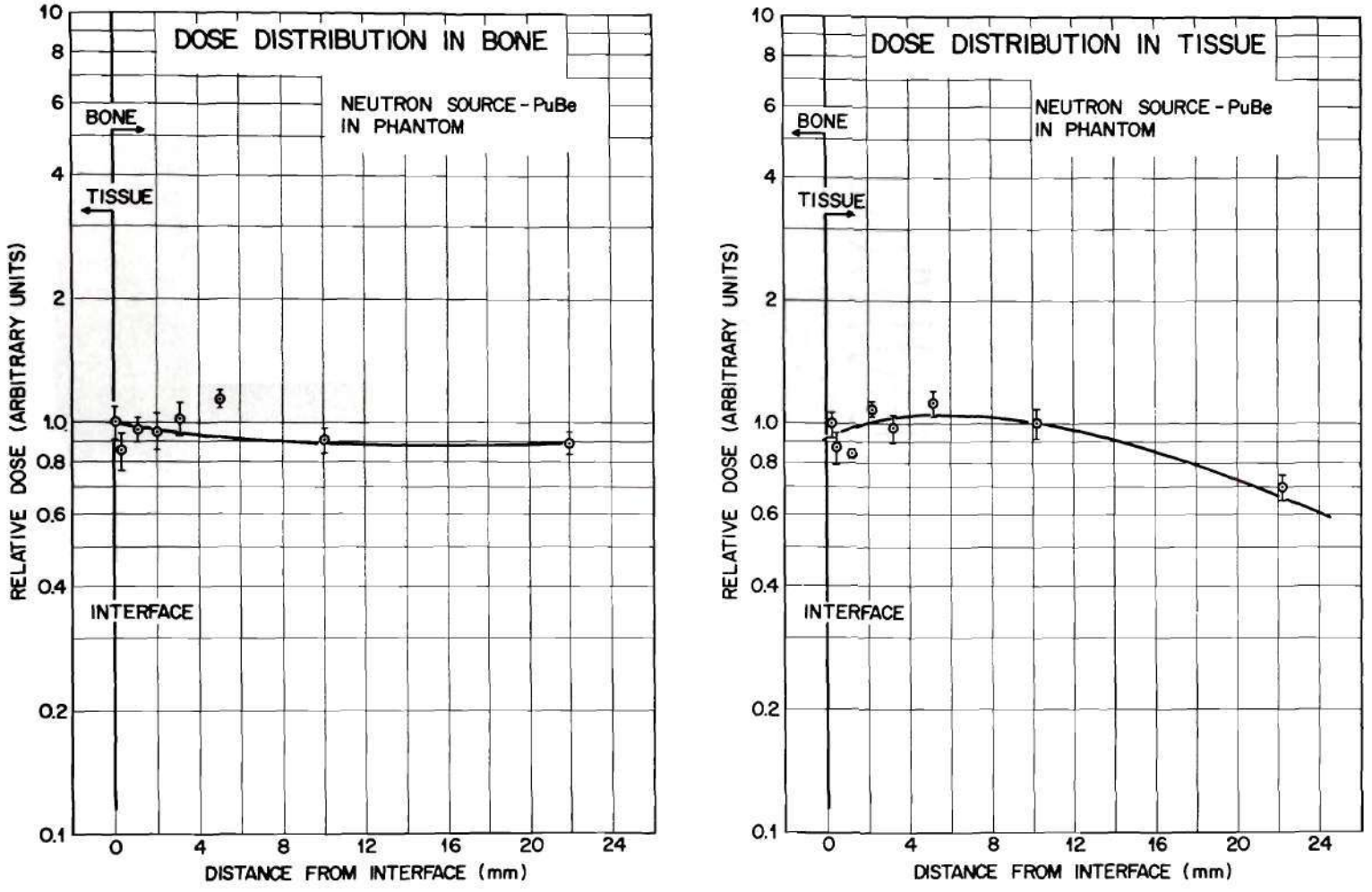

Figure 27. Dose Distributions at a Bone-Tissue Interface Due to Neutrons from a PuBe Source.

BIBLIOGRAPHY*

1. O. Glasser, E. H. Quimby, L. S. Taylor, J. L. Weatherwax, and R. H. Morgan, Physical Foundations of Radiology, 3rd Edition, Paul B. Hoeber, Inc., New York, 1961.

2. D. J. Pizzarello and R. L. Witcofski, Basic Radiation Biology, Lea and Febiger, Philadelphia, 1967.

3. W. D. Claus, ed., Radiation Biology and Medicine, Addison-Wesley Publishing Co., Inc., Reading, Mass., 1958.

4. H. E. Johns, The Physics of Radiology, 2nd Edition, Charles C. Thomas, Springfield, Ill., 1964.

5. F. W. Spiers, "Transition Zone Dosimetry," Chapter in Radiation Dosimetry, Vol. III, Academic Press, New York, 1970.

6. J. F. Fowler, "Neutrons in Radiotherapy: Slow Neutrons, Fast Neutrons and Other Heavy Particles," Biological Effects of Neutron and Proton Irradiations, Vol. II, 185-214, IAEA Vienna, (1964).

7. J. P. Barton and J. L. Boutaine, "Initial Development of Neutron Radiography in France," Isotopes and Radiation Technology 5, No. 3, 214-218 (1968).

8. J. P. Barton, "Neutron Radiography Using Nonreactor Sources," Isotopes and Radiation Technology 6, No. 2, 149-153 (1968-69).

9. J. A. Auxier, W. S. Snyder, and T. D. Jones, "Neutron Interactions and Penetration in Tissue," Chapter in Radiation Dosimetry, Vol.I, F. H. Attix and W. G. Roesch, eds., Academic Press, New York, 1968.

10. R. C. Lawson, "The Recoil Proton Dose at a Bone-Tissue Interface Irradiated by Fast Neutrons," Physics in Medicine & Biology 12, 551-554 (1967).

11. J. E. Turner, V. E. Anderson, H. A. Wright, W. S. Snyder, and J. Neufeld, "Radiation Dose from High-Energy Nucleons in Targets Containing Soft Tissue and Bone," Radiation Research 35, 596-611 (1968).

---

*The format used for this Bibliography is that required by the Oak Ridge National Laboratory.

12. T. F. Budinger, R. J. Howerton, and E. F. Plechaty, "Neutron Radiography and Dosimetry in Humans," Second Symposium on Accelerator Radiation Dosimetry and Experience, SLAC, Nov. 1969.

13. W. S. Snyder, personal communication.

14. "Measurement of Absorbed Dose of Neutrons, and of Mixture of Neutrons and Gamma Rays," National Bureau of Standards Handbook 75, U.S. Dept. of Commerce, 1961.

15. S. Glasstone and A. Sesonske, Nuclear Reactor Engineering, D. Van Nostrand Co., Inc., Princeton, N. J., 1967.

16. W. H. Wilkie, "Theoretical Modulation Transfer Functions and Dosimetry for Fast-Neutron Radiography," Thesis, Georgia Institute of Technology, Atlanta, Georgia, May, 1970.

17. D. Nachtigall, "Average and Effective Energies, Fluence-Dose Conversion Factors and Quality Factors of the Neutron Spectra of Some (α,n) Sources," Health Physics 13, 213-219 (1967).

18. "Physical Aspects of Irradiation," NBS Handbook 85, U.S. Department of Commerce, 1964.

19. H. H. Rossi, G. S. Hurst, W. A. Mills, and H. E. Hungerford, Jr., "Intercomparison of Fast Neutron Dosimeters," Nucleonics 13, No. 4, 46 (1955).

20. R. H. Ritchie, "The Physical Basis of Radiation Dosimetry," Chapter in Principles of Radiation Dosimetry, Morgan and Turner, eds., John Wiley and Sons, Inc., New York, 1967.

21. H. H. Rossi and G. Failla, "Tissue-Equivalent Ionization Chambers," Nucleonics 14, No. 2, 32-37, (1956)

22. G. Failla, "The Measurement of Tissue Dose in Terms of the Same Unit for All Ionizing Radiations," Radiology 29, 202-215 (1937).

23. J. W. Boag, "Ionization Chambers," Chapter in Radiation Dosimetry, Vol. II, Attix and Roesch, eds., Academic Press, New York, 1966.

24. C. L. Wingate, W. Gross, and G. Failla, "Experimental Determination of Absorbed Dose from X-rays Near the Interface of Soft Tissue and Other Material," Radiology 79, 984-999 (1962).

25. R. E. Simpson, E. Tochilin, and N. Goldstein, "Neutron and Gamma-Ray Dosimetry in an Animal Exposure Volume at a Pulsed Triga Reactor, Health Physics 9, 1021-2030 (1963).

26. K. C. Humphreys, ed., Neutron and Gamma Dosimetry Measurements at Walter Reed Army Institute of Research, E.G.&G. S-324-R (1966).

27. G. S. Hurst, "An Absolute Tissue Dosimeter for Fast Neutrons," British Journal of Radiology 27, 353 (1954).

28. E. B. Wagner and G. S. Hurst, "Advances in the Standard Proportional Counter Method of Fast Neutron Dosimetry," Review of Scientific Instruments 29, 153 (1958).

29. H. H. Rossi and W. Rosenzweig, "Measurements of Neutron Dose as a Function of Linear Energy Transfer," Rad. Res. 2, 417-425 (1955).

30. H. H. Rossi and W. Rosenzweig, "A Device for the Measurement of Dose as a Function of Specific Ionization," Radiology 64, 404 (1955).

31. F. W. Chambers, Jr., Georgia Institute of Technology, private communication.

32. J. E. Turner, R. D. Birkhoff, V. E. Anderson, and D. R. Johnson, "Unfolding of LET Spectra from Pulse Height Measurements," Health Physics Society, 14th Annual Meeting, Pittsburgh, Pa., June, 1969.

33. D. E. Watt, R. C. Lawson, and D. M. Clare, "An Experimental Appraisal of the Validity of Neutron Dosimetry Theory *in Radiation Protection*," Neutron Monitoring, 27-40, IAEA, Vienna, 1967.

34. M. O. Thurston, J. M. Swartz, R. R. Speers, and W. O. Closser, "A Silicon Fast-Neutron Dosimeter with a Wide Sensitivity Range," Neutron Monitoring, 245-252, IAEA, Vienna, 1967.

35. J. A. Auxier et al., Neutron Accident Dosimeter Intercomparison Study, ORNL-3849, part IV, 172-175 (1965).

36. F. H. Attix, ed., Luminescence Dosimetry, AEC Symposium Series No. 8, Division of Technical Information, Washington, D.C., 1967.

37. Solid State and Chemical Radiation Dosimetry in Medicine and Biology, IAEA, Vienna, 1967.

38. K. Becker and E. M. Robinson, "Integrating Dosimetry by Thermally Stimulated Exoelectron (After-) Emission," Health Physics 15, 463-466 (1968).

39. J. A. Auxier et al., Dosimetry by Thermally Stimulated Exoelectron Emission, ORNL-4316, part IV, 246-249 (1968).

40. W. C. Roesch and F. H. Attix, "Basic Concepts of Dosimetry," Chapter in Radiation Dosimetry, Vol. I., Attix and Roesch, eds. Academic Press, New York, 1968.

41. "Radiation Quantities and Units," Report 10a of the International Commission on Radiological Units and Measurements, National Bureau of Standards (U.S.) Handbook 84. 1962.

42. R. E. Zirkle, Journal of Cellular and Comparative Physiology 39 Suppl. No. 1, 75 (1952).

43. J. W. Boag, "Ion Density for Fast Neutrons in Water," Rad. Res. 1, 323-341 (1954).

44. H. H. Rossi, "Microscopic Energy Distribution in Irradiated Matter," Chapter in Radiation Dosimetry, Vol. I, Attix and Roesch, eds., Academic Press, New York, 1968.

45. W. Rosenzweig and H. H. Rossi, "Determination of the Quality of the Absorbed Dose Delivered by Monoenergetic Neutrons," Rad. Res. 10, 532-544 (1959).

46. W. S. Snyder, "The LET Distribution of Dose in Some Tissue Cylinders," Biological Effects of Neutron and Proton Irradiations, Vol. I, 3, IAEA Vienna, 1964.

47. T. D. Jones, W. S. Snyder, and J. A. Auxier, "Dose and LET Distributions in a Man Equivalent Cylinder Due to a Collimated Beam of Monoenergetic Neutrons," Annual Meeting of Health Physics Society, Pittsburgh, Pa. (June, 1969).

48. R. C. Lawson and D. E. Watt, "The LET Distribution of the Recoil Proton Dose from DD and DT Neutrons," Phys. Med. Biol. 12, 217-228 (1967).

49. R. C. Lawson and D. E. Watt, "The LET Distribution of the Recoil Proton Dose from Poly-energetic Neutron Sources," Phys. Med. Biol. 13, 619-626 (1968).

50. W. C. Roesch, "Dose for Nonelectronic Equilibrium Conditions," Rad. Res. 9, 399 (1958).

51. Frank H. Attix, "The Meanings of First Collision Dose," Health Physics 12, 793-799 (1966).

52. Harald H. Rossi, "Absorbed Dose Versus Kerma," Health Physics 11, 779-780 (1965).

53. J. A. Auxier, "Kerma Versus First Collision Dose: The Other Side of the Controversy," Health Physics 17, 342-343 (1969).

54. H. G. Ebert, ed., "Proceedings of the Symposium on Microdosimetry," Ispra, Italy, Nov. 13-15, 1967.

55. H. G. Ebert, ed., "Second Symposium on Microdosimetry, Stresa, Italy, October 20-24, 1969.

56. Radiological Health Handbook, 190, U.S. Dept. of Health, Education, and Welfare, 1960.

57. "Protection Against Neutron Radiation Up to 30 Million Electron Volts," NPS Handbook 63, U.S. Dept. of Commerce, 1957.

58. J. J. Ritts, E. Solomito, and P. N. Stevens, Calculations of Neutron Fluence-to-Kerma for the Human Body, ORNL-TM-2079 (1968).

59. Isabel H. Tipton, Elemental Composition of Total Body and Certain Tissues, ORNL-4446, part V., Oct., 1969.

60. L. J. Goodman, "A Modified Tissue Equivalent Liquid," Health Physics 16, 763 (1969).

61. F. R. Shonka, J. E. Rose, and G. Failla, "Conducting Plastic Equivalent to Tissue, Air, and Polystyrene," in Progress in Nuclear Energy, Series XII, Vol. I, 160-166, Pergamon Press, New York, 1959.

62. F. S. Williamson and P. Mitacek, Jr., "Calculations of Kerma Due to Fast Neutrons in Tissue-Like Materials," in Neutron Monitoring, 17-26, IAEA, Vienna, 1967.

63. M. L. Randolph, "Energy Deposition in Tissue and Similar Materials by 14.1 MeV Neutrons," Rad. Res. 7, 47-57 (1957).

64. J. A. Auxier and W. S. Snyder, The Calculation of Kerma as a Function of Neutron Energy, ORNL-4168, 223-225 (1967).

65. A. A. Maximow and W. Bloom, A Textbook of Histology, 6th Edition, W. B. Saunders Co., Philadelphia, 1952.

66. Helen Q. Woodard, "The Elementary Composition of Human Cortical Bone," Health Physics 8, 513-517 (1962).

67. H. Q. Woodward and E. Holodny, "A Summary of the Data of Mechanik on the Distribution of Human Bone Marrow," Phys. Med. Biol. 5, 57 (1960).

68. R. E. Ellis, "The Distribution of Active Bone Marrow in the Adult" Phys. Med. Biol. 5, 255 (1961).

69. D. E. Charlton and D. V. Cormack, "Energy Deposition in Finite Cavities," Rad. Res. 17, 34-49 (1962).

70. Neutron Fluence, Neutron Spectra and Kerma, ICRU Report 13, Sept., 1969.

71. P. Capron, M. Faes, and G. C. Tavernier, "Tolerance Flux of Thermal Thermal Neutrons," Nature 163, 129 (1949).

72. J. S. Mitchell, "Provisional Calculation of the Tolerance Flux of Thermal Neutrons," Brit. J. Radiol 20, 79-82 (Feb., 1947).

73. W. S. Snyder, "Calculations of Maximum Permissible Exposure to Thermal Neutrons," Nucleonics 6, 46-50 (1950).

74. J. S. Mitchell, "Provisional Calculation of the Tolerance Flux of Fast Neutrons," Brit. J. Radiol. 20, 177-180 (1947).

75. J. H. Tait, "Calculation of the Energy Deposition by Fast Neutrons in Soft Tissue," Brit. J. Radiol. 23, 282-286 (1950).

76. W. S. Snyder and J. Neufeld, "Calculated Depth Dose Curves in Tissue for Broad Beams of Fast Neutrons," Brit. J. Radiol. 28, 342-350 (1955).

77. A. M. Kogan, G. G. Petrov, L. A. Chudov, and P. A. Yampolski, "The Neutron Tissue Dose," Atomnaya Energiva 7, 351-362 (1959).

78. Neda Stipčić, "Experimental Determination of the Neutron Radiation-Dose Distribution in the Human Phantom," in Neutron Monitoring, 57-62, IAEA, Vienna, 1967.

79. W. E. Kinney and C. D. Zerby, Calculation of Dose in Tissue Due to Nucleons Below 400 MeV, ORNL-3499, Vol. II (1963).

80. D. C. Irving, R. G. Alsmiller, Jr., and H. S. Moran, "Tissue Current-to-Dose Conversion Factors for Neutrons with Energies from 0.5 to 60 MeV," Nuclear Instruments and Methods 51, 129-135 (1967).

81. W. S. Snyder, J. A. Auxier, M. D. Brown, T. D. Jones, and R. T. Boughner, "Distribution of Dose and Dose Equivalent in an Anthropomorphic Phantom Resulting from Broad-Beam Sources of Monoenergetic Neutrons," Transactions of the American Nuclear Society 9, No. 2 (1966).

82. J. A. Auxier et al., Distribution of Dose and Dose Equivalent in a Cylindrical Tissue Phantom from Fission Sources of Neutrons ORNL-3849, part IV, 166-171 (1965).

83. J. A. Auxier et al., Depth Dose Studies, ORNL-4007, part IV, 195-196 (1966).

84. J. A. Auxier et al., The Effect of Slant Incidence of a Broad Parallel Beam of Neutrons on the Distribution of Dose in a Cylindrical Tissue Phantom, ORNL-4168, part IV, 219-222 (1967).

85. H. H. Hubbell and J. A. Auxier, "Review of Neutron Depth-Dose Theory and Experiments," Health Physics Society Annual Meeting, Pittsburgh, Pa. (June, 1969).

86. W. S. Snyder and J. Neufeld, "Maximum Permissible Flux for Fast and Thermal Neutrons," Symposium on the Biophysical and Biological Effects of Neutrons, March 17, 1953.

87. T. A. Barr and G. S. Hurst, "Fast Neutron Dose in a Large Tissue-Equivalent Phantom," Nucleonics 12, No. 8, 33-35 (1954).

88. W. A. Mills and G. S. Hurst, "Fast Neutron Dosimetry in a Small Tissue-Equivalent Phantom," Nucleonics 12, No. 4, 17-19 (1954).

89. A. M. Kogan, G. G. Petrov, L. A. Chudov, and P. A. Yampolski, "Reflections of Neutrons with Different Energies from Paraffin and Water," Atomnaya Energiya 7, No. 4, 385-386 (1959).

90. A. M. Kogan et al., "Distribution of the Absorption Density of Neutrons in Paraffin," Atomnaya Energiya 7, No. 4, 386-388 (1959).

91. N. A. Frigerio, "Neutron Penetration During Neutron Capture Therapy," Phys. Med. and Biol. 6, No. 4, 541 (1962).

92. G. S. Hurst, R. H. Ritchie, F. W. Sanders, P. W. Reinhardt, J. A. Auxier, E. B. Wagner, A. D. Callihan, and K. Z. Morgan, "Dosimetric Investigation of the Yugoslav Radiation Accident," Health Physics 5, 179-202 (1961).

93. J. W. Smith and S. J. Boot, "The Variation of Neutron Dose with Depth in a Tissue Equivalent Phantom," Phys. Med. Biol. 7, 45 (1962-3).

94. S. J. Boot and J. A. Dennis, "Flux Density Distributions in and Around a Man Sized Phantom Irradiated with Thermal Neutrons," Phys. Med. Biol. 13, No. 4 573-583 (1968).

95. T. V. Blosser and R. M. Freestone, Jr., Absorbed Dose in a Water-filled Spherical Phantom Due to 14-MeV and PoBe Neutrons, ORNL-3499, Vol. II, 85-89 (1963).

96. G. F. Stone and J. H. Thorngate, Experimentally Determined Proton-Recoil Spectra in Tissue-Equivalent Material from 3 and 15 MeV Neutrons, ORNL-TM-1927 (October, 1967).

97. R. C. Lawson, D. M. Clare, and D. E. Watt, "(D,D) and (D,T) Neutron Depth Dose Measurements in a Tissue-Equivalent Phantom," Phys. Med. Biol. 12, No. 2, 201-215 (1967).

98. David Greene and R. L. Thomas, "An Experimental Unit for Fast Neutron Radiotherapy," Brit. J. Radiol. 41, 455-463 (1968).

99. C. E. Clifford, "Dose Distributions in Phantoms Exposed to 2.95 MeV Neutrons," Health Physics 15, 527-534 (1968).

100. D. E. Watt, R. C. Lawson, and J. H. Martin, "The Measurement of Energy Deposited at Depth in Tissue for an Incident PuBe Spectrum," in Biological Effects of Neutron Irradiations, Vol. I, 21-34, IAEA, Vienna, 1964.

101. D. R. Johnson and J. W. Poston, Experimental Depth-Dose Studies in Water Phantoms, ORNL-4007, 196-198 (1966).

102. T. D. Jones, J. A. Auxier, J. W. Poston, and D. R. Johnson, "Dose Distributions Functions for Neutrons and Gamma-Rays in Anthropomorphous and Radiobiological Phantoms," Proceedings of the First International Congress of Radiation Protection, 1461, Sept., 1966.

103. D. Hightower and H. M. Swartz, "Measurement of Neutron Penetration by Tissue Activation," Biological Effects of Neutron Irradiations, Vol. I, 141-155, IAEA, Vienna, 1964.

104. J. J. Broerse, "Effects of Energy Dissipation by Monoenergetic Neutrons in Mammalian Cells and Tissue," Radiobiological Institute TNO, Rijswijk, The Netherlands (1966).

105. F. H. Attix, L. de la Vergne, and V. H. Ritz, "Cavity Ionization as a Function of Wall Material," Journal of Research of the National Bureau of Standards 60, No.3, 235 (1958).

106. "Clinical Dosimetry," in NBS Handbook 87, U. S. Dept. of Commerce, 1963.

107. J. A. Auxier, "The Health Physics Research Reactor," Health Physics 11, 89 (1965).

108. D. R. Johnson and J. W. Poston, Radiation Dosimetry Studies at the Health Physics Research Reactor, ORNL-4113 (June, 1967).

109. J. A. Auxier, et al., DOSAR Low-Energy Accelerator, ORNL-4007, part IV, 207-208 (1966).

110. Linear Energy Transfer, ICRU Report No. 16, June, 1970.

111. Radiological Health Handbook, PB121784R, September, 1960.

112. Henry Margenau and George M. Murphy, The Mathematics of Physics and Chemistry, p. 504ff, D. Van Nostrand Company, Inc., Princeton, N.J., 1962.

113. Edward Fairstein, "Electrometers and Amplifiers," chapter in Nuclear Instruments and their Uses, A. H. Snell, ed., John Wiley and Sons, Inc., New York, 1962.

114. R. D. Evans, The Atomic Nucleus, 810-812, McGraw-Hill Book Co., Inc., New York, 1955.

115. T. D. Jones, private communication (1971).

116. J. A. Wall and E. A. Burke, "Gamma Dose Distribution At and Near the Interface of Different Materials, " submitted to the 1970 IEEE Conference on Nuclear and Space Radiation Effects (1970).

117. P. H. McGinley, Georgia Institute of Technology, private communication, 1971.

118. D. M. Drake, J. C. Hopkins, J. T. Martin, and H. Condé, "The Use of Pu-α-Be as a Calibrated Gamma-Ray Source," Nucl. Instr. and Meth. 62, 349-350 (1968).

VITA

John Ware Poston, Sr. was born in Sparta, Tennessee and educated in the secondary schools of Tennessee, Pennsylvania, and Virginia. He received the B.S. degree in Mathematics from Lynchburg College in Lynchburg, Virginia in 1958.

During the years 1958 through 1963, Mr. Poston was employed as an experimental reactor physicist by the Babcock and Wilcox Company, Lynchburg, Virginia. In this position, his primary research was in the area of critical experiments for reactor core design. He was certified by the U.S. Atomic Energy Commission as a reactor operator and later a senior reactor operator for all the critical experiment facilities and reactors in operation at the company site. During this period, he was the author or coauthor of 14 papers and reports dealing primarily with work on the NS Savannah and the Advanced Test Reactor critical experiments.

In 1964, he joined the Health Physics Division of the Oak Ridge National Laboratory, Oak Ridge, Tennessee. Principal research areas were dosimetry of coexistent neutron and gamma-radiation fields and pulsed fast reactor research. During this period, he has been the author or coauthor of 19 papers and reports.

Mr. Poston received the M.S. degree in Nuclear Engineering from the Georgia Institute of Technology in 1969. He is a member of the Health Physics Society, the East Tennessee Chapter of the Health Physics

Society, the International Radiation Protection Association, the American Nuclear Society, and Scientists and Engineers for Appalachia.

He is married to the former Yvonne Plunkett of Lynchburg, Virginia and has three children, daughters Martha and Vera, and a son, John Jr.